

1990

# Preparation of surface-enhanced resonance Raman scattering-active substrates: applications to heme-containing proteins

Vicki L. Schlegel  
Iowa State University

Follow this and additional works at: <https://lib.dr.iastate.edu/rtd>

 Part of the [Analytical Chemistry Commons](#)

## Recommended Citation

Schlegel, Vicki L., "Preparation of surface-enhanced resonance Raman scattering-active substrates: applications to heme-containing proteins " (1990). *Retrospective Theses and Dissertations*. 9888.  
<https://lib.dr.iastate.edu/rtd/9888>

This Dissertation is brought to you for free and open access by the Iowa State University Capstones, Theses and Dissertations at Iowa State University Digital Repository. It has been accepted for inclusion in Retrospective Theses and Dissertations by an authorized administrator of Iowa State University Digital Repository. For more information, please contact [digirep@iastate.edu](mailto:digirep@iastate.edu).

1  
91

10561

U·M·I

MICROFILMED 1991

## **INFORMATION TO USERS**

The most advanced technology has been used to photograph and reproduce this manuscript from the microfilm master. UMI films the text directly from the original or copy submitted. Thus, some thesis and dissertation copies are in typewriter face, while others may be from any type of computer printer.

**The quality of this reproduction is dependent upon the quality of the copy submitted.** Broken or indistinct print, colored or poor quality illustrations and photographs, print bleedthrough, substandard margins, and improper alignment can adversely affect reproduction.

In the unlikely event that the author did not send UMI a complete manuscript and there are missing pages, these will be noted. Also, if unauthorized copyright material had to be removed, a note will indicate the deletion.

Oversize materials (e.g., maps, drawings, charts) are reproduced by sectioning the original, beginning at the upper left-hand corner and continuing from left to right in equal sections with small overlaps. Each original is also photographed in one exposure and is included in reduced form at the back of the book.

Photographs included in the original manuscript have been reproduced xerographically in this copy. Higher quality 6" x 9" black and white photographic prints are available for any photographs or illustrations appearing in this copy for an additional charge. Contact UMI directly to order.

# **U·M·I**

University Microfilms International  
A Bell & Howell Information Company  
300 North Zeeb Road, Ann Arbor, MI 48106-1346 USA  
313/761-4700 800/521-0600



**Order Number 9110561**

**Preparation of surface-enhanced resonance Raman scattering -  
active substrates: Applications to heme-containing proteins**

**Schlegel, Vicki Lynn, Ph.D.**

**Iowa State University, 1990**

**U·M·I**  
300 N. Zeeb Rd.  
Ann Arbor, MI 48106



Preparation of surface-enhanced resonance  
Raman scattering-active substrates:  
Applications to heme-containing proteins

by

Vicki L. Schlegel

A Dissertation Submitted to the  
Graduate Faculty in Partial Fulfillment of the  
Requirements for the Degree of  
DOCTOR OF PHILOSOPHY

Department: Chemistry  
Major: Analytical Chemistry

**Approved:**

Signature was redacted for privacy.

**In Charge of Major Work**

Signature was redacted for privacy.

**For the Major Department**

Signature was redacted for privacy.

**For the Graduate College**

Iowa State University  
Ames, Iowa

1990

## TABLE OF CONTENTS

	Page
PURPOSE AND SCOPE OF RESEARCH	1
REVIEW AND DISCUSSION OF SERS/SERRS LITERATURE	6
Historical Survey	6
Surface-Enhanced Raman Scattering	8
Surface-Enhanced Resonance Raman Scattering	14
SERS/SERRS Experimental Observations	15
PAPER I APPLICATIONS OF SURFACE-ENHANCED RESONANCE RAMAN SCATTERING SPECTROSCOPY TO HEME-CONTAINING PROTEINS	35
ABSTRACT	36
INTRODUCTION	38
EXPERIMENTAL	42
Materials and Instrumentation	42
Experimental Procedures	46
RESULTS AND DISCUSSION	56
RRS and SERRS Studies of Cytochrome P-450 <sub>b</sub>	56
RRS and SERRS Studies of Myoglobin	66
RRS and SERRS Studies of Cytochrome c	79
CONCLUSIONS	93
ACKNOWLEDGEMENTS	95
LITERATURE CITED	96
PAPER II RESONANCE RAMAN AND SURFACE-ENHANCED RESONANCE RAMAN SCATTERING STUDIES OF CYTOCHROME C <sub>3</sub>	101
ABSTRACT	102
INTRODUCTION	103
EXPERIMENTAL	106
Materials and Instrumentation	106

Experimental Procedures	108
RESULTS AND DISCUSSION	111
RRS and RRS Comparison Studies of Oxidized and Reduced Cytochrome $c_3$	111
Investigations of the Intermediate Redox States of Cytochrome $c_3$ using RRS Spectroscopy	116
Investigations of the Intermediate Redox States of Cytochrome $c_3$ using SERRS Spectroscopy	119
CONCLUSIONS	126
ACKNOWLEDGEMENTS	128
LITERATURE CITED	129
PAPER III SILVER-ISLAND FILMS AS SUBSTRATES FOR ENHANCED RAMAN SCATTERING: EFFECT OF DEPOSITION RATE ON INTENSITY	133
ABSTRACT	134
INTRODUCTION	136
EXPERIMENTAL	141
Materials and Instrumentation	141
Experimental Procedures	142
RESULTS AND DISCUSSION	145
Characterization of Silver-Island Film Surface Morphology	145
Zinc Tetraphenylporphine Optical/SERRS Investigations	151
4,4'-Bipyridine Optical/SERS Investigations	162
CONCLUSIONS	168
ACKNOWLEDGEMENTS	169
LITERATURE CITED	170

<b>PAPER IV APPLICATION OF SURFACE-ENHANCED RESONANCE RAMAN SCATTERING SPECTROSCOPY TO THE ANALYSIS OF COVALENTLY MODIFIED ELECTRODE SURFACES</b>	<b>174</b>
<b>ABSTRACT</b>	<b>175</b>
<b>INTRODUCTION</b>	<b>176</b>
<b>EXPERIMENTAL</b>	<b>180</b>
<b>Materials and Preparation of Modified     Electrode Surfaces</b>	<b>180</b>
<b>Characterization of Modified Electrode Surfaces</b>	<b>183</b>
<b>RESULTS AND DISCUSSION</b>	<b>186</b>
<b>Optimization of Silver Overlayer Thickness</b>	<b>186</b>
<b>Detection of Covalently Bound Species by SERRS</b>	<b>190</b>
<b>Determination of Detection Limits</b>	<b>205</b>
<b>CONCLUSIONS</b>	<b>209</b>
<b>ACKNOWLEDGEMENTS</b>	<b>210</b>
<b>LITERATURE CITED</b>	<b>211</b>
<b>PAPER V RAMAN MICROPROBE INVESTIGATIONS OF RESONANTLY-ENHANCED DYE MOLECULES AT SILVER-ISLAND FILMS</b>	<b>214</b>
<b>ABSTRACT</b>	<b>215</b>
<b>INTRODUCTION</b>	<b>216</b>
<b>EXPERIMENTAL</b>	<b>221</b>
<b>Materials and Instrumentation     Experimental Procedures</b>	<b>221</b>
<b>RESULTS AND DISCUSSION</b>	<b>225</b>
<b>Raman Microprobe SERRS Studies of Zinc     Tetraphenylporphine</b>	<b>225</b>
<b>Concentration Dependence Studies</b>	<b>231</b>
<b>Determination of Detection Limits</b>	<b>233</b>
<b>Laser Irradiation Time Dependence Studies</b>	<b>236</b>

<b>Raman Microprobe SERRS Studies of Magnesium Phthalocyanine and 1,1'-Diethyl-2,2'-Cyanine Iodide</b>	<b>242</b>
<b>CONCLUSIONS</b>	<b>247</b>
<b>ACKNOWLEDGEMENTS</b>	<b>248</b>
<b>LITERATURE CITED</b>	<b>249</b>
<b>CONCLUDING REMARKS</b>	<b>252</b>
<b>LITERATURE CITED</b>	<b>254</b>

## PURPOSE AND SCOPE OF RESEARCH

The technique of surface-enhanced resonance Raman scattering (SERRS) has evolved into an acceptable surface analytical method since the initial observation of the Raman surface effect in 1973. The experimental features unique to SERRS coupled with the additional strengths of Raman spectroscopy permit the acquisition of surface vibrational information pertaining to a variety of samples.

An advantage of applying optical spectroscopic methods to the study of surfaces is that solid-gas and solid-liquid interfaces can be examined in situ. Conventional ultra-high vacuum surface techniques are limited to solid interface investigations. Vibrational spectroscopies are viable methods for the characterization of surfaces because information pertaining to the nature of the adsorbed molecules, the adsorbate surface bonding, and the surface chemical reactions can be obtained readily. However, the general applicability of infrared vibrational spectroscopy to samples in aqueous solutions is difficult because of the high absorption of water. In contrast, water has a relatively weak scattering cross-section; hence, Raman spectra of a species in this medium are easily acquired. In addition to sample preparation flexibility, high quality Raman spectra in the low-frequency region can be obtained

routinely because of the availability of high intensity light sources, sensitive detectors, and efficient double and triple monochromators. It is now feasible to examine Raman frequencies approximately  $3 \text{ cm}^{-1}$  from the excitation line.

Normal Raman scattering (NRS) spectroscopy lacks sufficient sensitivity for monolayer surface characterization. The resulting Raman spectra consist of low intensity signals indistinguishable from the background noise. The Raman sensitivity can be increased by using an excitation that coincides with an absorption band of the molecule of interest. Under these conditions, the electronic transition is accompanied by a large change in the polarizability of the molecule. The scattering cross-section is resonantly-enhanced by approximately  $10^6$ - $10^7$  compared to the normal Raman effect. Along with an increase in sensitivity, resonance Raman scattering (RRS) spectroscopy is a selective method in which the molecular distortions of the excited molecule can be probed. This feature of RRS is particularly beneficial to the study of biomolecules containing biologically-active chromophore sites. Vibrational modes of the chromophore are selectively enhanced over the nonchromophoric environment. Because of the high degree of sensitivity and selectivity, RRS spectroscopy requires only very low concentrations,  $10^{-3}$ - $10^{-6}$  M, of the biomolecule. The major disadvantage

associated with RRS is that fluorescence emitted from several molecules can completely obscure the RRS spectrum.

The sensitivity of Raman spectroscopy can be increased further by adsorbing the sample onto a rough metal surface. It has been repeatedly demonstrated that the Raman scattering efficiencies of a variety of molecules on certain types of metal substrates are increased by 3 to 6 orders of magnitude. The surface-enhanced Raman scattering (SERS) mechanism is attributed to adsorbate-metal interactions resulting in the modification of the molecule's electronic properties. To date, several theoretical models have been postulated to interpret the conflicting experimental evidence pertaining to SERS. It is now the general consensus that the different theories can be categorized into two dominant mechanisms, i.e., a molecular model and/or an electromagnetic model.

Surface-enhanced resonance Raman scattering (SERRS) combines RRS with SERS. Similar to SERS, the sample is adsorbed onto a metal surface, but an excitation wavelength that is in resonance with an electronic transition of the molecules is used as the radiation source. The advantage of SERRS is that the strong points arising from both RRS and SERS are coupled. Compared to normal Raman scattering efficiencies, SERRS enhancement factors can exceed  $10^9$  while allowing for selective examination of the adsorbate. As

discussed previously, resonantly-enhanced molecules may exhibit a high fluorescent background. In many cases, the fluorescence emission is quenched when the sample is adsorbed at a metal surface.

The majority of SERS/SERRS research has been directed at elucidating the mechanism from a theoretical perspective. Recently, studies have focused on exploiting the enormous analytical potential of the SERS/SERRS techniques. However, the SERRS technique has not been fully developed because several experimental parameters have not been characterized. The problem is especially apparent for the study of biological systems. In many cases, the biomolecules are perturbed upon adsorption onto a SERRS-active substrate. SERRS is not a viable method if the resulting spectra are representative of perturbed biological structures. It is the goal of our research to develop procedures for preserving the native structure and activity of proteins at SERRS-active substrates, including electrochemically-roughened silver electrodes, vapor-deposited silver-island films, and citrate-reduced silver sols. In particular, our work has focused on the heme-containing proteins, cytochrome P-450<sub>b</sub>, myoglobin, cytochrome c, and cytochrome c<sub>3</sub>. Depending on the nature of the biomolecule, the native structure of the protein can be retained by choosing the appropriate adsorption conditions.

Another aspect of our research is concerned with optimizing and characterizing the experimental parameters in the preparation of SERS/SERRS-active substrates. The experimental conditions that affect the intensity of the SERS/SERRS signals have been examined and methods are discussed for maximizing the Raman signals. Specific applications of the SERRS technique by using silver-island films as SERRS-active substrates include Raman microprobe investigations and the characterization of covalently modified electrodes.

In order to convey a better understanding of the specific areas of interest, a brief review of the current SERS/SERRS theories and the experimental observations is presented below.

**REVIEW AND DISCUSSION OF SERS/SERRS LITERATURE****Historical Survey**

Raman signals of pyridine adsorbed on an electrochemically-roughened silver electrode surface were first reported by Fleischmann, Hendra, and McQuillan in 1973 and 1974 [1,2]. The authors noted two distinct differences between the spectrum of the adsorbed molecule and that in solution. First, vibrational frequencies displayed by the adsorbate were shifted relative to the solution bands. Second, the intensity of the Raman signals of the adsorbed molecule were enhanced compared to the modes displayed by the free molecule. The results suggested that the spectrum originated from the adsorbed species. Fleischmann *et al.* [1,2] concluded that the increase in surface area arising from a roughened metal surface was responsible for the enhanced Raman signals.

Additional Raman studies pertaining to the pyridine/metal electrode substrate system were reported by two independent groups, Jeanmaire and Van Duyne [3] and Albrecht and Creighton [4] in 1977. Their experimental data showed an enhancement of 6 orders of magnitude for the average Raman cross section of the adsorbed pyridine molecule with respect to the molecule in solution. An

increase in the surface area alone could not have evoked this degree of amplification. Billman et al. [5] showed a monolayer of radioactive labeled  $CN^-$  covered both a smooth surface and a roughened surface.

Jeanmaire and Van Duyne [3] showed that the metal substrate must be subjected to a roughening process in order to induce the surface-enhanced effect. When pyridine was adsorbed onto a smooth silver surface, no spectrum was observed. The bands were exhibited only after an oxidation-reduction cycle (ORC) was applied to the electrode. Bergman et al. [6] examined the effect of the ORC roughening procedure as a function of Raman intensity signals from radioactive-labeled  $CN^-$ . By increasing the anodization time from 1 to 20 sec, the Raman intensity increased by approximately  $10^2$  and then remained constant for greater anodization periods. The SERS spectrum could also be obtained after the activation cycle was completed. The experimental evidence suggested that SERS is evoked only when the surface morphology is modified in some manner.

Since the initial SERS studies, a large body of conflicting experimental data has been collected. As a consequence, several theoretical mechanisms have been postulated accounting for these observations. Because of the amount of published material available on SERS/SERRS, only an overview of the theoretical models and the

experimental features will be presented. For more comprehensive treatments, the reader is directed to excellent reviews by Van Duyne [7], Chang and Furtak [8], Otto [9], Wokaun [10], Metiu and Das [11], Creighton [12], and Moskovits [13]. Each of these authors discuss SERS/SERRS from a slightly different perspective.

### Surface-Enhanced Raman Scattering (SERS)

The two dominant theories proposed to account for the SERS mechanism can be understood in terms of the Raman scattering process. The intensity of the Raman scattered light is proportional to the square of the induced molecular dipole moment ( $\mu$ ). The induced dipole moment is produced by the interaction of the incident electromagnetic field ( $E$ ) with the molecular polarizability ( $\alpha$ ) and is described by the following relationship:

$$\mu = E \cdot \alpha$$

The intensity of the scattered radiation is thereby enhanced by increasing the molecular polarizability component and/or the electromagnetic component. Experimental results indicate that one or both of these terms are enhanced when molecules are adsorbed onto a metal

surface. The postulated SERS mechanisms are thus categorized into two classes, the electromagnetic enhancement (EM) theory and the molecular enhancement theory.

#### Electromagnetic Enhancement Theory

The electromagnetic enhancement model attributes the augmented surface signals to an increase in the electric field (E) component that is experienced by the adsorbed molecule. Interaction of radiation with an appropriate substrate composed of metal particles produces large local fields at the metal surface, which are described effectively by an electrostatic method. This approach assumes that the dimensions of the metal particles are small relative to the exciting wavelength and that the EM field is constant across the particles. A detailed treatment of the EM theory is described by Wokaun [10], Moskovits [14], and McCall et al. [15] and is summarized here. When an applied field interacts with a roughened metal surface, electromagnetic resonances are generated. The metal particles become polarized producing local fields at the surface that are substantially larger than the incident field. The adsorbed molecule is polarized by the field and the induced dipole moment produces the Raman scattering. The field created by the vibrating adsorbed molecule in turn polarizes the metal

particle and the Raman scattered radiation is then amplified by the latter process. The enhancement of the Raman intensity is proportional to the square of the electric field at both the incident frequency and the Raman scattered frequency.

The EM mechanism requires certain types of metals couple the incident photons with the metal surface and produce plasma oscillations. The quanta of energy of the electrical oscillations in condensed matter are known as plasmons. Qualitatively, a metal can be classified as a plasma because the surface is essentially an electron gas with a fixed positive-ion background. A plasmon is created by fluctuations in the electron gas relative to the positive background. The background is no longer neutralized, and a Coulombic restoring force initiates propagating repulsive electric fields. In metals, an external force is required for plasmons to be excited, namely a photon with the same energy as the plasma oscillations. An incident photon in the visible region cannot sustain electron oscillations on smooth metallic surfaces because of momentum mismatches between the plasmon and the incident radiation. A rough surface, however, allows the momentum of the plasmon to be modified such that it matches the momentum of the photon [16]. A localized surface plasmon is excited at frequencies that are typically used in Raman experiments. These

electronic oscillations can be described as longitudinal electric field waves which propagate along the surface of the metal.

EM theory predicts that the magnitude of the SERS enhancement is dependent upon several experimental parameters, including the dielectric constant of the metal substrate, the frequency of the incident radiation, and the size/geometry of the metal particles [17-20]. The large local fields at the surface are produced when the real component of the dielectric vanishes and the imaginary component is small. This response correlates to the excitation of the surface plasmon. However, electromagnetic resonances are only excited when the incident radiation frequencies are equivalent to the frequencies of the electronic oscillations. Noble metal or alkali metal substrates generate electromagnetic resonances with frequencies that are used in Raman experiments. The dielectric constants of particles composed of these materials satisfy the conditions required for plasmon excitation when visible excitations are used. Moreover, the frequencies of the plasma oscillations are related to the shape and size of the metal surface particles. Zeman and Schatz [21] calculated the maximum field enhancement for ellipsoidal silver particles of varying sizes by using optimal incident radiation. With increasing particle

sizes, the absorption maximum shifted towards the red spectral region of the spectrum, and at the optimal excitations, the magnitude of the surface field was the greatest. The authors also demonstrated that the theoretical SERS enhancement factor for a molecule adsorbed onto various sizes of particles was similar to the enhancement of the surface field determined experimentally. SERS enhancement factors for molecules at spherical [18] and spheroidal [22] particles have been derived as well.

Localization of the electric field near the tip of the metal particle can substantially affect the magnitude of the SERS intensities. Enhancement factor of approximately  $10^{11}$  has been calculated for analytes adsorbed onto needle-like particles [11]. Although concentrating the field near the curvature of the particle reduces the field at other parts of the surface, the average value of the field increases. According to EM theory, SERS intensities are also influenced by dielectric properties of the adsorbate/solvent system [23,24] and by particle dipolar interactions [10,11].

#### Molecular Enhancement Theory

The development of molecular enhancement theories attracted considerable attention when calculations based upon the chemical effect predicted enhancement factors of as large as  $10^6$ . These theories propose that the large

enhancement of SERS is due to surface induced modifications of the molecular polarizability which result in an increase in the  $\alpha$  component. The molecular model accounts for certain experimental observations that cannot be adequately explained by the EM mechanism. Specific experimental observations, including frequency shifts exhibited by the adsorbate relative to the solution spectrum, molecular specificity, and the diversity of the degree of Raman enhancement at various surface sites support the chemical contribution to SERS.

The molecular process is described by a number of theories, i.e., electron-hole pair, charge-transfer, and modulated reflectance models [9,25,26]. Although the mechanism varies for each of these models, all of the theories require some type of interaction between the adsorbed molecule and the metal surface. For example, a chemisorption metal-molecule interaction occurs when the orbitals of the molecule overlaps with the metal orbitals. The electronic properties of the surface complex are different from those in the bulk. Raman scattering of the new surface-induced complex is resonantly enhanced at the appropriate incident wavelength [27]. Another type of interaction involves the formation of a charge-transfer complex or direct covalent bonding of the adsorbate with the surface. In these cases, the molecular polarizability is

modified due to an increase in the electron density of either the adsorbate or the metal surface [28].

It is now commonly believed that both the molecular enhancement mechanism and the EM enhancement mechanism play a role in the SERS phenomenon. The relative contribution of each mechanism to the overall Raman enhancement varies for different adsorbates and experimental conditions, and for a given system, is difficult to determine experimentally. The general consensus is that the magnitude of the SERRS intensity is predominantly dependent upon the local field effects at the surface [13].

#### **Surface-Enhanced Resonance Raman Scattering (SERRS)**

Surface-enhanced resonance Raman scattering (SERRS) signals have been documented for adsorbed molecules that are in resonance with the excitation line [3,7]. Early SERRS studies showed large Raman intensities when certain dye molecules were adsorbed onto suitable metal surfaces. Based upon these observations, it was proposed that resonant Raman scattering and surface-enhanced Raman scattering contributed independently to the overall SERRS enhancement. Additional, more detailed investigations indicated that the SERRS intensities were indeed larger relative to normal SERS, but the SERRS enhancement factors for most resonantly-

enhanced adsorbates were lower, i.e.,  $10^3$ - $10^5$  [29-33]. Similar to SERS, the intensity of the SERRS signals is dependent upon the local surface fields at the incident frequency and the field at the Raman shifted frequency. However, SERRS enhancement factors are also proportional to the resonance scattering tensors which describe the interaction of the electronic excited states with the surface. Possible explanations for the smaller SERRS enhancement factors relative to SERS include adsorbate-induced modifications of the dielectric environment of the substrate in the presence of highly absorbing molecules [34,35], separation of the chromophoric group from the metal substrate [36], and/or perturbation of the electronic properties of the molecule upon adsorption onto a SERRS-active substrate [37,38]. In the latter situation, an increase of the electronic state lifetime can result or the electronic absorption frequency can shift to a longer wavelength.

#### **SERS/SERRS Experimental Observations**

SERS/SERRS has been reported for many adsorbates representing a variety of classes of compounds. Several of these molecules are listed in a recent bibliography composed by Seki [39]. SERS/SERRS research was initially directed at

determining the types of molecules as well as the metal surface that exhibited the effect. However, the accumulated experimental evidence revealed other characteristics unique to SERS/SERRS. These features can be used to distinguish a SERS/SERRS signal from a bulk signal and/or EM enhancement from chemical enhancement. The criteria common to SERS/SERRS are summarized below.

#### SERS/SERRS-Active Metals

Although many types of metals evoke SERS/SERRS, the greatest enhancements observed experimentally are from a silver surface [12]. For this reason as well as its ease in handling, silver is the most commonly used metal for SERS/SERRS studies. Other metals that give rise to SERS/SERRS activity are gold and copper [40] and, next to silver, these surfaces are widely used. SERS intensities comparable to those obtained from gold and copper are also observed from lithium [8], potassium [41], sodium [41,42], aluminum [43], and indium [13] substrates. Low intensity signals have been collected from such metals as nickel [44,45], palladium [45,46], palladium hydride [47], and platinum [45,47,48].

#### Surface Roughness

Surface roughness is an important requirement for

SERS/SERRS. As discussed previously, SERS signals from pyridine adsorbed onto an electrode were observed only after the surface was subjected to an electrochemical-roughening cycle. Fleischmann et al. [1,2] conducted SERS experiments in which extensive potential cycling was used to create extremely rough surfaces. Later Jeanmaire and Van Duyne [3] showed similar SERS signals of pyridine adsorbed onto an electrode roughened with a single oxidation-reduction cycle (ORC). After the substrate was pretreated under the described conditions, a scanning-electron microscope was used for closer inspection of the electrode surface morphology [49]. The micrograph depicted a surface composed of coarse silver deposits ranging on a scale of 10-100 nm.

Because surfaces with varying degrees of metal roughness show SERS/SERRS activity, the specific scale of roughness necessary to induce the effect has not yet been completely characterized. SERS signals have been recorded from substrates with particle sizes ranging in the microscopic (500-2000 Å) [50], submicroscopic (<100 Å) [51], or atomic (adatom) [5] scale. It is difficult to establish the necessary degree of roughness because a substrate can contain several various surface particle sizes. When a surface is extensively roughened on the microscopic scale, submicroscopic and atomic metal deposits are always present. Other variables such as the type of metal and the

excitation frequency must be considered before determining the required scale of roughness.

The degree of surface roughness is dependent upon the specific adsorbate-metal interactions. Molecules that undergo EM enhancement must be adsorbed onto microscopic or submicroscopic metal particles with suitable dielectric properties. On the other hand, chemical enhancement requires direct interaction with the surface, and even atomically smooth substrates can evoke SERS/SERRS [52].

#### SERS/SERRS-Active Substrates

Subjecting a metal electrode to an ORC roughening process is only one means of activating a surface. Several other innovative SERS/SERRS-active substrates have been fabricated since the initial pyridine/electrode studies. A common feature of the various substrates is surface roughness. The SERS/SERRS-active substrates most widely used include electrochemically-roughened electrodes, metal colloids, and vapor-deposited metal films. A short discussion pertaining to each type of substrate is presented.

Electrodes. To date, metal electrodes pretreated with an ORC are the most common substrates used in SERS/SERRS experiments. The activation cycle creates a rough surface by initially oxidizing the silver. During this step, the

electrode surface is covered with a porous insoluble silver salt. When the electrode is exposed to the cathodic sweep, the silver ions in the diffusion layer are reduced and redeposited at the surface. A major advantage associated with electrode substrates is that the surface potential can be monitored and electrogenerated species can be studied by using SERS/SERRS.

Many experimental parameters must be controlled in order to insure reproducible surface roughness, including nature of the electrolyte solution, the number of activation cycles, the potentials of the oxidation and reduction potentials, and the amount of charge passed during the oxidation step [7,8,13,53]. Moreover, it has been demonstrated that the SERS enhancement factor increases when the electrode surface is illuminated during the roughening cycle [54-57]. Photoreduction of silver ions occurs during illumination which thereby produces microstructures.

The manner in which the surface of the electrode is pretreated before the ORC also affects the SERS/SERRS intensities of the adsorbate. In order to evolve H<sub>2</sub> bubbles and to desorb organic materials accumulated on the electrode, proper pretreatment of the surface is essential. These problems are eliminated by applying a cathodic potential to the electrode before the roughening process. Barz et al. [58] showed an increase in the SERS intensity by

a factor of 10 when a cathodic sweep was applied prior to the anodization step.

SERS has been reported for a number of small neutral molecules and ions adsorbed onto silver and copper electrodes [7,58-63]. In addition, Pettinger et al. [64] observed SERS signals of pyridine on roughened gold electrodes. A comprehensive review pertaining to SERS of molecules at electrodes is presented by Chang [65].

Metal Sols. Creighton et al. [66] were the first to observe enhanced Raman signals of pyridine adsorbed onto gold and silver sols. The authors demonstrated that the particles aggregated upon addition of pyridine to a silver sol. The electronic absorption band of this system is shifted towards the red spectral region and the resulting excitation profile also displays a maximum in the red region. In later studies, Wetzel and Gerischer [67] developed a preparation method that prevented particle aggregation. Because of the presence of the smaller silver particles, the maximum of the sol absorption was approximately 400 nm. Depending upon the colloidal preparation procedure, gold sols have various colors: ruby, green, violet, or blue [68]. Thus, the fact that the sol particle roughness can be characterized by absorption spectroscopy is a major advantage associated with SERS/SEERS-active colloid suspensions.

A primary reason for the popularity of the metal sols is their ease in preparation. Colloidal suspensions are produced by chemically reducing silver, gold, or copper salts. Compared to electrochemically-roughened electrode substrates, metal sols consist of particles that are more separated and homogeneous. Scanning electron micrographs of silver and gold sols showed particle sizes ranging between 10-100 nm in diameter [8].

Nonetheless, certain disadvantages arise with the use of metal sols. As mentioned previously, aggregation of the colloid particles can occur when the analyte is adsorbed onto the surface. Because of the change in the surface morphology of the sol and the tendency for large particles to settle out of the solution, time dependent Raman spectra of changing intensity can result. The addition of stabilizers to the metal particle suspensions prevents aggregation [69,70]. However, partial aggregation is necessary to obtain the highest quality SERS/SERRS spectra. Investigations performed by Laserna et al. [71] indicated that intense SERS signals could only be obtained from partially aggregated borohydride sols. Soper and Kuwana [72] observed the same effect from partially aggregated citrate-reduced sols. A detailed discussion on the relationship between sol aggregation and the particle size effects on the SERS of citrate is presented by Siiman et al.

[73]. Aggregation of gold sols was also required in order to obtain SERS signals from adsorbed pyridine.

In addition, metal sols are limited as SERS/SERRS-active substrates because it is difficult to control the sol surface potential from one preparation to the next. Silver sols are especially susceptible to inconsistent surface potentials. The silver sol potential can be lowered by the addition of the reductant,  $\text{NaBH}_4$ , which tends to stabilize the suspension [74,75]. With negative potentials, the sol disaggregates due to repulsion between the negatively-charged particles. Although the stability of the sol is greater under these conditions, disaggregation leads to weaker SERS/SERRS enhancements.

Studies have shown that SERS/SERRS can be evoked by depositing a silver sol onto certain types of support matrices. Tran [76,77] acquired SERRS spectra from several dyes that were first adsorbed onto a silver sol and then deposited onto filter paper. Laserna et al. [78] observed Raman signals from samples adsorbed onto silver sols after the particles were deposited onto filter paper. Séquaris and Koglin [79] collected SERS data of derivatized nucleic purine deposited onto high-performance thin-layer chromatographic plates and coated with a silver sol suspension. As demonstrated by Soper and Kuwana [72] and Tran [76,77], the SERS/SERRS intensities are dependent upon

the supporting matrix used in the studies. Compared to solution-phase sols, the deposited sols displayed signals that were more stable as a function of time.

Metal sols have been used primarily to correlate experimental observations with predictions based on theoretical models [66,74,80-82]. Recently, sol substrates have attracted attention for analytical applications as well. Torres and Winefordner [83] reported trace analysis of nitrogen-containing drugs adsorbed onto metal sols. Freeman *et al.* [84], Berthod *et al.* [85], and Laserna *et al.* [86] coupled SERS with a flow injection system. The authors obtained a detection limit of 2 ng for pararosaniline at a SERS-active sol suspension. Studies pertaining to the conformation of cyclohexanethiol adsorbed onto silver sol surfaces were conducted by Kwon *et al.* [87]. At submonolayer coverages, the SERS spectra exhibited vibrational bands of both the equatorial and axial chair conformations, but at monolayer surface coverages only the equatorial chair conformation was observed. Sandroff *et al.* [88] studied high pressure effects at liquid-solid interfaces by using the SERS technique with gold colloids.

Metal Films. As in the case of metal sols, activated metal film substrates have been used mainly to verify SERS/SERRS theoretical predictions [8,10,89-92]. Metal films are particularly suitable for SERS/SERRS studies

because these substrates are more reproducible and stable compared to metal sols.

SERS/SERRS-active metal films are prepared by various methods, but metal films are commonly prepared by vacuum-depositing metal vapor onto appropriate substrates. Wood and Klein [93,94] were the first to report SERS of carbon monoxide at vacuum-deposited silver films under UHV conditions. Chen et al. [95] observed SERS signals from a nonconducting silver films with an average metal thickness of 50 Å. As revealed by scanning electron microscopy, the thin film surfaces were composed of isolated particles with diameters of approximately 200 Å. Earlier studies, which focused on the morphology of the thin films, showed that vacuum-deposited silver surfaces with thickness below 100 Å consisted of discontinuous island-like structures [96]. With increasing metal thickness, the particles merge and eventually a smooth surface is formed. Thick metal films are not submicroscopically or microscopically rough at room temperature, and, thus cannot induce EM enhancement. However, surface roughness is produced by depositing a thick film onto cold substrates [13,93,97]. Rough surfaces have also been fabricated by coating a thick film of metal onto CaF<sub>2</sub> films or onto polystyrene spheres deposited on filter paper or glass substrates [98-100].

In order to prepare the metal films, a vacuum

deposition instrument must be available. SERS/SERRS-active silver-island films can be produced by a chemical procedure as well. Ni and Cotton [101] reported SERS spectra of pyridine at chemically reduced silver films which were deposited onto frosted glass slides. Scanning electron micrographs of the chemically-deposited films indicated that the degree of surface roughness was dependent upon the  $\text{AgNO}_3$  concentration used in the preparation procedure. Isolated silver particles were formed with  $\text{AgNO}_3$  concentrations of approximately 2%. Higher concentrations produced surfaces consisting of larger, more aggregated particles. Corresponding SERS studies showed stronger signals of pyridine at the silver films prepared with the lower concentrations of  $\text{AgNO}_3$  solutions.

#### Inelastic Background in SERS/SERRS

Adsorbates at roughened SERS/SERRS-active substrates exhibit vibrational bands that are always superimposed on a high structureless background. Billman *et al.* [5] noted that the background was not present when pyridine was adsorbed onto a smooth silver electrode; however, it was observed after the electrode was roughened. The background is also displayed in the absence of an adsorbate. Hence, the intrinsic properties of the activated surfaces give rise to the inelastic continuum. The background is ascribed to

luminescence resulting from a continuum of metal electronic excitations [102-104].

#### Distance Dependence of SERS/SERRS

Molecules that undergo chemical enhancement must be in close contact with the SERS/SERRS-active surface. Investigation of pyridine chemisorbed onto a silver surface showed that the intensity of the SERS signals maximized at a surface coverage between one and two monolayers [105]. The results suggest complete saturation of the active sites at the surface. With successive monolayer coverages, SERS signals of a physisorbed species was observed beyond 20 monolayers. This long-range enhancement is fully rationalized by EM theory. The intensity of the signal is predicted to decrease with distance by  $(a/R)^{12}$  ( $a$  is the radius of curvature of the particle and  $R$  is the distance between the molecule and the center of the particle) [59]. Long-range enhancement was confirmed by spacer experiments in which the adsorbate was separated from a silver film by different thicknesses of polymer layers. SERS spectra of the adsorbate were acquired at polymer thicknesses of up to 100 Å [105]. Depending upon the type of molecule and the degree of surface roughness, adsorbates can be separated between 50 Å to 100 Å and still display SERS/SERRS signals [106-108].

Frequency Dependence of SERS/SERRS: Correlation with  
Optical Properties

Surfaces composed of discontinuous metal particles are characterized by a strong, broad absorption band. The optical properties of these surfaces are related to the excitation of surface plasma resonances. At a fixed frequency, the extinction band maximizes when the plasmon frequency of the metal particles is in resonance with the excitation frequency. As predicted by the EM mechanism, the SERS effect is dependent upon this resonance effect.

The electronic resonances contributing to the Raman enhancement can be established by SERS excitation profiles (SERS intensity vs excitation wavelength). The SERS excitation profile of pyridine at a silver sol surface shows an increase in the intensities of the SERS signals towards the blue spectral region. Furthermore, the SERS profile tracks the absorption spectrum of the silver sol suspension [109]. Absorption studies of thin silver films as a function of metal thickness showed that the extinction maximum is shifted towards the red spectral region with increasing film thicknesses [92]. The optical properties of the films were attributed to changes in the shapes, sizes, and packing densities of the metal particles. Silver sol suspensions exhibit similar optical properties with increasing particle sizes due to aggregation effects [110].

SERS excitation profiles of pyridine adsorbed onto the aggregated sol particles displayed a maximum in the red region which corresponded to the long-wavelength optical properties of the substrate. A quantitative treatment relating the absorption properties of the surface with the magnitude and the spectral dependence of the SERS excitation profile was developed by Weitz et al. [111].

SERRS excitation profiles show contributions from molecular resonances as well as from the plasmon resonances. Similar to SERS, the SERRS excitation profiles reflect the absorption spectra of the substrate/adsorbate system, but the qualitative characteristics of the spectra change with increasing coverages of strongly absorbing molecules. The local electromagnetic environment surrounding the surface metal particles is modified by the presence of a resonantly-enhanced molecule. As a consequence, the electromagnetic resonances are perturbed thereby altering the optical properties and the SERRS excitation profiles. The absorption spectra usually exhibit an anomalous splitting due to interactions involving the molecular resonances and the plasmon resonances of the metal [112].

Experimentally, SERS/SERRS excitation profiles are broad and vary slowly. This behavior is ascribed to the discontinuous shapes and sizes of metal deposits that are found on a rough surface. Therefore, experimental results

and EM theoretical calculations do not always agree. In order to compare accurately plasmon resonance theories with the observed SERS results, Liao et al. [113] developed a microlithographic technique to produce a surface composed of a regular array of isolated, uniform silver particles. The experimental excitation resonances correlated with the shape-dependent resonance frequencies predicted by EM theory. The EM mechanism can successfully predict observed SERS/SERRS excitation profiles of adsorbates at irregular metal particles by accounting for the measured optical properties of an adsorbate/substrate system [110]. Experimental excitation profiles are usually red shifted compared to calculated profiles because intermolecular dipole interactions are neglected in the theoretical treatments.

For an adsorbate that undergoes chemical enhancement, the greatest SERS/SERRS intensities occur when the excitation line coincides with the resonance molecular energy. Both EM- and chemically-enhanced adsorbates display excitation profiles that diverge greatly from the  $\nu^4$  dependence of the normal Raman scattering process.

#### Coverage Dependence of SERS/SERRS

The enhancement factor of SERS/SERRS is influenced by the adsorbate surface coverage. Typically, a nonlinear

relationship between surface coverage and signal intensities exists for both nonresonantly-enhanced molecules and resonantly-enhanced molecules [40,50,97,114-118]. Early studies of pyridine showed an increase in the SERS intensity with coverages up to 0.5 monolayer. At higher surface coverages, the intensity was observed to decrease [118], remain constant [118], or increase slowly [50]. The differences in the surface coverages were attributed to variations in experimental procedures. A nonlinear behavior was documented for SERRS of rhodamine 6G and basic fuchsin [116]. Zeman et al. [119] examined the SERRS intensities exhibited by cobalt phthalocyanine (CoPc) at CaF<sub>2</sub> roughened silver films as a function of surface coverage. The results indicated that the maximum signal was measured at approximately 0.07 monolayer. The intensity of the SERRS signals decreased quickly at greater coverages and remained constant for coverages higher than 2 monolayers. Enhancement factors obtained at very low surface coverages show the SERRS amplification comparable to nonresonance enhancement. The effect of dye coverages on the SERRS intensities of cyanine dye was further examined using Langmuir-Blodgett monolayers [120]. The results showed a nonlinear behavior with a maximum at submonolayer coverages. The relationship of the adsorbate concentration and the SERS/SERRS intensities was attributed to modifications in

the dielectric properties of the adsorbent/adsorbate system and/or dipole-dipole coupling of the molecules with increasing surface coverage [119]. For molecules that are chemisorbed onto the surface, the nonlinear behavior is due to a complete saturation of the special bonding sites at the surface.

Spectral Features of SERS/SERRS: Relaxation of Raman Selection Rules

Because SERS/SERRS involves a chemical and/or an electromagnetic interaction between the molecule and the surface, the characteristic Raman selection rules are relaxed for adsorbates at metal substrates. Vibrational bands that are normally Raman inactive in the bulk may be observed in the surface spectrum of the adsorbed molecule. For example, free pyrazine has an inversion center, therefore, symmetry constraints dictate the Raman exclusion of IR active modes [121]. When pyrazine was adsorbed onto an activated silver electrode, the SERS spectrum exhibited vibrational bands that were Raman inactive in solution [61,122]. Moskovits and DiLella [123] demonstrated that the normally inactive Raman and IR modes for free benzene were enhanced for the adsorbed species. By reducing or breaking the molecular symmetry of the molecule upon adsorption onto a SERS/SERRS-active substrate, Raman forbidden bands may be

observed in the surface spectrum. Alternatively, surface interactions can perturb and change the bond polarizabilities giving rise to scattering for Raman inactive modes. Both the EM mechanism and the chemical mechanism account for the relaxation of the symmetry requirements; however, the selection rules differ for each model.

The SERS/SERRS spectra for molecules that undergo a chemical enhancement may display changes in relative intensities and/or frequency shifts with respect to those bands observed in the solution Raman spectrum. The type and the strength of the bonding interactions of the metal-adsorbate complex influence the relative intensities and the frequencies of the modes. Selective enhancement is expected for vibrational modes that correlate to bonds involved in the chemical interaction. From these spectral changes, the orientation of the adsorbate relative to the surface can be deduced. Gao and Weaver [124] showed a downshift of 15-25  $\text{cm}^{-1}$  in the frequency of the symmetric ring breathing mode of benzene at gold electrodes. The authors concluded that the molecule adopted a flat orientation relative to the surface. The flat adsorption of the molecule occurred through  $\pi$  bonding to the metal resulting in a downshift of those vibrational bands of the atoms interacting with the surface. A similar orientation for benzene at a silver

surface was determined from the SERS spectra [123]. Alkenes and alkynes at gold surfaces displayed large decreases in the frequencies of the carbon-carbon double band and triple bond stretching frequencies, i.e., 70-140  $\text{cm}^{-1}$  [125]. Downshifts of only 35-50  $\text{cm}^{-1}$  were observed for alkenes adsorbed onto silver surfaces which suggests that the chemical interactions were stronger at the gold substrate [126]. For chemical interactions that involve surface-induced resonance mechanisms or charge-transfer mechanisms, the intensities of the modes are dependent upon the orientation of the transition dipole moment in the surface complex [127,128].

The orientation of a molecule that undergoes EM enhancement can be determined from surface selection rules as presented in detail by Creighton [129], and Moskovits and Suh [130]. Evidence has shown preferential enhancement for those modes that are perpendicular to the surface. These vibrational bands are amplified because the highest local field exists in the direction normal to the surface [133,134]. Hence, information can be obtained regarding the orientation of an adsorbate by monitoring the changes in the relative intensities of the bands in the surface spectrum with respect to those exhibited in the solution spectrum.

As reflected by the SERS/SERRS results, the orientation of certain molecules is affected by the applied potential

and/or the adsorbate concentration [131,132,133]. An example of this behavior was shown in the SERS of  $\text{Ru}(\text{pyridine})_6(\text{BF}_4)_2$  at a silver electrode. The spectra exhibited changes in the relative intensities of the pyridyl ligand vibrations bands as a function of potential [134]. Based on the results, the authors proposed that the  $\text{Ru}(\text{pyridine})_6(\text{BF}_4)_2$  assumed a different orientation with applied potential which changed the symmetry of the surface complex. Moskovits et al. [131] studied the effects of surface coverage on the spectra of aromatic compounds at vacuum-deposited silver films. Spectral changes that were observed included differences in relative intensities, shifts in frequencies, and the appearance of Raman forbidden bands. The variations displayed in the SERS spectra with surface coverage were attributed to molecular reorientations at the surface. Moreover, the presence of the large electric field near the sharp surface particles modified the polarizabilities of the normally inactive modes such that these bands were present in the SERS spectra.

An additional feature that is observed the SERS/SERRS spectra is the strong depolarization of all the adsorbate modes. Vibrational bands that are normally polarized for the molecule in solution are depolarized at the surface because of multiple scattering effects caused by the roughened metal substrate.

**PAPER I APPLICATION OF SURFACE-ENHANCED RESONANCE RAMAN  
SCATTERING SPECTROSCOPY TO HEME-CONTAINING PROTEINS**

**ABSTRACT**

Surface-enhanced resonance Raman scattering (SERRS) studies of cytochrome P-450<sub>b</sub>, myoglobin, and cytochrome c have demonstrated that the native structure of heme-containing proteins can be retained at SERRS-active substrates. However, certain adsorption parameters must be maintained in order to preserve the native state of the adsorbed species. Our work shows that the optimal adsorption conditions depend upon the nature of the protein. Spectra relevant to unperturbed cyt P-450<sub>b</sub> were obtained only when SERRS-active electrodes were subjected to liquid nitrogen temperatures. Under these same conditions, the band frequencies of myoglobin indicated that the heme environment was indeed perturbed. The native state of the protein was retained only when myoglobin was adsorbed onto citrate-reduced sols or onto an electrode roughened in the presence of citrate. In contrast, cyt c is stable at different SERRS-active substrates, including electrochemically-roughened silver electrodes, silver-island films, and citrate-reduced silver sols. In order to retain the native integrity of cyt c, the adsorption conditions at the SERRS-active substrates must also be established. The results support the enormous potential of SERRS as a

biocompatible probe for the investigation of complex biological molecules.

## INTRODUCTION

Heme-containing proteins are important biomolecules that are involved in a variety of biological functions. Such processes include electron transfer along the respiratory chain, oxygen transport, and the metabolism of toxic materials [1-3]. Because these proteins are involved in many different reactions, an all-encompassing method for their investigation is essential.

Resonance Raman scattering (RRS) spectroscopy has become a powerful technique for studying biochemical systems. This method is particularly useful for examining proteins containing a chromophore site. When the frequency of the excitation line coincides with an absorption transition, the electronic and vibrational structure of the biologically-active site is selectively enhanced [4]. The vibrational bands of the surrounding protein matrix are observed only when ultraviolet (UV) resonance Raman scattering spectroscopy is employed. Hence, RRS can be used to study the structure as well as the function of the biomolecule. Alterations in the protein matrix and the amino acid residues surrounding the chromophore group can be monitored if these changes are transmitted to the heme. If the interactions affect the spectroscopic properties of the heme, RRS can be used to probe the relationship between the

heme and the protein matrix.

Cotton et al. [5] were the first to study cyt c and myoglobin with surface-enhanced resonance Raman scattering (SERRS) spectroscopy. Since these initial investigations, (SERRS) has been applied to a variety of biological systems containing heme groups [6-24]. Compared to conventional Raman or RRS techniques, SERRS provides several advantages for studying protein biomolecules. First, the enormous sensitivity of the SERRS effect enables examination of protein concentrations that are equivalent to or lower than those found in the membrane systems. Second, fluorescence is quenched when the heme-containing protein is adsorbed at a metal surface [13,14]. Third, the SERRS-active substrate can be used to simulate a membrane directly or by coating the substrate with a lipid layer. Fourth, the redox properties of the protein can be monitored at an electrode/electrolyte interface.

Although the biologically-active site is separated from the surface by the protein matrix, the vibrational modes associated with the chromophore are selectively enhanced. However, alteration of the protein structure may occur upon adsorption onto a SERRS-active substrate. The observed spectra are not useful if the data represent a perturbed heme environment. Therefore, one aspect of our research has focused on developing procedures for the application of

SERRS to heme-containing proteins. Specifically, we are concerned with retaining the native structure of the protein at SERRS-active substrates, including silver electrodes, silver-island films, and citrate-reduced silver sols. Three types of heme-containing proteins with different biochemical functions were studied at SERRS-active substrates. These biomolecules include cytochrome P-450<sub>b</sub> (cyt P-450<sub>b</sub>), and myoglobin, cytochrome c (cyt c). Our studies show that for a particular heme-containing protein, the native state of the protein at SERRS-active substrates is preserved by proper choice of adsorption parameters.

The biologically-active site of heme-containing proteins is a highly conjugated protoporphyrin IX macrocycle which is complexed to an iron atom. The delocalized  $\pi$  system is characterized by a strong B (Soret) absorption band in the high-energy violet region and two less intense Q bands in the red region of the spectrum. The central iron atom is in an octahedral coordination with the nitrogen atoms of the pyrrole groups serving as equatorial ligands. The axial ligands depend upon the type of heme-containing protein. In all cases, the iron is coordinated to at least one amino acid residue from the surrounding protein matrix. Extensive normal coordinate calculations determined with model compounds have assigned the RRS modes arising from excitation in the Q bands and the Soret band [25,26]. Based

upon these investigations, certain bands display greater sensitivity to the oxidation, spin, and ligation state of the chromophore. The  $\nu_4$  mode resulting from C-N vibrational stretch is assigned as the oxidation-state marker. Upon reduction of the iron atom, the C-N bonds weaken due to increased back-donation of electrons into the antibonding orbitals of the porphyrin. As a result, the  $\nu_4$  band shifts from approximately  $1370\text{ cm}^{-1}$  to  $1360\text{ cm}^{-1}$ . Vibrational bands arising from C-C stretches,  $\nu_{10}$ ,  $\nu_{19}$ ,  $\nu_3$ , are sensitive to the spin and ligation states. These modes downshift in frequency when the ligation state of the heme changes from a low-spin (LS) to a high-spin (HS) conformation. The radius of the iron is larger in the HS state which thereby weakens the C-C bonds of the expanded macrocycle. Six-coordinated HS species also produce greater shifts in frequency compared to five-coordinated HS states. To determine if the native state of the protein at a SERRS-active substrate was retained the modes discussed above were monitored in the RRS and SERRS studies discussed herein.

**EXPERIMENTAL****Materials and Instrumentation****Sample Preparation and Materials**

Cyt P-450<sub>b</sub> was isolated from the liver microsomes of phenobarbital pretreated Sprague-Dawley male rats according to the literature procedure [27,28]. The protein was purified from the microsomes by the method of Waxman and Walsh [29]. The samples were buffered to pH 7.4 with 50 mM potassium phosphate buffer and contained 20% v/v glycerol. Reduction of the enzyme was accomplished by slowly bubbling carbon monoxide through the solution and by adding a small quantity of sodium dithionite. Type I and Type II substrate binding was achieved by adding benzphetamine and metyrapone to the protein solution.

Cyt c, type VI, (Sigma) was purified by passing the sample through an ion-exchange column. In some of the experiments, the protein was used as received. The protein was buffered to pH 7.0 with 50 mM or 85 mM potassium phosphate buffer. Myoglobin (Sigma) was used as received and was buffered to pH 7.0 with 85 mM potassium phosphate buffer.

Silver nitrate (Aldrich) and citric acid (Sigma) were used as received for the preparation of silver sols.

The silver used in the metal vapor deposition and for the construction of the electrodes was 99.99% pure (AESAR).

### Instrumentation

Raman data were collected by means of the instrumental arrangement diagramed in Figure 1. Raman spectra were acquired with excitation lines from an Ar<sup>+</sup> laser (INNOVA 90-5, Coherent Inc.) and from a Kr<sup>+</sup> laser (INNOVA 100-K3, Coherent Inc.). Removal of plasma lines from the laser emission was accomplished by passing the beam through a premonochromator (Anaspec 300-S). Because the premonochromator reduces the power by approximately 30%, the laser power was monitored after the beam exited through the premonochromator. The power was measured with a conventional power meter (Coherent Model 2109) and values were recorded frequently throughout the Raman experiments.

The samples were mounted on a holder placed on an X-Y-Z micropositioner, and the beam was directed onto the samples at an angle of approximately 60°. The scattered radiation from the irradiated samples was collected in a back-scattering configuration. A two lenses collection system, which consisted of a fused silica collection lens (Oriel Model 6236) and a focusing lens (Oriel Model 6236), directed the scattered radiation onto the entrance slit. The focused light was dispersed by a monochromator/spectrograph (Spex

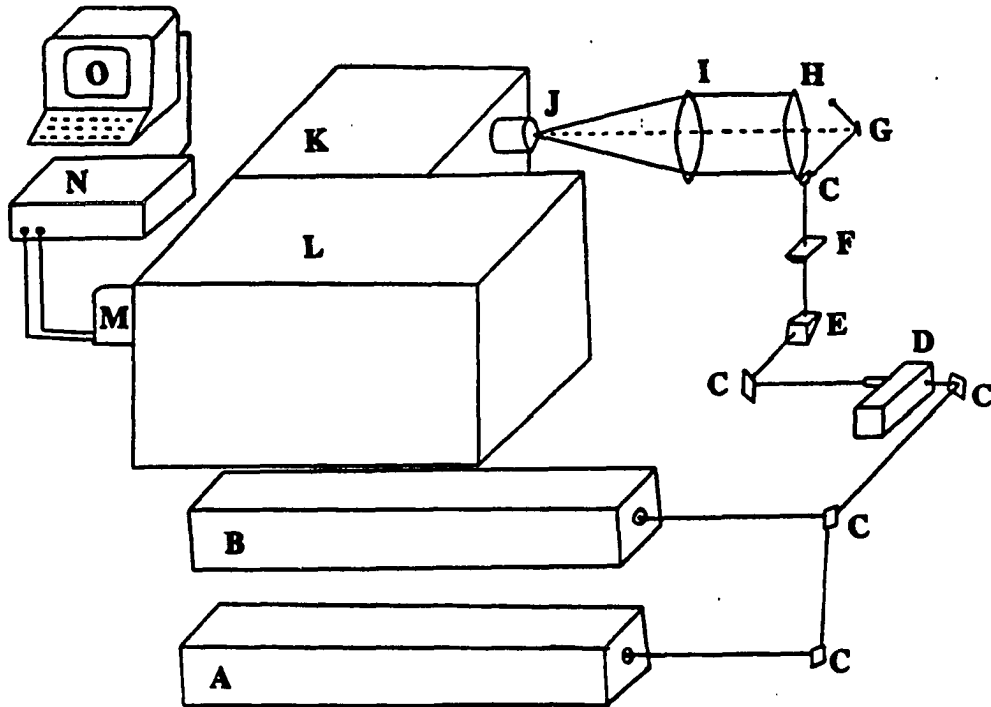


Figure 1. Diagram of Raman Instrumentation: A) Ar<sup>+</sup> laser; B) Kr<sup>+</sup> laser; C) mirrors; D) premonochromator; E) prism; F) cylindrical lens; G) sample holder; H) collecting lens; I) focusing lens; J) entrance slit; K) monochromator stage; L) spectrograph stage; M) diode-array detector; N) detector controller; O) operating system and computer.

Triplemate Model 1877). The monochromator stage has two 600 grooves/mm gratings. The gratings used in the spectrograph stage were 1800 grooves/mm ( $D^{-1} = 0.93$  nm/mm) or 1200 grooves/mm ( $D^{-1} = 1.4$  nm/mm). The Raman signals were detected and processed with an intensified silicon diode-array detector (Princeton Applied Research, model 1420) interfaced to a multichannel analyzer (Princeton Applied Research OMA II). Indene was used to calibrate the RRS and SERRS frequencies.

Deposition of silver films onto glass slides was performed with a commercial vacuum system (Edwards High Vacuum, Model E306A). The average mass thickness of deposited metal and the metal deposition rate was monitored with a film thickness monitor (Edwards High Vacuum, model FTM4) equipped with a quartz piezoelectric crystal oscillator. A potentiostat constructed in our laboratory was used to roughen the electrodes and a standard calomel electrode (SSCE) served as the reference.

Absorption measurements were acquired with a Hewlett Packard single beam UV-Vis spectrometer.

## Experimental Procedures

### Preparation of SERRS-Active Substrates

Silver-Island Films. Silver-island films were commonly incorporated as the SERRS-active substrates in our studies. The films were prepared by vacuum depositing silver vapor onto clean glass microscope slides. Prior to deposition, the microscope slides were cleaned according to the following steps. The slides were cut into smaller pieces of approximately 2 cm x 1 cm. The slides were positioned upright in a Teflon holder which was placed in a beaker. Surface contamination was removed from the glass slides by soaking the substrates in a 3 M KOH/methanol solution for a minimum of 1 hr. For additional cleaning, the slides were sonicated and rinsed in distilled or deionized water. Slides that were not used immediately were stored in deionized water. The substrates were rinsed a final time with fresh deionized water and were dried in a oven for a minimum of 20 min. The slides were placed on the sample holder in the deposition instrument and the work chamber was evacuated. At a base pressure of approximately  $<3.0 \times 10^{-6}$  Torr, the metal was heated by passing a current through the DC boat source. The average metal mass thickness and the evaporation rate were 50 Å and 0.1 Å/sec, respectively.

Electrochemically-Roughened Electrodes. Electrochemically-roughened silver electrodes were also employed extensively in these investigations. This SERRS-active substrate was constructed by sealing flattened polycrystalline silver wire into glass tubing. Similar to the silver-island films, the electrodes were subjected to a cleaning procedure prior to the roughening process. The cleaning routine included a three-step polishing sequence. The first step consisted of polishing the electrode on a polishing wheel with 5.0  $\mu\text{m}$  alumina/water slurry. The electrode was then polished using polishing clothes with successively finer alumina/water slurries, i.e., 0.30  $\mu\text{m}$  and 0.05  $\mu\text{m}$ . To remove excess alumina from the metal surface, the electrode was rinsed and sonicated with distilled water after each polishing step. Adsorbed organic compounds and surface oxides were removed from the surface by holding a potential at approximately -2.2 V for 30 sec.

The electrode was roughened by subjecting the silver surface to an oxidation-reduction cycle (ORC). In most cases, a solution of 0.1 M  $\text{Na}_2\text{SO}_4$  that had been purged with  $\text{N}_2$  served as the electrolyte. The ORC was initiated by stepping the potential from -600 mV to +450 mV (vs sodium saturated calomel electrode, SSCE) during which a total charge of 25  $\text{mC}/\text{cm}^2$  was passed in the oxidation step. The voltage was then returned back to -600 mV until a reduction

current of less than 10  $\mu$ amps was achieved. Reproducible surface roughness was insured by means of the integrator/comparative circuit of the potentiostat which controlled the potential changes.

Silver sols. Silver sols were prepared by the procedure developed by Lee and Meisel [30] and Rospendowski [31]. A silver nitrate solution was prepared by dissolving 90 mg of the solute in 500 ml of distilled water. After the solution was heated to the boiling point, 1% sodium citrate was added to the silver nitrate solution. The solution was heated for an additional hr with continuous stirring. The unaggregated silver sol was characterized by an extinction maximum of 406 nm.

#### Sample Adsorption

The protein samples were stored at temperatures ranging from -95 to 0 C. The frozen samples were thawed in an ice bath and maintained at this temperature unless otherwise noted. Prior to adsorption of the samples, the island-films and/or electrodes were cooled to the temperature of the protein solution by placing the substrates in an appropriate solvent cooled to 0 C for approximately 5 min.

In most cases, samples were adsorbed onto the SERRS-active substrates by a dipping technique. For the silver-island films, sample adsorption was accomplished by

submerging the substrates into a solution of the desired adsorbate. The films were exposed to the solution for approximately 15 min. The silver film was transferred to a dewar filled with nitrogen before the protein dried on the surface. In addition, samples were adsorbed onto an electrochemically-roughened electrode by inserting the substrate into the adsorbate solution for approximately 15 min. To prevent drying of the surface, the electrode was immediately transferred to a low-temperature dewar or a SERRS spectroelectrochemical cell.

Silver sols. The proteins were adsorbed onto silver sols by adding the anylyte directly to the dispersion. The proportion of protein to sol ratio was 1:30.

#### Optical Arrangement for Raman Spectroscopy

The SERRS spectra were collected by various methods. The procedures depended upon several variables, including the type of substrate used and the nature of the experiment to be conducted, i.e., potential studies, low-temperature studies, etc. A feature common to all of the described methods is that the scattered radiation from the samples was collected in a backscattering geometry. The spectra were measured with various integration times and the signals were accumulated by multiple scans. The background dark current was subtracted automatically from the spectra by the

software resident in the OMA II. In some cases, correction of the diode gain was necessary when a weak Raman spectrum was superimposed on a high background. The background was eliminated from the spectra by using a third-degree polynomial. The polynomial background fit was produced by selecting points that represented the background and the polynomial calculation was then performed by the OMA II software.

Silver-Island Films. The glass slide coated with the metal film was placed on the Raman sample holder. The laser beam was directed at the metal surface at an angle of approximately  $60^\circ$  and the slide was positioned at the focal point of the collection lens.

Electrochemical Studies. Roughened silver electrodes were used for the SERRS experiments involving potential dependent measurements. As shown in Figure 2, the SERRS-active electrode/adsorbate system was inserted into a electrochemical cell which was filled with an  $N_2$  purged electrolyte solution. The flattened silver surface was positioned at the front window and the SERRS cell was placed on the sample holder. The laser beam was directed through the glass onto the roughened surface and by adjusting the X-Y-Z micropositioner of the collection lens, the scattered light was directed onto the entrance slit. Potentials were monitored with the same potentiostat used for the ORC

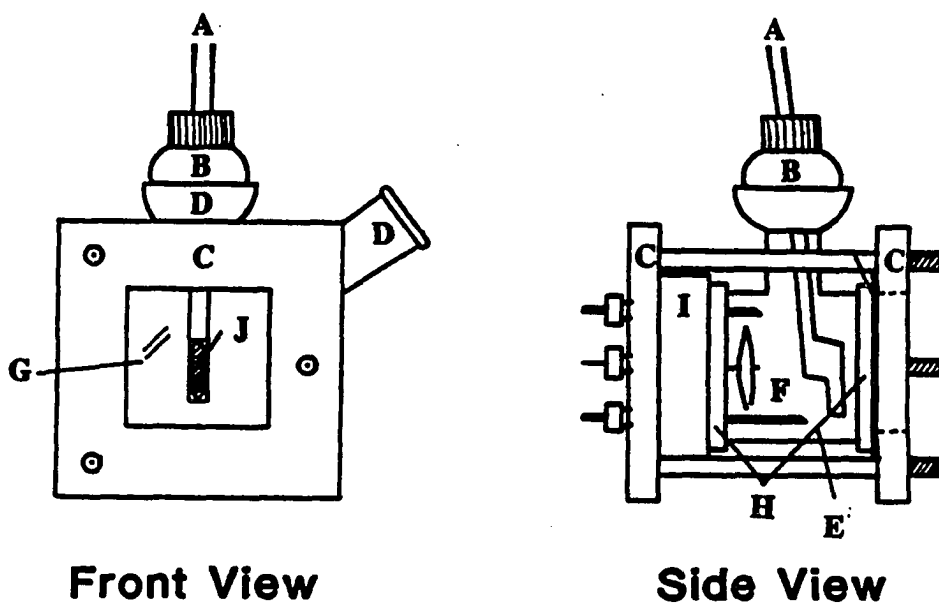


**Figure 2.** Diagram of SERRS electrochemical cell: A) SERRS electrode submerged in cell; B) thermometer clamp; C) cell clamp assembly; D) cell body openings; E) nitrogen blanket inlet; F) platinum auxiliary electrode; G) front window of glass; H) O-rings; I) rear plate; J) SERRS electrode surface.

roughening procedure. The potential was applied to the electrode and the SERRS spectrum was recorded. After the spectrum was collected at a specific potential, the laser was moved to another area on the substrate for the next potential step. Degradation of the adsorbate was minimized by this procedure. A sodium saturated calomel electrode (SSCE) was used to record the potentials and a platinum wire served as the auxiliary electrode.

Silver sols. The laser beam was directed at the sol/adsorbate sample which was positioned on the Raman sample holder. The scattered light was collected and focused onto the entrance slit of the monochromator.

Time Dependence Studies. SERRS studies performed as a function of laser irradiation time were conducted with electrodes and silver-island films. In both cases, the laser light was directed onto a defined area of the substrate. The sample/substrate system was irradiated for a specific time span. Raman spectra were acquired at various intervals during this period of time.

Low-Temperature Studies. Low-temperature SERRS experiments were performed at liquid nitrogen temperature, i.e., 77 K. After the sample was adsorbed onto a activated surface, excess solvent was removed from the surface of the electrode or silver-island film by gently blotting the substrate with a tissue. This step prevented ice from

forming on the surface. The substrate and adsorbate was immediately submerged into a Raman dewar flask filled with liquid nitrogen. The laser beam was focused onto the roughened surfaces and the Raman signals were collected through the dewar's transparent double glass wall. Figure 3A illustrates this arrangement with an electrode serving as the activated surface. High-quality spectra were obtained with this flask even in the presence of the bubbling liquid nitrogen.

The electrodes used in the low-temperature investigations were longer and thinner compared to the substrates employed in the electrochemical studies. The fabrication of the former SERRS-active surface is depicted in Figure 3B. Silver-island films were prepared as previously described.

#### Resonance Raman Scattering Experiments

Resonance Raman scattering investigations were conducted by placing the solution into a small test tube. The laser line was directed onto the samples and the tube was positioned at the focal length of the optics. Studies performed at temperatures below room temperature were accomplished with the Raman dewar flask. These experiments were typically carried out at temperatures ranging from 0-5 C. The RRS sample tube was inserted into the dewar filled

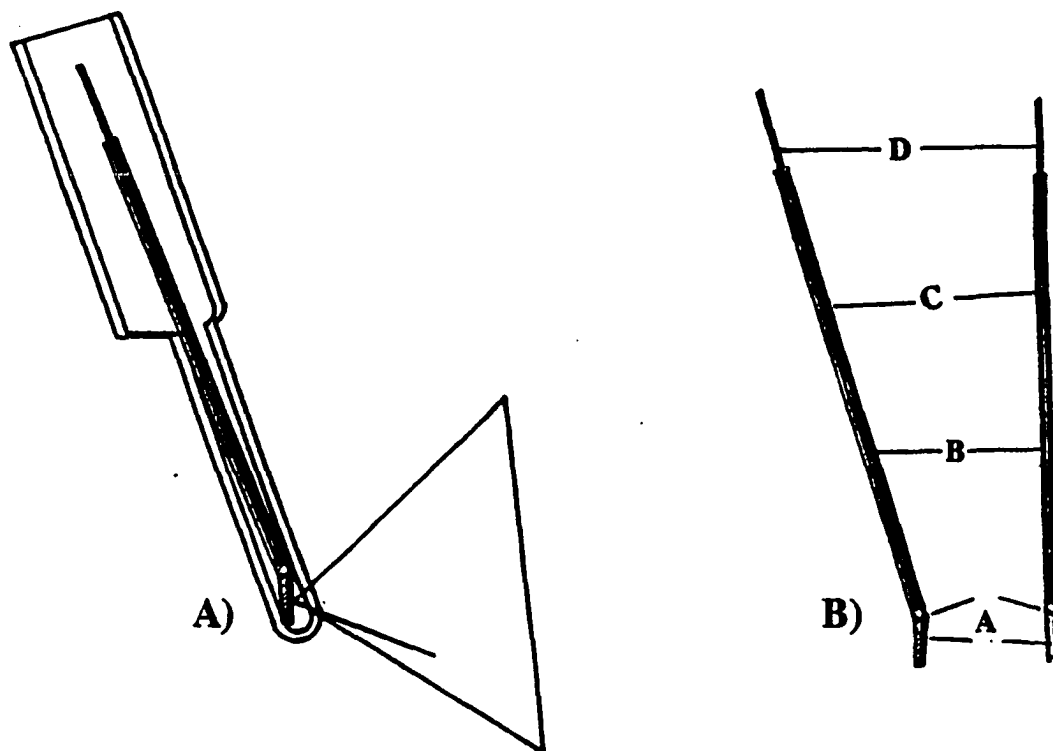


Figure 3. A) Low-temperature Raman dewar flask with electrode. The collection configuration of the scattered light is depicted. B) SERRS-active electrode construction: A - silver electrode surface; B - epoxy seal; C - glass tube body; D - copper wire connection to silver.

with ice water. The temperature of the surrounding media was checked periodically throughout the experiment.

**RESULTS AND DISCUSSION****RRS and SERRS Studies of Cytochrome P-450<sub>b</sub>**

Cytochromes P-450 (cyt P-450) are enzyme catalysts which function in the metabolism of drugs and foreign materials [32]. The proteins catalyze the oxidation of a large variety of exogenous and endogenous compounds through the transfer of oxygen atom into the substrate [32,33]. The mechanism involves a one-electron reduction of the heme when the substrate binds to the protein. The reduced protein binds molecular oxygen which regenerates the ferric state of the heme-containing protein. Cytochromes P-450 participate in various types of reactions, including hydroxylation reactions which oxidize C-H bonds, and the insertion of an oxygen at nitrogen and sulfur atoms [33,34]. The products produced in the latter reaction can be electrophilic in nature. The electrophilic compounds may interact with DNA resulting in mutations and cancer.

Cytochromes P-450 are a multigene family which, to some extent, explains their specificity to many various types of compounds. Some forms of the heme-containing protein catalyze the detoxification of environmental materials while other types activate the materials [32]. In spite of their diverse functions, these proteins are closely related in

structure. Cytochromes P-450 contain one heme surrounded by a single polypeptide chain resulting in a molecular weight of approximately 50,000. The heme is coordinated to a cysteine amino acid residue in the fifth coordinate position while the substrate and/or molecular oxygen occupies the sixth position during the catalytic reaction. Although information relating to the primary amino acid sequence of the proteins is increasing, it is still unclear as to how this sequence affects the interaction between the protein structure and its substrate. Hence, sensitive techniques are needed to provide information about the heme environment and heme-protein interactions. RRS and SERRS are powerful techniques to investigate these effects as demonstrated by several studies [20,34,35]. The present study examines the behavior of cyt P-450<sub>b</sub> adsorbed onto SERRS-active silver electrodes. Based on a comparison with RRS spectra, the native state of the heme environment and the activity of the enzyme can be preserved at the surface under controlled conditions.

A comparison of cyt P-450<sub>b</sub> in solution and at an electrochemically-roughened silver electrode is shown in Figure 4. Figure 4A depicts the RRS spectrum of a typical oxidized mixed spin-state species. The LS markers include the  $\nu_{19}$  mode at  $1582\text{ cm}^{-1}$  and the  $\nu_3$  at  $1501\text{ cm}^{-1}$ . The  $\nu_{19}$  at  $1565\text{ cm}^{-1}$  is also characteristic of a HS component.

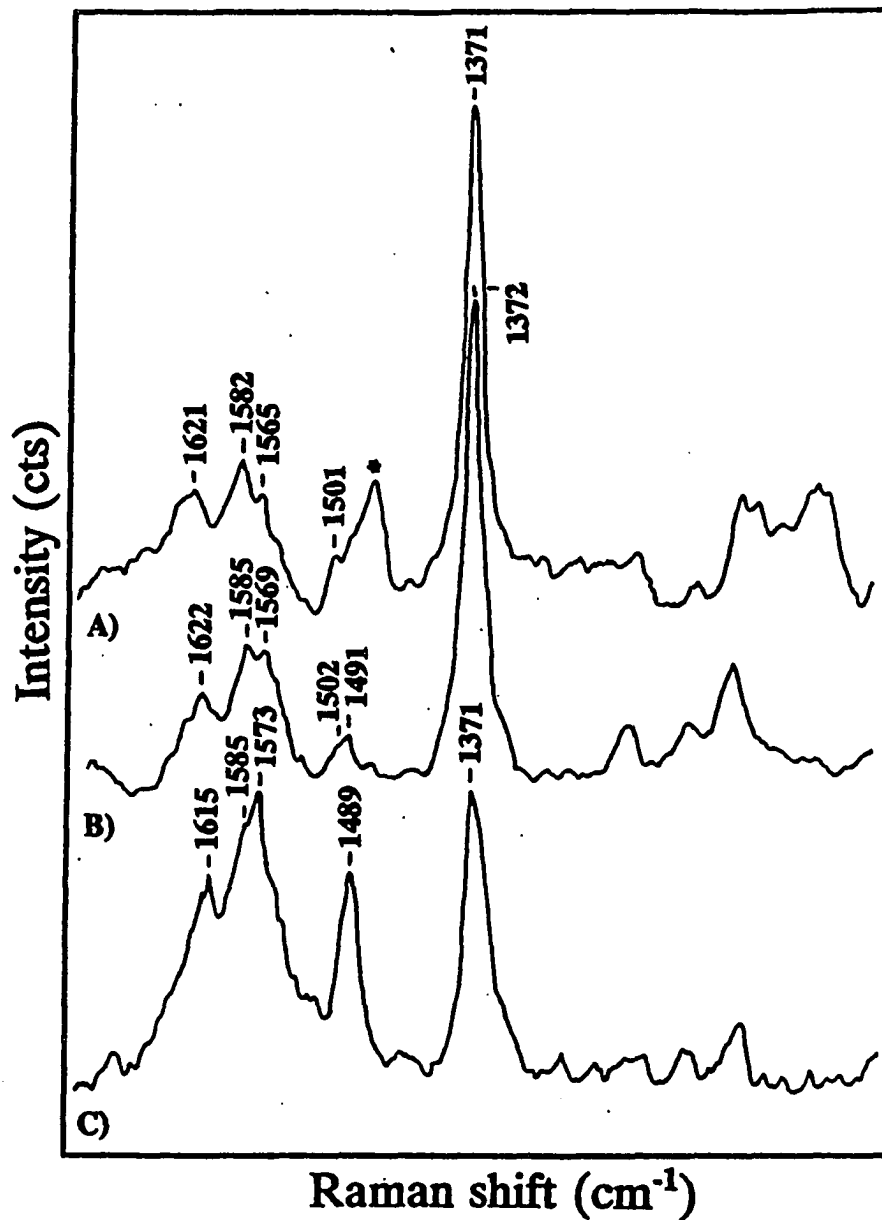


Figure 4. Spectra of cyt P-450: A) RRS; B) low-temperature SERRS; C) room-temperature SERRS. Experimental conditions: SERRS-active substrate, electrochemically-roughened electrode; excitation wavelength; 406.7 nm; integration time, 1 sec; scans, 25.

Because cytochromes P-450 are isolated from various sources and have different heme environments, the proteins can exist in low-spin, high-spin, or mixed-spin states [2,36].

Parallel absorption studies were performed to insure the RRS spectrum is relevant to the native cyt P-450<sub>b</sub> structure. The oxidized form of cyt P-450<sub>b</sub> has a Soret absorption maximum at 416 nm. When the solution is bubbled with carbon monoxide and reduced with sodium dithionite, the Soret band shifts to 450 nm. This behavior is similar to that of the native carbon monoxide adduct of reduced cyt P-450 induced by phenobarbital [37]. In contrast, the inactive protein displays a Soret absorption band at 420 nm. In addition, the RRS spectrum does not produce a vibrational mode at 398 cm<sup>-1</sup>. RRS studies of the protein have shown that this band is indicative of the inactive P-420 form [35].

Figure 4C shows the SERRS spectrum of the cyt P-450 at an electrochemically-roughened silver electrode under room-temperature conditions. Compared to the RRS spectrum of the protein, the SERRS spectrum is significantly different. In particular, the SERRS spectrum displays a greater contribution from the HS state markers at 1573 cm<sup>-1</sup> and 1489 cm<sup>-1</sup>. The SERRS frequencies compare to those in solution spectrum when the electrode is maintained at low-temperature conditions (77 K) as shown in Figure 4B. A HS marker at

1491  $\text{cm}^{-1}$  is evident in the low-temperature SERRS spectrum, but the corresponding RRS band is not observed. The glycerol solvent band (starred in Fig 4A) found in this region may be superimposed on the HS marker. The asymmetrical shape of the solvent peak suggests that the band is composed of more than one vibrational band.

Based upon the above results, the protein structure is perturbed at the SERRS-active substrate at room temperature whereas its native structure is preserved under low-temperature conditions. Structural alterations may be induced by unfolding of the protein matrix which in turn leads to the exposure of the heme to the silver surface. The shift of the 1622  $\text{cm}^{-1}$  band to 1615  $\text{cm}^{-1}$  shown in Figure 4C suggests that there may be interaction between the heme and the metal surface. This band is attributed to vibrational stretching of the vinyl substituent located on the periphery of the macrocycle. Previous SERRS studies of ferric protoporphyrin IX showed that the vinyl group downshifted 7  $\text{cm}^{-1}$  relative to the corresponding RRS [38,39]. Sanchez and Spiro [38] proposed that the vinyl group interacted with the silver surface because of the tendency of silver ions to bind to double bonds.

Protein perturbation at the electrode may reflect photodamage as a result of continued laser irradiation. By submerging the electrode/adsorbate system into liquid

nitrogen, the photodegradation effect is eliminated. The spectrum shown in Figure 4B is similar to that reported for cyt P-450 LM2 adsorbed onto a silver colloid suspension [35]. Although the silver sol was rotated continuously during the SERRS experiments, the protein sample was not cooled.

The RRS and the low-temperature SERRS spectra of substrate bound cyt P-450<sub>b</sub> with metyrapone are shown in Figure 5A and Figure 5B, respectively. A comparison of the Raman signals of the protein in the presence and in the absence of the substrate (Figure 4) shows that substrate binding produces an increase in the LS state. In both the RRS and SERRS spectra, the high spin state marker,  $\nu_2$  at 1562  $\text{cm}^{-1}$  decreases in intensity. The change in spin state was monitored with absorption spectroscopy as well. Figure 6A shows that the electronic difference spectrum of metyrapone-bound cyt P-450<sub>b</sub> displays a maximum at 420 nm. These results correspond to the LS state species which absorb in this region [40]. Figure 6B depicts the electronic difference spectrum of benzphetamine-bound cyt P-450<sub>b</sub>. In this case, the maximum is at 319 nm corresponding to absorption of the HS state conformation [40]. The SERRS spectrum (Figure 7) of the benzphetamine-bound cyt P-450<sub>b</sub> shows an increase in the intensity of the HS-state marker band,  $\nu_2$  at 1571  $\text{cm}^{-1}$ , relative to the  $\nu_2$  mode of the

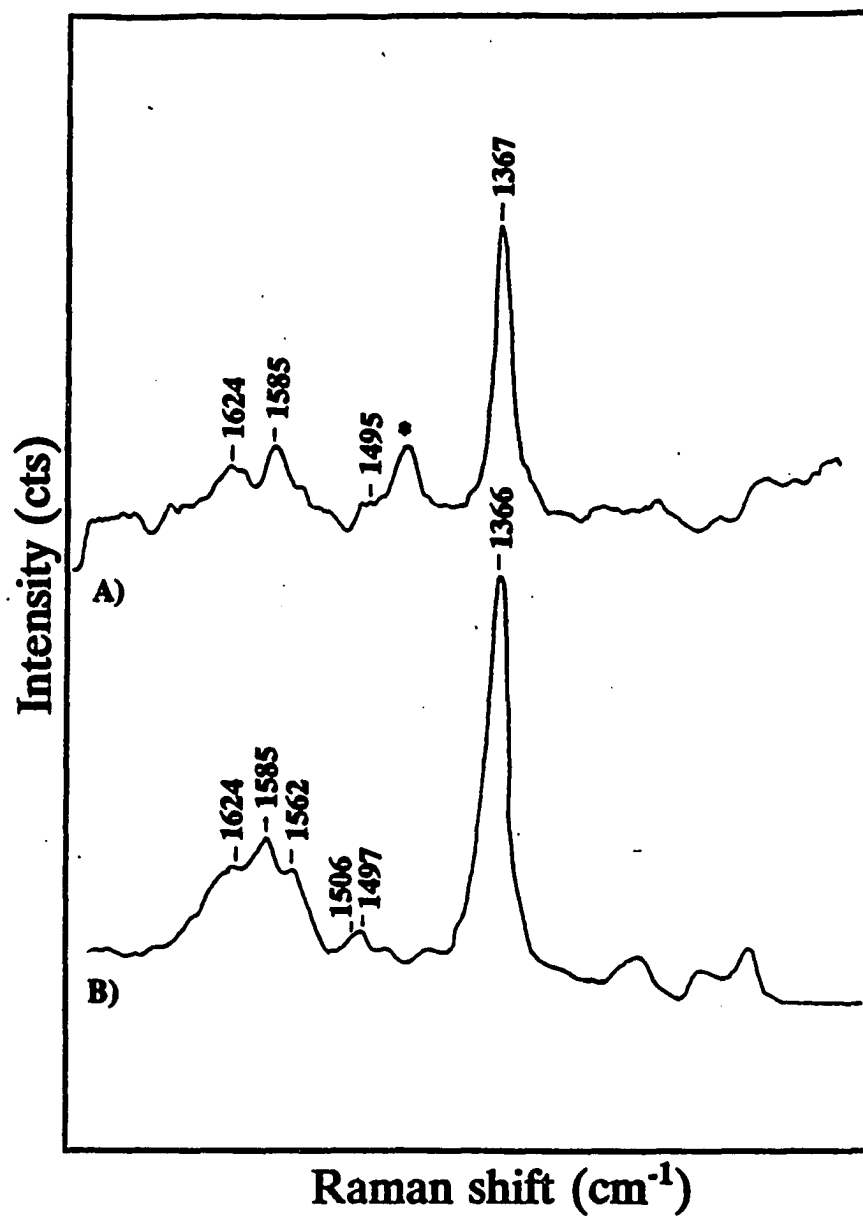


Figure 5. Spectra of substrate-bound cyt P-450<sub>b</sub> with metyrapone: A) RRS (\* indicates glycerol solvent band); B) low-temperature SERRS. Experimental conditions: SERRS-active substrate, electrochemically-roughened electrode; excitation wavelength, 406.7 nm; integration time, 1 sec; scans, 25.

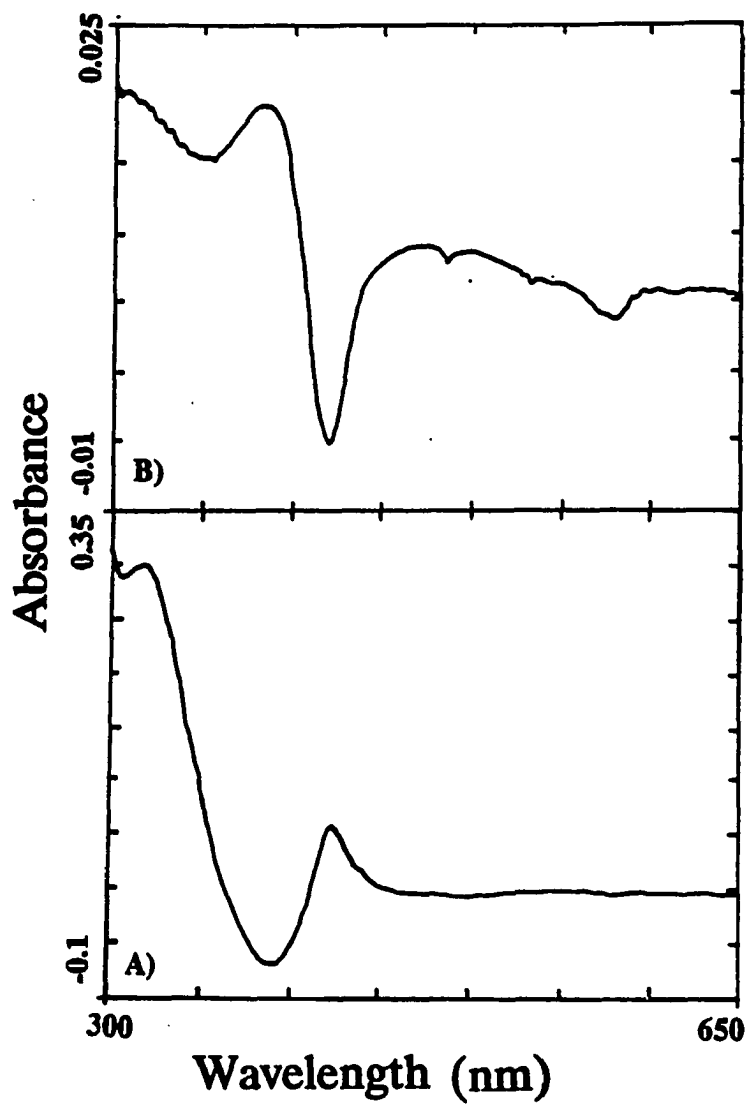
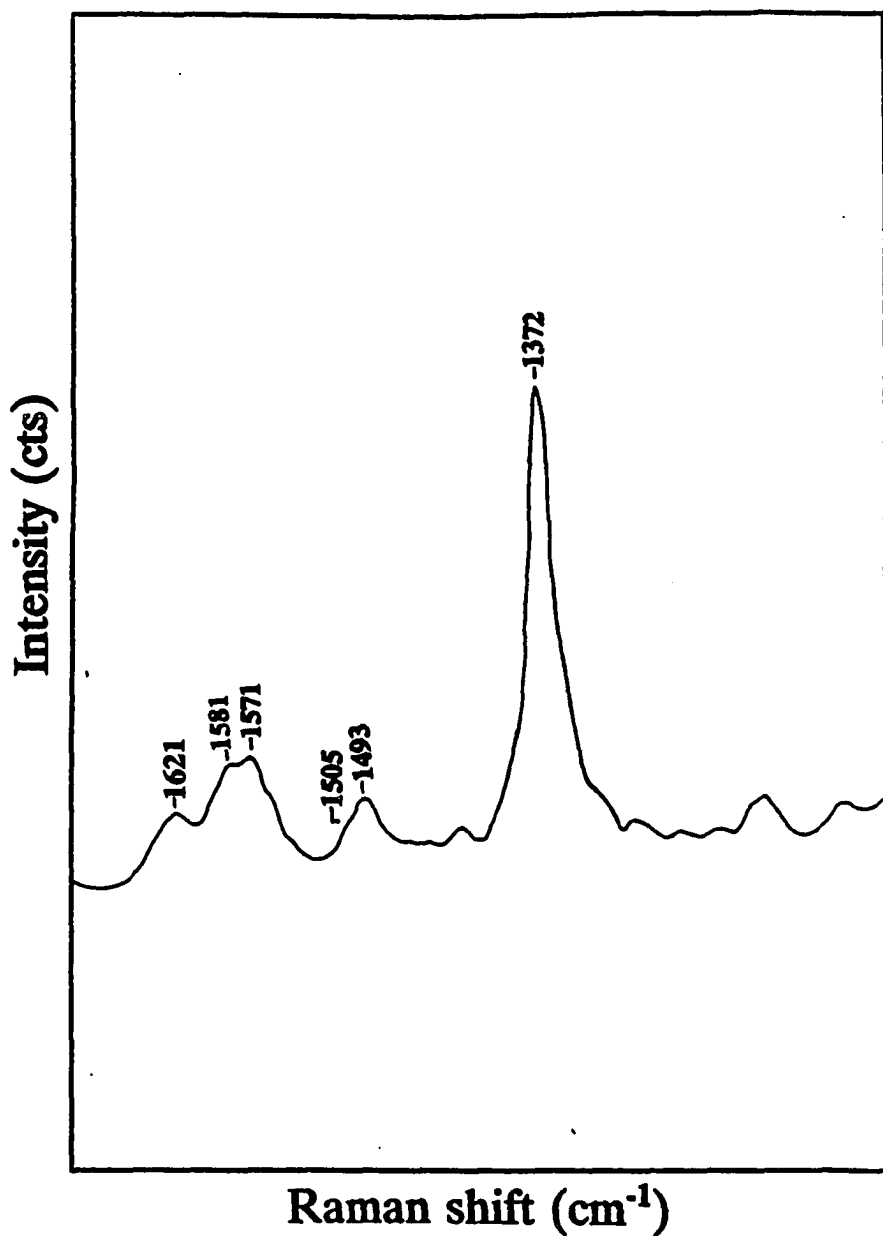


Figure 6. Electronic difference spectra: A) substrate-bound cyt P-450<sub>b</sub> with metyrapone; B) substrate-bound cyt P-450<sub>b</sub> with benzphetamine.



**Figure 7.** Low-temperature SERRS spectrum of substrate-bound cyt P-450, with benzphetamine. Experimental conditions: SERRS-active substrate, electrochemically-roughened electrode; excitation wavelength, 406.7 nm; integration time, 1 sec; scans, 25.

unbound SERRS spectrum (Figure 4B).

Our work agrees with absorption studies previously reported for substrate-bound cyt P-450<sub>b</sub> [2]. Two types of spectral changes occur upon substrate binding, i.e., type I and type II. Type I substrate binding results in reduction in the Soret band at 420 nm and an increase in the 390 nm absorption region. The spectral change produced by type II binding consists of a shift of the Soret band to a lower frequency. Based upon their electronic properties, benzphetamine and metyrapone have been categorized as type I and type II binding substrates, respectively [2]. Type I substrates are believed to bind to the protein through hydrophobic or electrostatic interactions resulting in a conversion from a LS state to a HS state. On the other hand, type II binding substrates ligate to the heme macrocycle. This ligation may be reflected in the RRS and SERRS spectra of metyrapone-bound cyt P-450<sub>b</sub>. In the spectra of the unbound protein (Figure 4) the oxidation-state marker is present at 1372 cm<sup>-1</sup>; however, this band shifts down to 1366 cm<sup>-1</sup> upon substrate binding (Figure 5). Studies have indicated that the  $\nu_4$  band is sensitive to the axial ligation of the heme [34,40]. The ligands can induce  $\pi$ -back donation from the ligand to the porphyrin or  $\pi$ -forward donation from the porphyrin to the ligand. The C-N stretching vibrations which give rise to the Raman

oxidation-state marker are sensitive to the  $\pi$ -donations. The spectra of the metyrapone-bound protein indicate that upon substrate binding, a  $\pi$ -back donation occurs between the ligand to the  $\pi^*$  orbitals of the heme macrocycle. The C-N bond is weakened which results in a downshift of the  $\nu_4$  frequency. The effective substrate binding as shown by our Raman studies further suggest that the native structure and the biological function of cyt P-450<sub>b</sub> is preserved in the adsorbed state.

#### RRS and SERRS Studies of Myoglobin

Myoglobin is a heme-containing molecule found in muscle tissues. The role of myoglobin is to store oxygen until it is needed for metabolic oxidation [41]. Detailed studies of the atomic structure of this globular protein have been conducted with with X-ray diffraction crystallography [42,43]. The heme is surrounded by a single polypeptide chain composed of eight  $\alpha$  helix sections. The helices form a pocket for the heme. Thus, the chromophore is completely buried within the matrix with the exception of one exposed edge. Histadine serves as the fifth octahedral ligand whereas an oxygen molecule occupies the sixth position. For metmyoglobin, the ferric species which does not bind to oxygen, a water molecule occupies the sixth ligand site.

The heme group is not covalently bound to the protein matrix, and therefore, is easily removed from the protein.

The first SERRS spectrum of myoglobin was obtained by Cotton et al. [5]. The authors showed that the protein heme environment was perturbed at a SERRS-active electrode. For this reason, myoglobin has not been investigated extensively by SERRS. The present work demonstrates, however, that the protein behaves differently at various SERRS-active substrates. Similar to cytochrome P-450<sub>b</sub>, the native structure of myoglobin can be retained by utilizing the appropriate adsorption conditions.

Figure 8 shows spectra of myoglobin obtained in solution (A), at an electrochemically-roughened electrode (B), and at a citrate-reduced silver sol (C). The RRS frequency bands shown in Figure 8A are similar to those of myoglobin bound to H<sub>2</sub>O as reported by Kitagawa et al. [40]. The spectrum of myoglobin in solution indicates that the heme is in an oxidized 6-coordinate HS state ( $\nu_3$  at 1483 cm<sup>-1</sup>,  $\nu_2$  at 1564 cm<sup>-1</sup> and the  $\nu_4$  at 1372 cm<sup>-1</sup>). Compared to the RRS results, the SERRS spectrum of myoglobin at an electrochemically-roughened electrode changes significantly as depicted in Figure 8B. In particular, the  $\nu_3$  band shifts down to 1472 cm<sup>-1</sup> and shoulders are present on the  $\nu_2$  band at 1576 cm<sup>-1</sup> and on the  $\nu_4$  band at 1355 cm<sup>-1</sup>. The presence of the shoulder on the oxidation state marker ( $\nu_4$ ) indicates

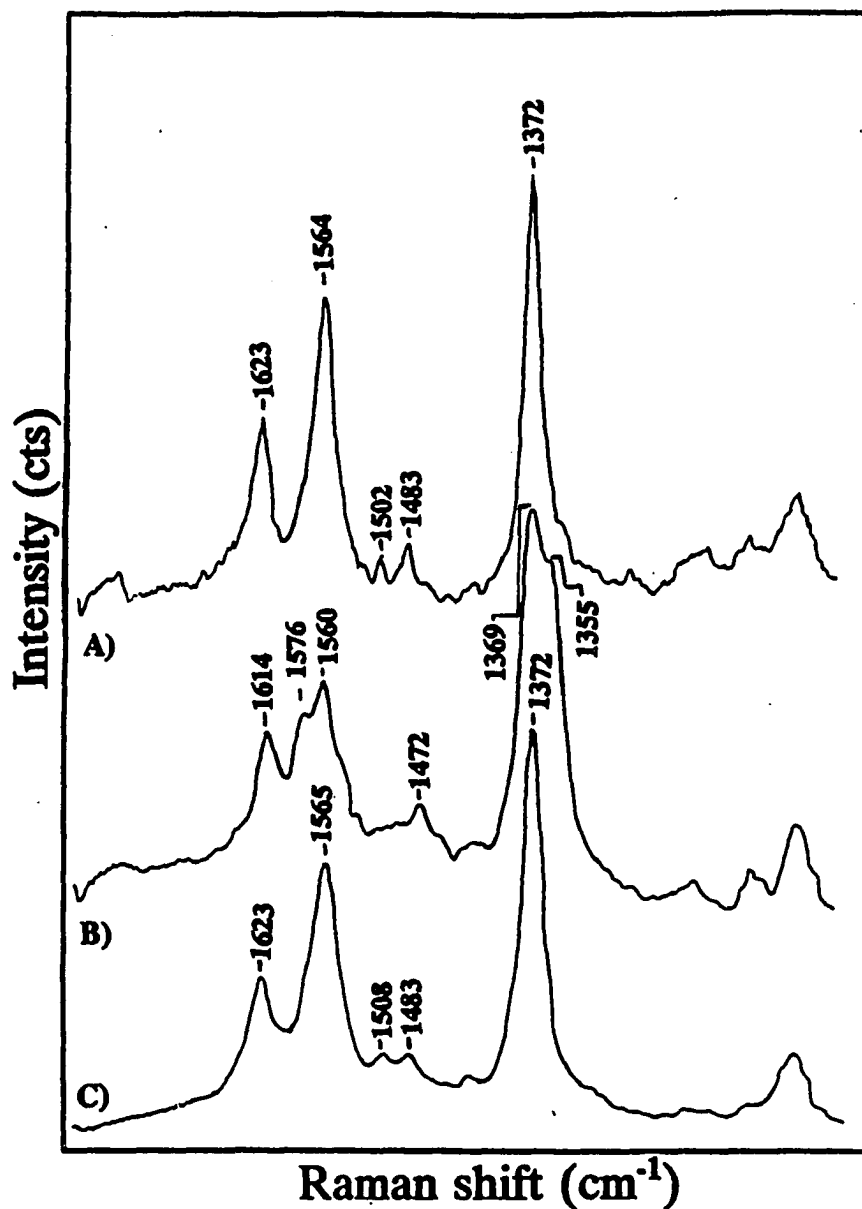
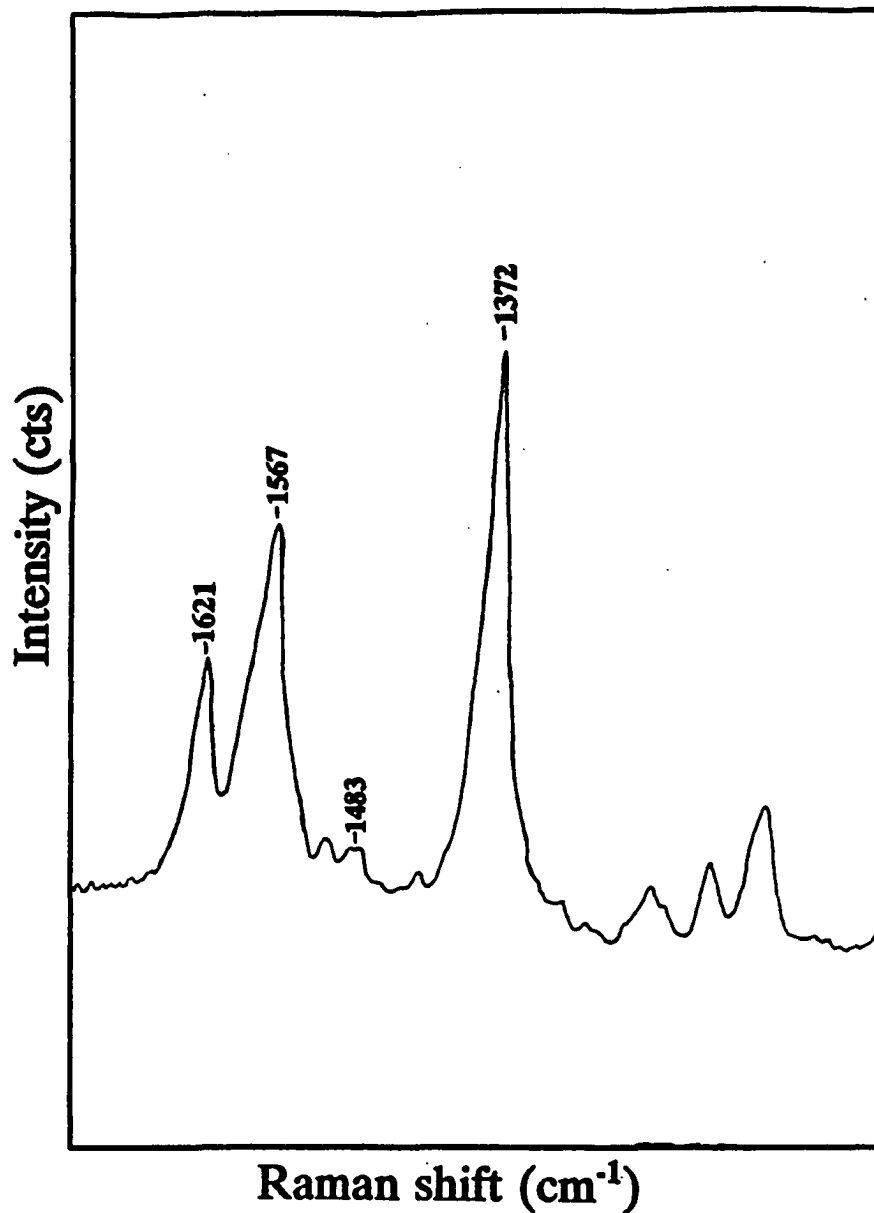


Figure 8. Spectra of myoglobin: A) RRS; B) low-temperature SERRS (electrochemically-roughened electrode); C) room-temperature SERRS (citrate-reduced sols). Experimental conditions: excitation wavelength, 413.1 nm; integration time, 1 sec; scans, 25.

reduction of the protein. Photoreduction of myoglobin mutants has been observed when the sixth ligand is lost [44]. In addition, deoxymyoglobin RRS spectra produce comparable band frequencies to those depicted in Figure 8B [40]. The results suggest that the protein loses its water ligand and is subsequently photoreduced at the activated electrode surface. Hence, the native structure of myoglobin is not retained at an electrode substrate, under low-temperature conditions, i.e., 77 K.

The loss of the sixth ligand may be caused by electrostatic interactions between the electrode and the protein. Separation of the protein from the surface may reduce changes in the ligand coordination and thus prevent photoreduction. Figure 8C shows the spectrum of myoglobin at a citrate-reduced silver sol. The SERRS band frequencies are similar to those displayed in the RRS spectrum. The citrate ion may be separating the protein from the silver surface so that the electrostatic effect is minimized. Therefore, a SERRS spectrum characteristic of the native structure of myoglobin is obtained. Further support of the stabilizing effect of the citrate ion was obtained by roughening an electrode in the presence of citrate as shown in Figure 9. A comparison of the RRS spectrum (Figure 8A) and the SERRS spectrum (Figure 9) show similar band frequencies.



**Figure 9.** Low-temperature SERRS spectrum of myoglobin at a silver electrode roughened in the presence of citrate. Experimental conditions: excitation wavelength, 413.1 nm; integration time, 1 sec; scans, 25.

It is also necessary to control the adsorption conditions at a citrate-reduced silver sol in order to preserve the native structure of myoglobin. The concentration of the adsorbing protein solution must be considered when silver sols are used as the SERRS-active substrate. Figure 10 shows spectra of myoglobin obtained at adsorbing solution concentrations of  $10^{-7}$  M (A),  $10^{-8}$  M (B), and  $10^{-9}$  M (C). Figure 10A indicates that the native structure of the protein is retained at adsorbing solution concentrations of  $10^{-7}$  M. However, Figure 10B depicts changes in the spin-state of the adsorbed myoglobin with respect to the corresponding RRS spectrum (Figure 8A). In particular, a shoulder is observed on the  $\nu_2$  band at  $1583\text{ cm}^{-1}$  and the  $\nu_3$  band is broader and shifts to a higher frequency. Figure 10C illustrates a similar spin-state conversion as shown in Figure 10B. The results suggest that the heme environment is perturbed when very low adsorbing concentrations of the protein are used. Rospendowski noted that the structure of cyt c is altered with decreasing adsorbing solution concentrations [31]. This effect can be attributed to an electrostatic interaction of the protein with the surface. With decreasing concentrations, the protein is exposed to a larger area of the silver surface. The interaction between the silver surface and the protein may result in perturbation of the

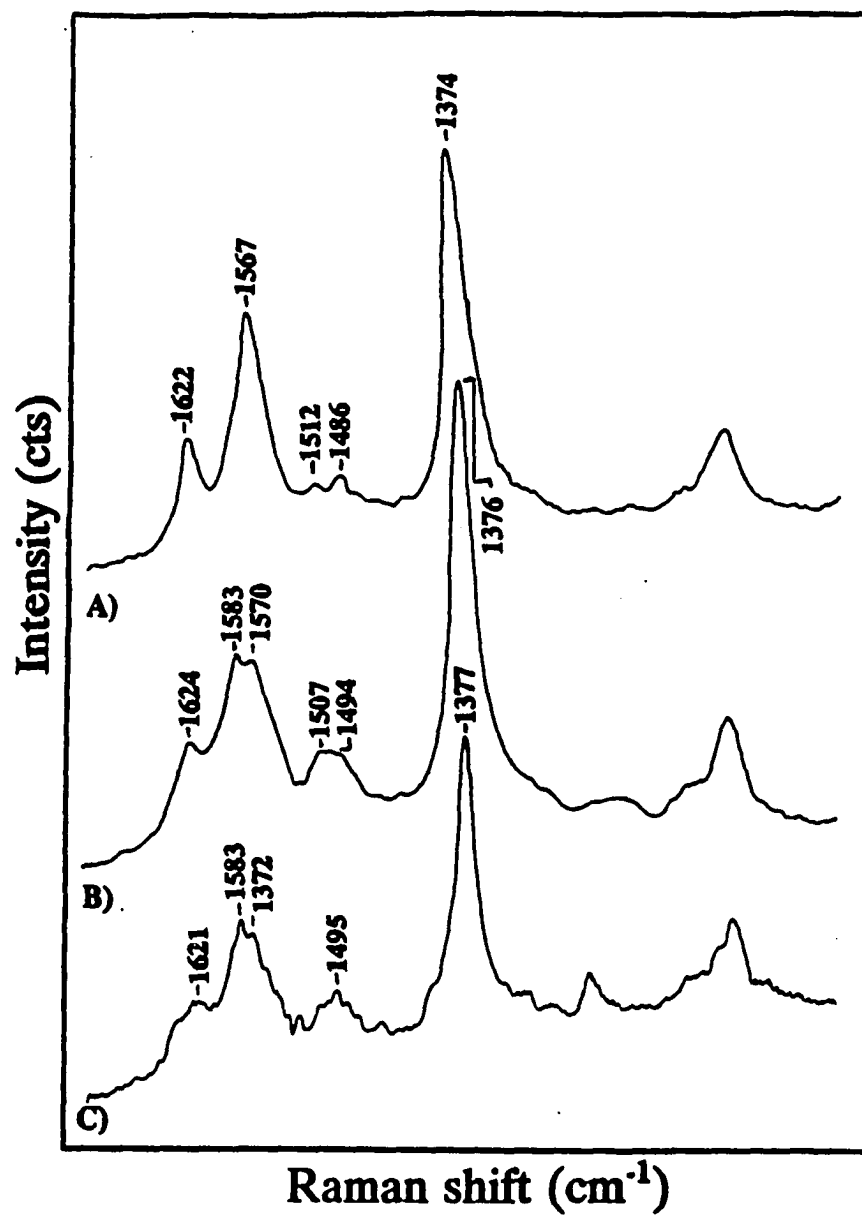


Figure 10. SERRS spectra of myoglobin as a function of adsorbing concentrations: A)  $10^{-7}$  M; B)  $10^{-8}$  M; C)  $10^{-9}$  M. Experimental conditions: SERRS-active substrate, citrate-reduced sols, excitation wavelength, 413.1 nm; integration time, 1 sec; scans, 25.

chromophore. Another possibility is that the protein orients differently at the silver sol particles at lower adsorbing solution concentrations. The heme may be located closer to the silver surface and, as a consequence, the heme environment is perturbed by the electrostatic effects of the substrate.

In any case, the absence of the shoulder at  $1355\text{ cm}^{-1}$  indicates that photoreduction of the heme does not occur at the silver sol. Although the heme environment is perturbed, the water ligand may still be coordinated to the iron atom. Alternatively, the protein may not be susceptible to photoreduction at a silver sol surface even following the loss of the water molecule.

The presence of phosphate ions in the silver sol suspension is another requirement for the preservation of the native myoglobin structure. Figures 11A and 11B show the RRS spectrum and the SERRS spectrum of myoglobin dissolved in water, respectively. The solution spectrum indicates that myoglobin does not undergo coordination or spin-state changes. Conversion of spin states ( $\nu_2$  at  $1578\text{ cm}^{-1}$  and  $\nu_3$  at  $1496\text{ cm}^{-1}$ ) occurs only when the protein is adsorbed at the SERRS-active substrate. These spin-state changes were not observed when phosphate buffer was used as the solvent (Figure 8C). Phosphate ions may also play a role in separating the protein from the surface which thereby

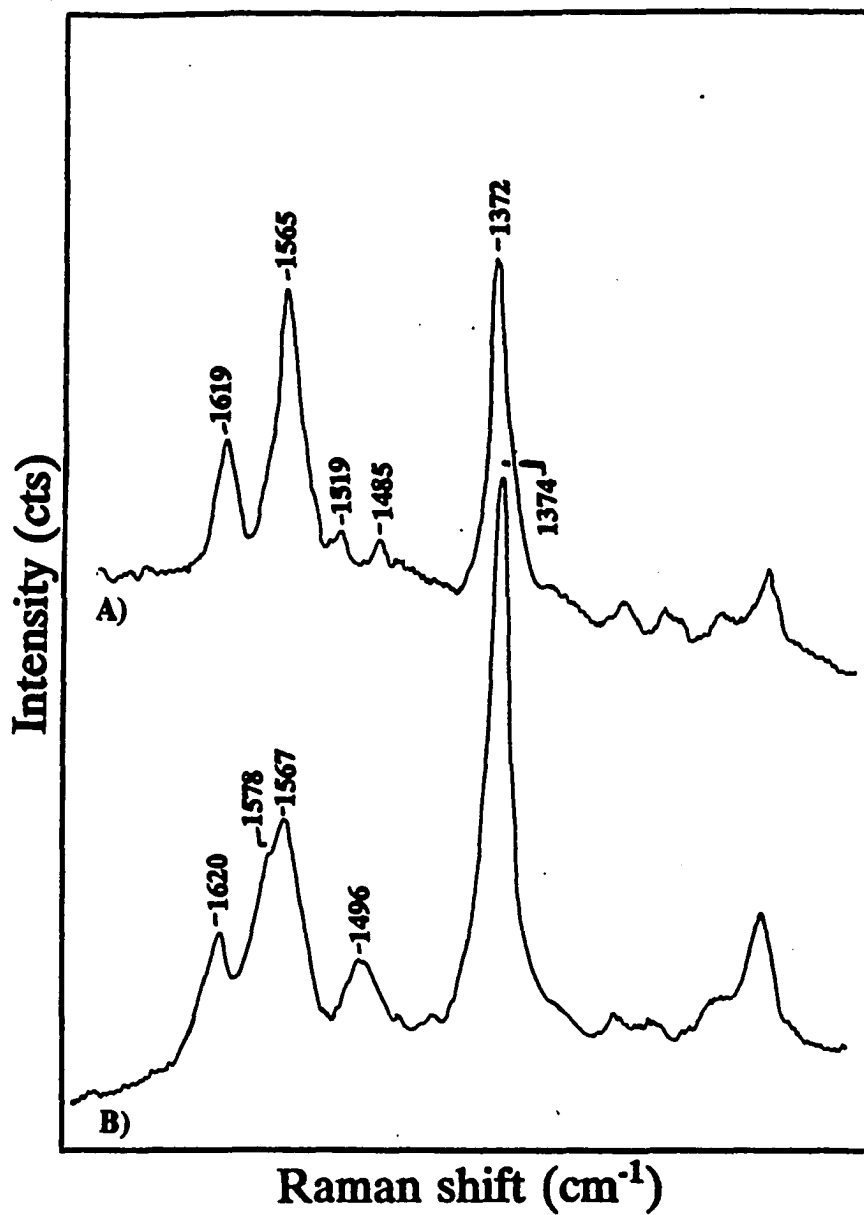


Figure 11. Spectra of myoglobin in H<sub>2</sub>O: A) RRS; B) SERRS. Experimental conditions: SERRS-active substrate, citrate-reduced sols; excitation wavelength, 413.1 nm; integration time, 1 sec; scans, 25.

prevents protein denaturation. Another explanation is that the phosphate ions may orient the heme at the substrate such that the macrocycle environment is not perturbed by the surface. Rospendowski et al. [45] demonstrated that the orientation of cyt c at a silver sol surface is influenced by the presence of phosphate ions.

The age of the sol is an important experimental parameter. Figure 12 shows the spectrum of myoglobin adsorbed onto a silver colloid suspension which was previously stored in a sealed container for four weeks. With respect to the solution spectrum of myoglobin (Figure 8A), the most significant difference in the SERRS spectrum is the shift of the  $\nu_3$  band from  $1483\text{ cm}^{-1}$  to  $1498\text{ cm}^{-1}$ . Comparable band frequencies were observed for myoglobin at a silver-island film surface under low-temperature conditions as shown in Figure 13B. Figure 13A depicts a RRS spectrum of myoglobin adsorbed onto a bare glass slide at 77 K. Based upon these results, the changes occur only at a metal substrate. The presence of an oxide layer at the silver surfaces may cause the protein structure to denature. Metal-island films readily oxidize when exposed to atmosphere. In addition, oxide formation at the surface of a silver sol is expected after a month of storage.

The electrostatic effect of the surface cannot be ignored when silver-island films are used as the SERRS-

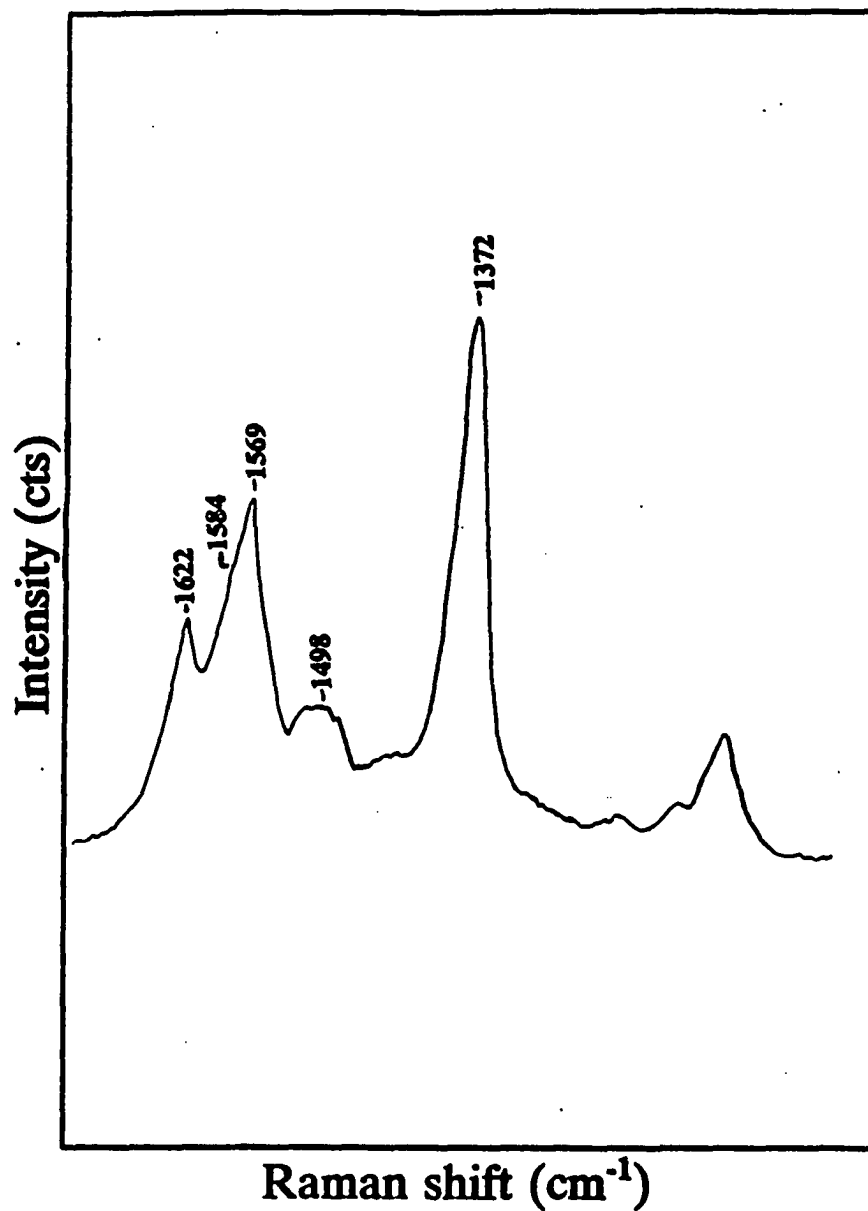


Figure 12. SERRS spectrum of myoglobin at a citrate-reduced sol stored for 1 month. Experimental conditions: excitation wavelength, 413.1 nm; integration time, 1 sec; scans, 25.

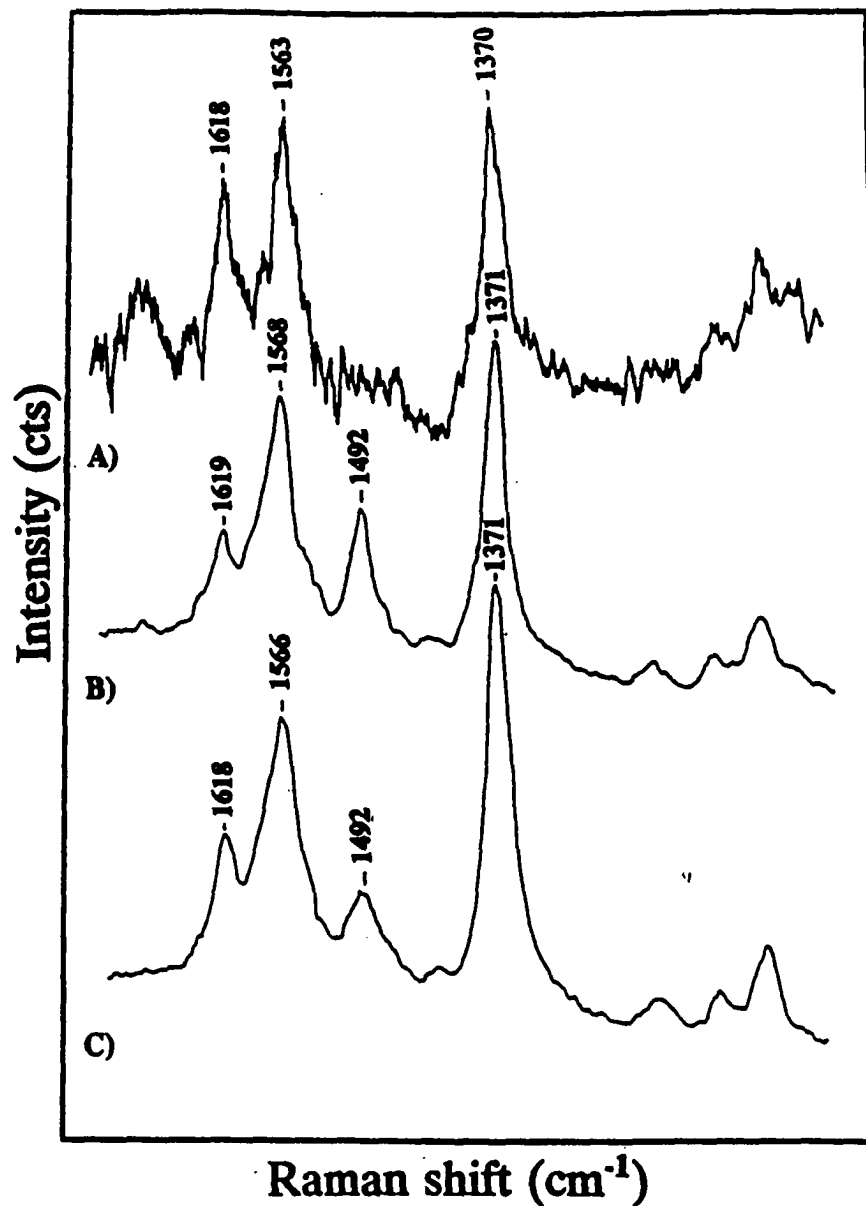


Figure 13. Low-temperature spectra of myoglobin: A) RRS of myoglobin on glass; B) SERRS of myoglobin at a 50 Å silver-island film; C) SERRS of myoglobin at a citrate-coated 50 Å silver-island film. Experimental conditions: excitation wavelength, 413.1 nm; integration time, 1 sec; scans, 25.

active substrate. Although photoreduction of the protein does not occur at the silver-island film surface, the SERRS spectrum shows that the native structure was not preserved. In order to examine the protein/surface interaction, the myoglobin was separated from the surface by initially coating the surface with citrate ions. Figure 13C depicts the SERRS spectrum of the cyt  $c$  at a citrate-coated silver film. The band frequencies are the same as those observed at a bare metal film. However, it should be noted that the vinyl stretch at  $1618\text{ cm}^{-1}$  increases in intensity whereas the band at  $1492\text{ cm}^{-1}$  decreases in intensity. The changes in the relative intensities of the bands of the protein at the citrate-coated metal film suggest that the protein adopts a slightly different orientation relative to myoglobin at a bare film.

The surface potential may influence the orientation of the protein at the substrate as well. Studies relating the effect of potential on the structure of myoglobin are currently being pursued in our lab. The open circuit potentials are expected to vary slightly for each type of substrate and for different experimental preparations. Although the differences may be very small, the surface potentials may significantly affect the adsorption interaction and the conformation of the adsorbed protein.

**RRS and SERRS Studies of Cytochrome c**

Cytochrome c (cyt c) functions as a one electron carrier in the terminal end of the respiratory assembly. This heme-containing protein has been well-characterized by several techniques [1,3,4]. Thus, cyt c is an ideal model compound for investigating the physiological and structural properties of the biomolecule at SERRS-active substrates. These studies have elucidated the oxidation-, ligation-, spin-state and protein structure of the protein. Cyt c is a relatively small spherical protein with a molecular weight of approximately 13,000 and a diameter of 34 Å. The protein matrix is composed of a single polypeptide which completely surrounds the porphyrin with the exception of one exposed edge. The heme is covalently attached to the backbone through thioether linkages between two cysteine residues and the vinyl substituents of the chromophore whereas the axial ligation sites are occupied by a histadine and a methionine in the fifth and sixth coordination positions, respectively. Under physiological conditions, cyt c exists in a 6-coordinate LS state in both the oxidized and reduced forms. Although the three-dimensional structure of cyt c has been deduced by x-ray diffraction crystallography at nearly atomic resolution [46], the mechanisms of electron transfer reactions in vivo and at electrode surfaces are not

understood. Initial research of cyt c at a silver electrode showed that the frequencies displayed by the SERRS spectrum corresponded to the RRS band frequencies. Several studies conducted in our lab indicate that the native state of cyt c can be preserved at SERRS-active substrates.

Figure 14 shows a comparison of the RRS spectrum (A) with the SERRS spectra of cyt c at an electrochemically-roughened silver electrode obtained at room temperature (B) and at low temperature, i.e., 77 K (C). The RRS spectrum is characteristic of oxidized 6-coordinate LS species as indicated by the oxidation state marker,  $\nu_4$  at  $1377\text{ cm}^{-1}$ , and the spin-state markers,  $\nu_{10}$  at  $1640\text{ cm}^{-1}$ ,  $\nu_2$  at  $1590\text{ cm}^{-1}$ , and  $\nu_3$  at  $1506\text{ cm}^{-1}$ . The SERRS spectrum obtained at room temperature is typical of an oxidized 5-coordinate HS heme, with spin-state markers at  $1629\text{ cm}^{-1}$  ( $\nu_{10}$ ),  $1577\text{ cm}^{-1}$  ( $\nu_2$ ) and  $1491\text{ cm}^{-1}$  ( $\nu_3$ ). By subjecting the adsorbed protein to liquid nitrogen temperature, the iron porphyrin moiety retains its physiological 6-coordinate LS state as shown in Figure 14C. Hildebrandt and Stockburger observed a 5-coordinate HS-state conformation of cyt c when the protein was adsorbed onto a silver sol suspension [24,47]. Moreover, a conversion from the HS state to the LS state occurred at low temperatures, i.e., 196 K. The authors concluded that cyt c existed in a thermal equilibrium state between both spin configurations. Comparable results are

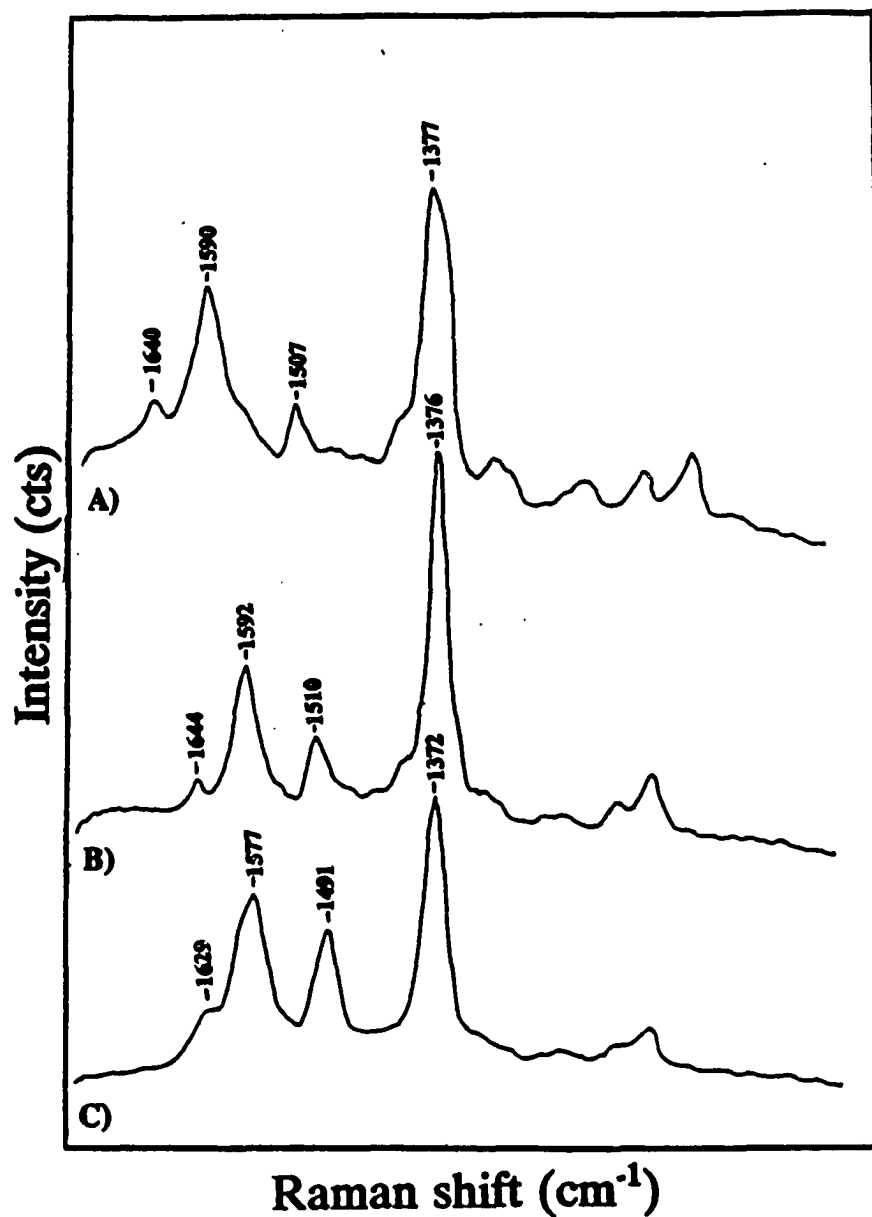


Figure 14. Spectra of cyt c: A) RRS; B) low-temperature; SERRS; C) room-temperature SERRS. Experimental conditions: SERRS-active substrate, electrochemically-roughened electrode; excitation wavelength, 406.7 nm; integration time, 1 sec; scan, 1.

shown in the spectra of cyt c at a silver electrode surface (Figure 14B and Figure 14C).

A time dependence study on the effect of laser irradiation on the spin-state configuration suggests that photodegradation is partially responsible for the structural changes as shown in Figure 15. The electrode was maintained at room temperature and the substrate was continuously irradiated throughout a five minute time period. The spectra were obtained after an irradiation period of 1 sec (A), 2 min (B) and 5 min (C). Although the signal-to-noise ratio is low, it is nevertheless apparent from the spectra that the protein changes quickly from the native 6-coordinate LS state to 5-coordinate HS state with continued laser irradiation. Figure 16 also shows spectra that were collected as a function of irradiation time, but the signal-to-noise ratio is higher because the spectra were collected by summing 25 1-second scans. The spectra were recorded after an irradiation time of 25 sec (A), 2 min (B), 5 min (C), 10 min (D), 15 min (E), and 25 min (F). Based upon the results, conversion from a LS state to a HS state occurs after only 25 sec of irradiation. In addition, the overall spectral intensity decreases with continuous laser irradiation. However, when the excitation was moved to a different area on the same electrode surface, the spectral intensity and the band frequencies were similar to those

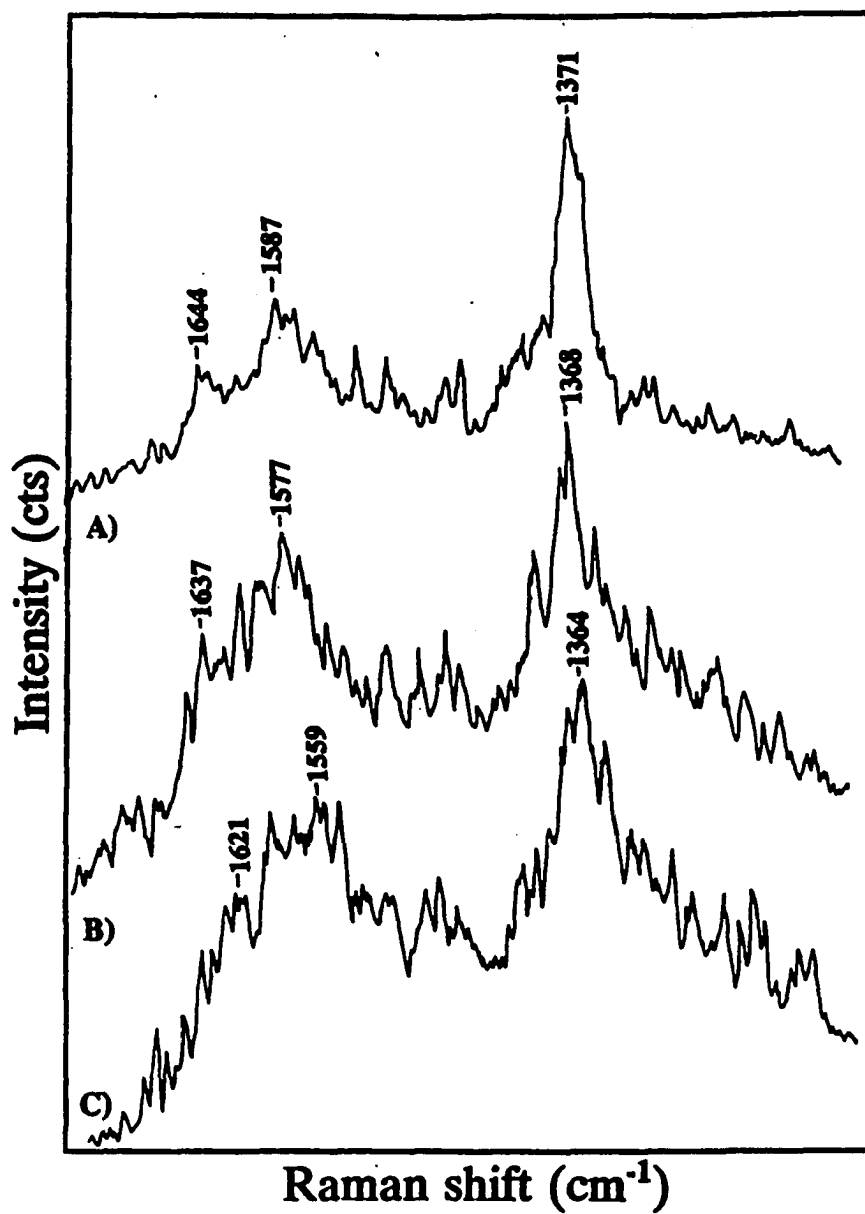


Figure 15. SERRS spectra of cyt *c* as a function of laser irradiation time: A) 25 sec; B) 2 min; C) 5 min. Experimental conditions: SERRS-active substrate, electrochemically-roughened electrode; excitation wavelength, 406.7 nm; integration time, 1 sec; scan, 1.

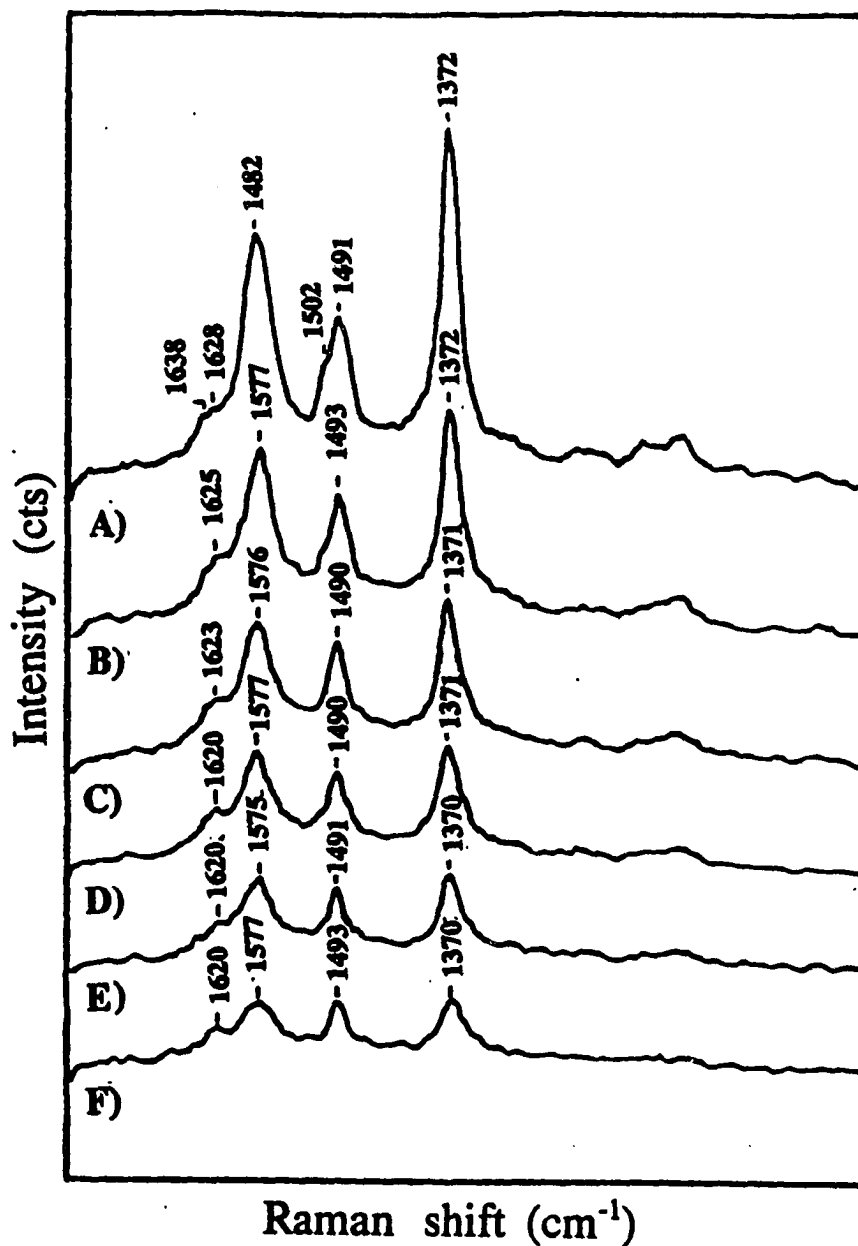


Figure 16. SERRS spectra of cyt c as a function of laser irradiation time: A) 25 sec; B) 2 min; C) 5 min; D) 10 min; E) 25 min. Experimental conditions: SERRS-active substrate, electrochemically-roughened electrode; excitation wavelength, 406.7 nm; integration time, 1 sec; scans, 25.

initially observed before prolonged irradiation. In contrast, the spectrum of cyt c obtained under low-temperature conditions did not change as a function of irradiation time.

The redox properties of the adsorbed protein were also monitored by acquiring SERRS spectra as a function of potential. Figure 17 shows the spectra of cyt c obtained when the electrode was maintained at potentials of -65 mV (A), -165 mV (B), -265 mV (C), -365 mV (D), -465 mV (E), and -565 mV (F). The entire spin-state/oxidation state band region was collected in a single scan. The spin-state markers at each potential indicate the protein is predominantly in the 6-coordinate LS state. The oxidation state marker, however, shifts from 1370  $\text{cm}^{-1}$  to 1358  $\text{cm}^{-1}$  in a potential range of -365 mV to -565 mV. Electrochemical studies of cyt c in solution have shown that its redox potential is +0.1 mV [24]. Because the spectra displays spin-state markers that correspond to the LS state, the negative redox properties of the adsorbed protein cannot be due to protein denaturation. Similar redox properties of the adsorbed protein were observed by Hildebrandt and Stockburger [24]. The authors showed that the redox potential of the adsorbed species was influenced by the initial adsorbing potentials of the protein. At negative adsorbing potentials, the redox properties of cyt c were

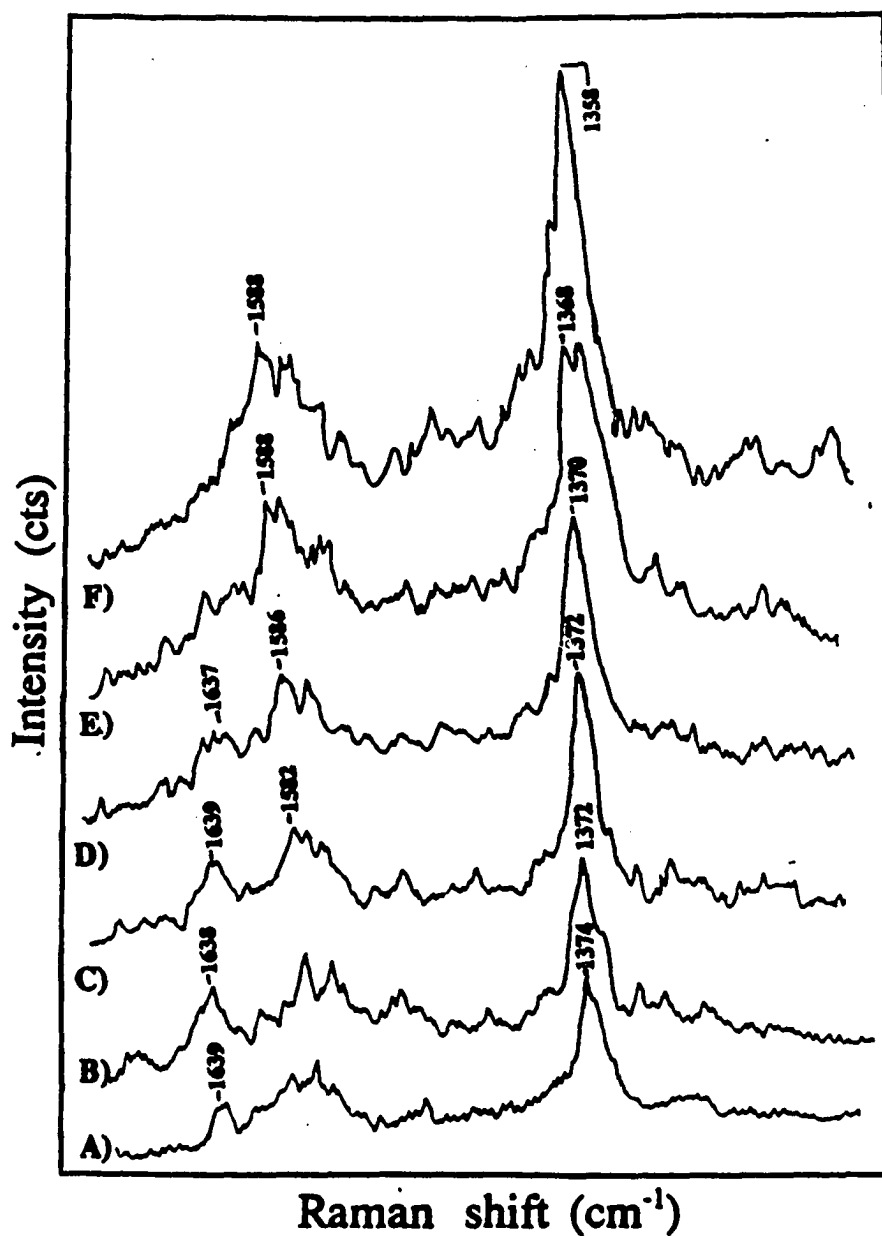


Figure 17. SERRS spectra of cyt *c* as a function of potential: A) -100 mV; B) -200 mV; C) -300 mV; D) -400 mV; E) -500 mV; F) -600 mV. Experimental conditions: SERRS-active substrate, electrochemically-roughened electrode; excitation wavelength, 406.7 nm; integration time, 1 sec; scans, 25.

comparable to values obtained for the protein in solution. In contrast, when the biomolecule was adsorbed onto the electrode at positive potentials, the redox potential was significantly more negative. The results suggest that the electron transfer reaction is dependent upon the orientation of the protein at the electrode surface. As proposed by the authors, cyt c can bind to the electrode surface through two sites. At negative potentials, the interaction site involves the positively-charged lysine residues that surround the exposed heme edge. Alternatively, at positive potentials, binding is believed to occur in the region of negatively charged amino acids which are located on the other side of the protein. The studies showed that the latter conformation is susceptible to perturbation of the heme environment as a result of electrostatic interaction between the protein and the substrate.

Recent investigations in our lab showed that the protein is quite stable at an electrode surface when cyt c is adsorbed in the reduced state. Figure 18 compares the RRS spectrum (A) with the SERRS spectra collected at room temperature (B) and low temperature (C). The spectra are characteristic of reduced 6-coordinate LS heme. The spin-state markers include the  $1592\text{ cm}^{-1}$  band ( $\nu_3$ ) and the  $1492\text{ cm}^{-1}$  ( $\nu_2$ ) band, the frequency of the oxidation-state marker is the  $1361\text{ cm}^{-1}$  frequency ( $\nu_4$ ). In contrast to the results

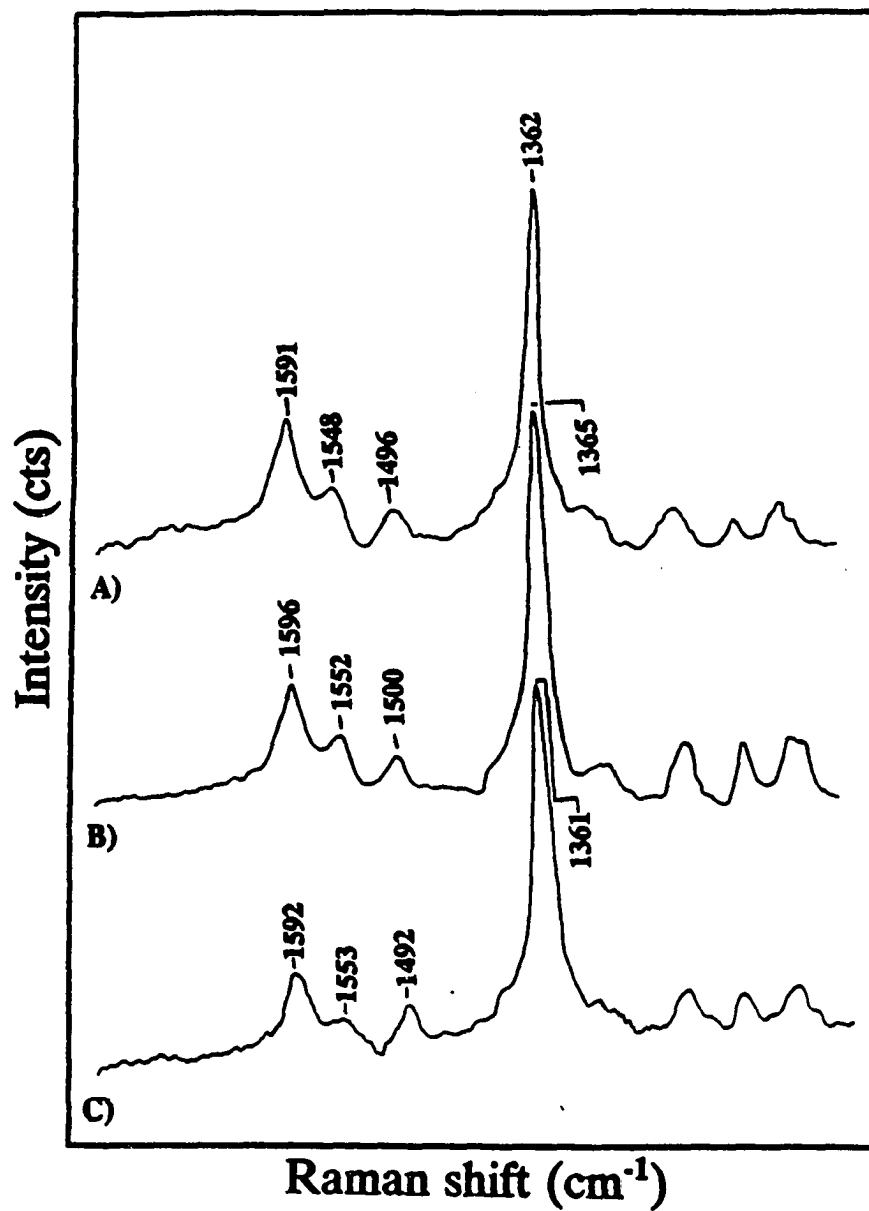


Figure 18. Spectra of reduced cyt *c*: A) RRS; B) low-temperature SERRS; C) room-temperature SERRS. Experimental conditions: SERRS-active substrate, electrochemically-roughened electrode; excitation wavelength, 413.1 nm; integration time, 1 sec; scans, 25.

discussed previously (Figure 14), the SERRS frequencies obtained at room temperature are identical to RRS frequencies obtained from the protein in solution. Additional SERRS studies from the protein of reduced cyt c as a function of potential showed a comparable redox potential was comparable to that in solution. These results suggest that the reduced protein binds to the surface through the lysine amino acid residues. As discussed previously, this conformation of cyt c is stable at the metal substrates. However, following prolonged laser irradiation, the overall spectral intensity of the reduced protein decreases under room-temperature conditions.

The SERRS spectra of cyt c at silver-island films were further studied under low-temperature conditions (Figure 19A) and at 5 C (Figure 19B). Figure 19A depicts the SERRS spectrum of the oxidized LS species. Alternatively, the oxidized HS state is evident when the spectrum is acquired at a higher temperature as shown in Figure 19B. The behavior of the protein was monitored as a function of laser irradiation time. Figure 20 illustrates the spectra obtained after an irradiation time of 25 sec (A), 85 sec (B), and 325 sec (C). After 25 sec of laser irradiation, the protein still retains its native 6-coordinate LS state. With continued laser irradiation, spin-state conversion occurs until the protein exists in a predominantly HS state.

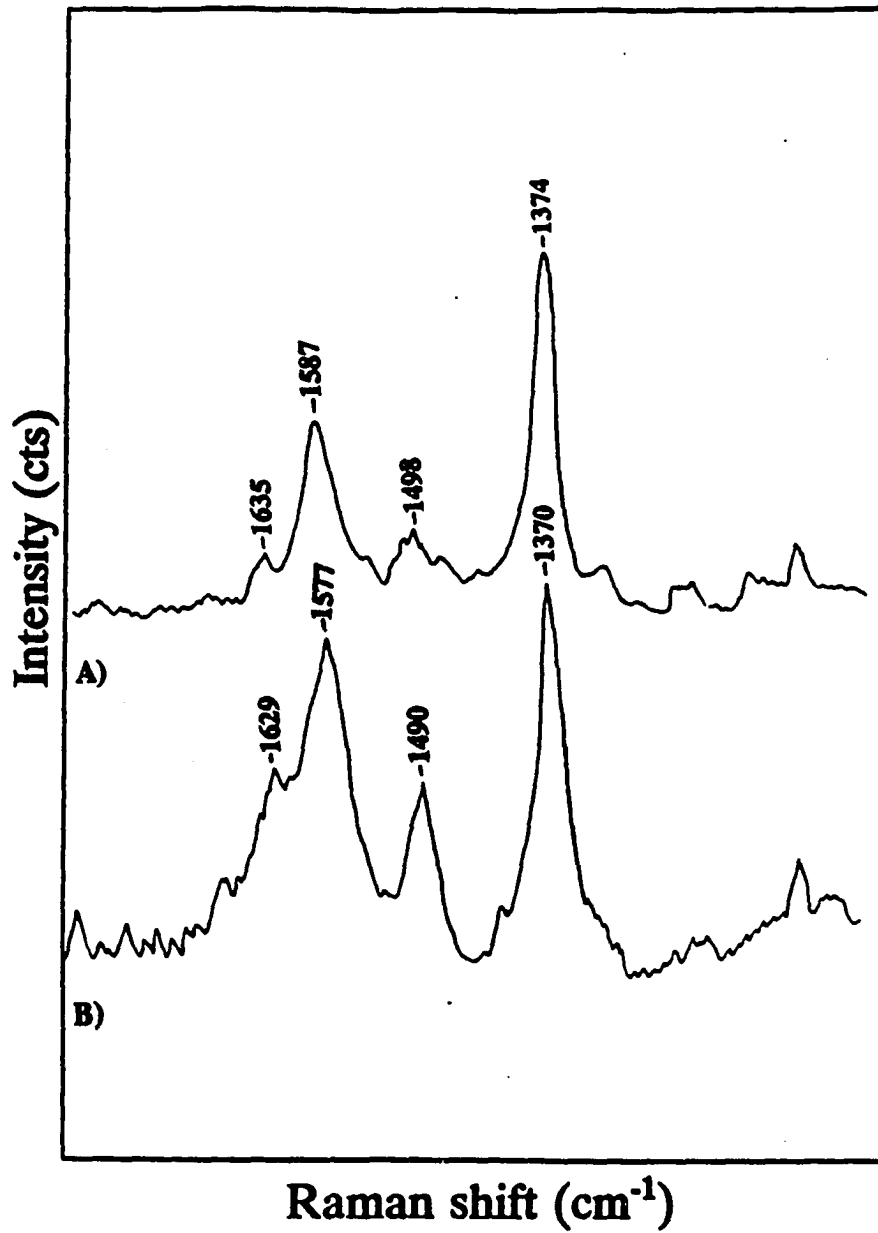


Figure 19. SERRS spectra of cyt *c*: A) low-temperature SERRS; B) room-temperature SERRS. Experimental conditions: SERRS-active substrate, 50 Å silver-island film; excitation wavelength, 413.1 nm; integration time, 1 sec (A), 5 sec (B); scans, 25.

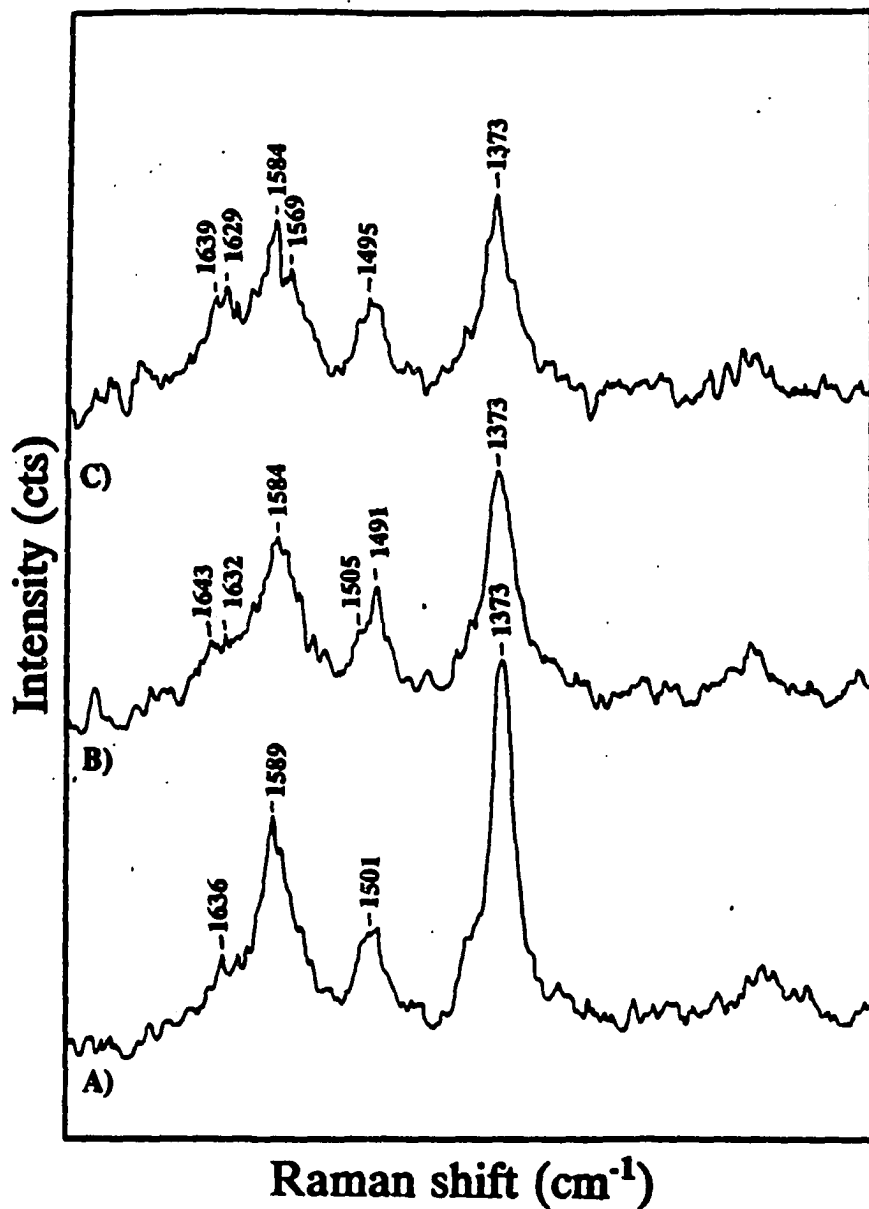


Figure 20. SERRS spectra of cyt *c* as a function of laser irradiation time: A) 25 sec; B) 1 min 25 sec; C) 5 min 25 sec. Experimental conditions: SERRS-active substrate, 50 Å silver-island film; excitation wavelength, 413.1 nm; integration time, 1 sec; scans, 25.

The results observed for cyt c at silver-island films are similar to those obtained for the oxidized species at the electrode surface (Figures 14-15). Hence, the binding site of the protein at the metal film surface must be through negatively-charged amino acid groups. This conformation readily undergoes conversion between the two spin states under various adsorption conditions.

## CONCLUSIONS

The following points have been established based upon SERRS studies of heme-containing proteins.

1. The native structure of the heme-containing proteins can be preserved at SERRS-active substrates, including electrochemically-roughened silver electrodes, silver-island films, and citrate-reduced silver sols.

2. The stability of the protein at the different SERRS-active substrates is dependent upon the nature of the heme-containing proteins. The interaction of a protein with the substrates is influenced by its overall charge, size, and structure. For example, the native structure of myoglobin is more easily perturbed upon adsorption as compared to cyt *c* because the heme group of the former protein is not covalently bound to the protein matrix and is more susceptible to electrostatic effects. In contrast, cyt P-450<sub>o</sub> is stable at an electrochemically-roughened surface under low-temperature conditions because the heme is sufficiently separated from the surface due to the large amino acid envelope. The reduced state of cyt *c* is stable at an electrode under room- and low-temperature conditions. The stability of the various heme-containing protein must therefore be considered in choosing suitable substrates and adsorbing conditions.

3. The structure of the heme-containing protein is stable at citrate sols under the appropriate conditions. The adsorbing solution concentration as well as the buffer must be controlled in order to retain the native integrity of the protein.

4. Bare silver electrodes and silver-island films tend to perturb the heme environments of most of the proteins. Alterations in the protein structure are induced by photodegradation and/or an electrostatic effect. Proteins sensitive to photodegradation can be stabilized by submerging the SERRS-active substrate into liquid nitrogen. Electrostatic interactions between the substrate and the protein are reduced by separating the protein from the surface. This is accomplished by coating the surface with a citrate layer.

5. As in the case of cyt c, the adsorbing potential may influence the stability of myoglobin. SERRS studies of myoglobin as a function of potential are currently underway.

**ACKNOWLEDGEMENTS**

The authors are grateful for the support of the National Institutes of Health (GM 35108). We thank Dr. Bernard Rospendowski and Dr. Randall Holt for their assistance and many helpful suggestions. We also thank Dr. P. Ortiz de Montellano and Barbara Swanson (Department of Pharmaceutical Chemistry, University of California) for extracting and purifying the cyt P-450<sub>b</sub> samples and Dr. Kostic (Department of Chemistry, Iowa State University) for purifying the samples of cyt c. And lastly, the work performed by John P. Neddersen is greatly appreciated.

## LITERATURE CITED

1. Dickerson, R. E., Timkovich, R. In The Enzymes, Boyer, P., Ed.; Academic Press: New York, 1975, Vol. 4, p 397.
2. Ortiz de Montellano, P. R., Ed.; Cytochrome P-450, Structure, Mechanism, and Biochemistry, Plenum Press: New York, 1986.
3. Dolphin, D., Ed.; The Porphyrins, Academic Press: New York, 1978; Vol. VII.
4. Dolphin, D., Ed.; The Porphyrins, Academic Press: New York, 1978; Vol. III, p 347.
5. Cotton, T. M., Schlutz, S. G., Van Duyne, R. P. J. Am. Chem. Soc. 1980, 102, 7960.
6. Cotton, T. M., Timkovich, R., Cork, M. S. FEBS Lett. 1981, 133, 39.
7. Hildebrandt, P., Heimburg, T., Marsh, D., Powell, G. L. Biochemistry 1990, 29, 1661.
8. Bobinger, R., Schweitzer-Stenner, R., Dreybrodt, W. J. of Raman Spectrosc. 1989, 20, 191.
9. Champion, P. M., Albrecht, A. C. J. Chem. Phys. 1979, 71, 1110.
10. Sage, T. J., Morikis, D., Champion, P. M. J. Chem. Phys. 1989, 90, 3015.
11. de Groot, J., Hester, R. E., Kaminaka, S., Kitagawa, T.

- J. Phys. Chem. 1987, 91, 1693.
12. Spiro, T. G. Biochim. Biophys. Acta 1975, 416, 169.
  13. Baranov, A. V., Bobovich, Y. S. Opt. Spectrosc. 1982, 52, 231.
  14. Hildebrandt, P., Stockburger, M. J. Phys. Chem. 1984, 84, 5935.
  15. Weitz, D. A., Garoff, S., Gersten, J. I., Nitzan, A. J. Chem. Phys. 1983, 78, 5824.
  16. Hildebrandt, P., Stockburger, M. Biochemistry 1989, 28, 6710.
  17. Hildebrandt, P., Stockburger, M. Biochemistry 1989, 28, 6722.
  18. Cotton, T. M. In Spectroscopy of Surfaces, Clark, J. H., Hester, R. E., Eds.; John Wiley & Sons Ltd.: New York, 1988; p 91.
  19. Kelly, K., Rospendowski, B. N., Smith, W. E., Wolf, C. R. FEBS Lett. 1987, 222, 120.
  20. Kelly, K., Rospendowski, B. N., Smith, W. E. Wolf, C. R. In Cytochrome P-450: Biochemistry and Biophysics, Schuster, I., Ed.; Taylor and Francis: London, 1989; p 375.
  21. de Groot, J., Hester, R. E., Kaminaka, S., Kitagawa, T. J. Phys. Chem. 1988, 92, 2044.
  22. Hildebrandt, P., Stockburger, M. J. Phys. Chem. 1986, 90. 6017.

23. McMahon, J. J., Baer, S., Melendres, C. A. J. Phys. Chem. 1986, 90, 1571.
24. Hildebrandt, P., Stockburger, M. In Vibrational Spectra and Structure, in press.
25. Kitagawa, T., Abe, M., Ogoshi, O. H. J. Chem. Phys. 1978, 69, 4516.
26. Abe, M., Kitagawa, T., Kyogoku, Y. J. Chem. Phys. 1978, 69, 4526.
27. Komives, E. A., Ortiz de Montellano, P. R. J. Biol. Chem. 1987, 262, 9793.
28. Ortiz de Montellano, P., Mico, B. A., Mathews, J. M., Kunze, K. L., Miwa, G. T., Lu, A. Y. H. Arch. Biochem. Biophys. 1981, 206, 43.
29. Waxman, D. J., Walsh, C. J. Biol. Chem. 1982, 257, 10446.
30. Lee, P. C., Meisel, D. J. Phys. Chem. 1982, 86, 3391.
31. Rospendowski, B. N., Department of Chemistry, Iowa State University, unpublished results.
32. Wolf, C. R. Trends Genet. 1986, 2, 209.
33. Adesnik, M., Atchison, M. CRC Crit. Rev. Biochem.
34. Wolf, C. R., Miles, J. S., Seilman, M., Burke, D., Rospendowski, B. N., Kelly, K., Smith E. W. Biochemistry 1987, 27, 1597.
35. Hildebrandt, P., Greinert, R., Stier, A., Stockburger, M., Taniguchi, H. FEBS Lett. 1988, 227, 76.

36. Arzenbacher, P., Sipal, Z., Strauch, B., Twardowski, J., Proniewicz, L. M. J. Am. Chem. Soc. 1981, 103, 5928.
37. Sato, R., Omura, T., Eds.; Cytochrome P-450, Academic Press: New York, 1978.
38. Sanchez, L. A., Spiro, T. G. J. Phys. Chem. 1985, 89, 763.
39. Muhs, M. A., Weiss, F. T. J. Am. Chem. Soc. 1982, 84, 1962.
40. Kitagawa, T., Kyogoku, Y., Iizuka, T., Saito, M. I. J. Am. Chem. Soc. 1976, 98, 5169.
41. Dickerson, R. E., Geis, I., Eds.; The Structure and Action of Proteins, Harper & Row, Publishers: New York; 1969.
42. Kendrew, J. C., Dickerson, R. E., Strandberg, B. E., Hart, R. G., Davies D. R., Phillips, D. C., Shore, V. C. Nature 1960, 185, 422.
43. Kendrew, J. C., Watson, H. C., Strandberg, B. E., Dickerson, R. E., Phillips, D. C., Shore, V. C. Nature 1961, 190, 665.
44. Morikis, D., Champion, P. M., Springer, B. A., Egeberg, K. D., Sligar,
45. Rospendowski, B. N., Schlegel, V. L., Holt, R. E., Cotton, T. M. In Charge and Field Effects in Biosystems-2, Allen, M. J., Cleary, S. F., Hawkrige,

R. M., Eds.; Plenum Publishing Corp.: New York, 1989;  
p 43.

46. Kallai, O. B., Swanson, R., Dickerson, R. E. J. Biol. Chem. 1973, 248, 5244.
47. Hildebrandt, P., Stockburger, M. J. Phys. Chem. 1986, 90, 6016.

**PAPER II RESONANCE RAMAN SCATTERING AND SURFACE-ENHANCED  
RESONANCE RAMAN SCATTERING STUDIES OF  
CYTOCHROME C<sub>3</sub>**

**ABSTRACT**

The tetra-heme protein, cytochrome  $c_3$  (cyt- $c_3$ ), isolated from the sulfate-reducing bacteria, Desulfovibrio desulfuricans, strain NCIMB 8372 was examined with the RRS and SERRS techniques. A comparison of the protein in solution and at a citrate-reduced silver sol shows the native structure of cyt- $c_3$  is retained at a SERRS-active substrate. Therefore, SERRS is a viable technique for the examination of this protein. Additional RRS spectra were collected as a function of concentration of  $\text{Na}_2\text{S}_2\text{O}_4$ . Five distinct intermediate states were observed which correlate to the stepwise reduction of each heme.

In addition, SERRS spectra were acquired at an electrochemically-roughened SERRS-active substrate as a function of potential. As shown by the SERRS spectra, the redox properties of the adsorbed protein differ to those observed in solution with RRS. The protein is completely reduced at a potential that corresponds to the reduction of heme-1 as determined by electrochemistry. The RRS and SERRS results of cyt- $c_3$  isolated from Desulfovibrio desulfuricans, strain NCIMB 8372 are similar to data reported previously of cyt- $c_3$  from other strains of bacteria.

## INTRODUCTION

Cytochromes  $c_3$  (cyt- $c_3$ ) are multiheme proteins found in the anaerobic bacteria of the genus, Desulfovibrio [1,2]. This class of heme-containing proteins is distinguished from other c-type cytochromes by their unique structure and redox properties. Each cyt- $c_3$  molecule contains four heme macrocycles covalently bound to a single polypeptide producing a molecular weight ranging between 13,000 and 14,000 [3]. The fifth and sixth axial ligand position of each of the chromophores are coordinated to an imidazole group of a histidine amino acid residue. Cytochromes  $c_3$  thereby adopt a hexacoordinated low-spin form in both the oxidized state and reduced state. Although the amino acid sequences vary significantly for different strains of Desulfovibrio [4-6], the relative conformation of the hemes within the molecule are similar as revealed by x-ray crystallography studies [7,8]. The heme irons are separated by distances of 11 Å to 18 Å; however, the pyrrole atoms of individual chromophores are in close proximity to other pyrrole groups of nearby hemes. Moreover, studies have indicated that the interheme separation is smaller in the oxidized state as compared to the reduced form [9].

Cytochromes  $c_3$  act as electron carriers in reduction metabolism of sulfate. Physiologically, the proteins are

reduced reversibly with hydrogen at very negative redox potentials in the presence of the catalyst, hydrogenase [10,11]. Several studies have shown that electron transfer occurs between the chromophore groups in a stepwise process at four distinct redox potentials [3,12-22]. Despite a number of spectroscopic and electrochemical investigations, the nature of the heme-heme interactions and the conformational changes in the native and the adsorbed molecular states are still obscure.

Surface-enhanced Raman scattering (SERS) spectroscopy have several advantages for the characterization of heme-containing proteins. This technique provides a highly sensitive method (submonolayer coverages) for the examination of species adsorbed onto roughened metal surfaces, including electrodes, colloids, and metal-island films [23-27]. When SERS is coupled with resonance Raman scattering (RRS), the sensitivity is further increased for the surface-enhanced resonance Raman effect (SERRS). Hence, high quality structural information can be readily obtained from very low sample concentrations of the valuable scarce proteins. SERRS is particularly conducive to the study of hemoproteins because vibrations of the biologically-active prosthetic group are selectively enhanced over modes arising from the protein backbone [28]. Thus, SERRS can be used as a bioanalytical probe to study both the structure and

function of the protein. It is well established that the electrochemical behavior of cytochromes  $c_3$  depends upon the particular bacteria strain. In addition, electrochemical studies have shown various redox properties of the adsorbed protein at different electrode surfaces [29]. SERRS is a powerful technique for monitoring electron-transfer processes at the metal surfaces. SERRS also provides information regarding conformational changes of the adsorbed biomolecules [30]. In the present study, we report the first application of RRS and SERRS to the study of cyt- $c_3$  isolated from Desulfovibrio desulfuricans, strain NCIMB 8372. The redox states of the protein were monitored by obtaining RRS spectra of cyt- $c_3$  as a function of sodium dithionite ( $\text{Na}_2\text{S}_2\text{O}_4$ ) concentration. In addition, the redox behavior of the adsorbed protein and the its probable orientation at the substrate surface were examined with SERRS. The analytical merits and limitations of RRS and SERRS to the application of cyt- $c_3$  are discussed herein.

**EXPERIMENTAL****MATERIALS AND INSTRUMENTATION**Sample Preparation and Materials

Cyt- $c_3$  was isolated from Desulfovibrio desulfericans, strain NCIMB 8372, and was purified according to the published procedure [31]. The purity index of this cyt- $c_3$  protein  $((A_{553\text{red}} - A_{570\text{red}})/A_{280\text{ox}})$  was 3.25,  $I_{p_{\text{ox}}} > 9$ ,  $I_{p_{\text{red}}} = 6.7$ . The sample was dissolved in 30 mM phosphate buffer at pH 7. The concentration of cyt- $c_3$  was maintained at 1 mM and 2  $\mu\text{M}$  for the RRS and SERRS experiments, respectively. Sodium dithionite ( $\text{Na}_2\text{S}_2\text{O}_4$ ) served as the reducing agent in all the experiments.

Citric acid (Aldrich) and silver nitrate (Sigma) were used as received for the preparation of the SERRS-active silver sol.

Instrumentation

The cell used in the RRS and SERRS experiments was designed as shown in Figure 1. The cell was filled with 0.1 M KCl and was sealed with porous vycor (BAS).

The RRS and SERRS spectra were obtained with the 514.5 nm excitation from an Ar<sup>+</sup> laser (Coherent, INNOVA 90-5). The scattered light was collected in a backscattering

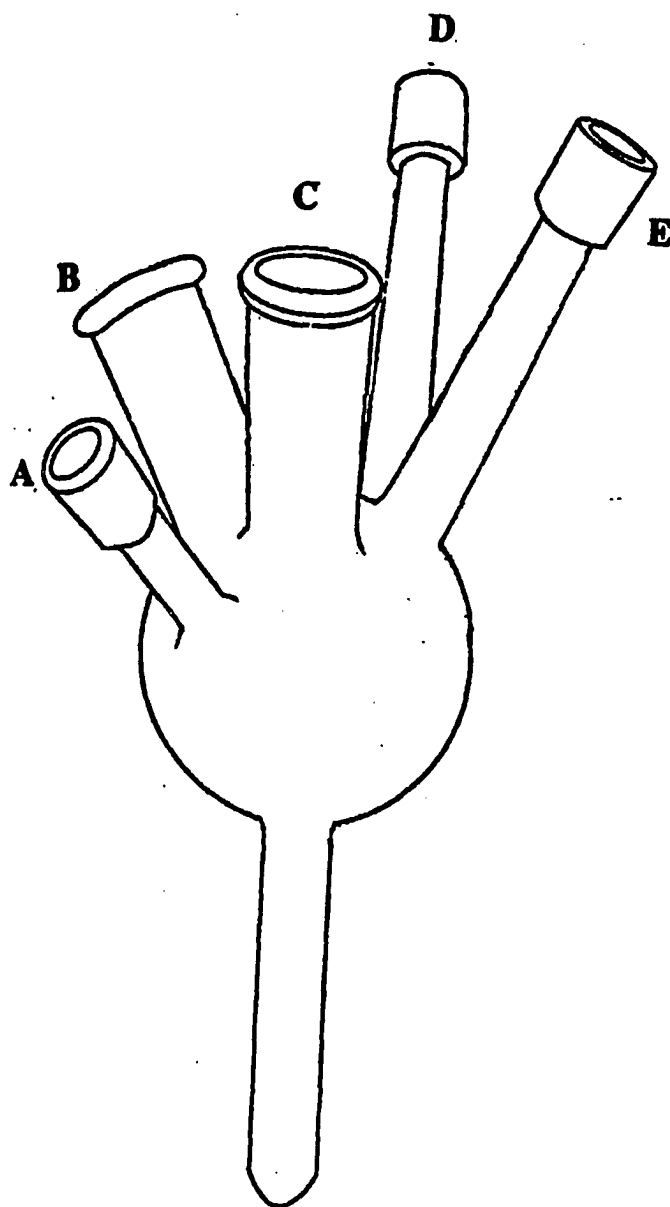


**Figure 1.** Cell used for collection of RRS and SERRS spectra: A) reductant inlet; B) reference electrode inlet; C) working electrode inlet; D) nitrogen inlet; E) nitrogen outlet.

configuration and was focused onto the entrance slit of a monochromator/spectrograph (Triplemate 1877). The monochromator stage contains two 600 grooves/mm gratings and the spectrograph stage is equipped with an 1800 grooves/mm grating (Dispersion = 0.93 nm/mm, bandpass = 10 cm<sup>-1</sup>). The exit slit was maintained at 0.200 mm for the RRS and the SERRS experiments. An intensified diode array detector (PARC 1420) interfaced to a multichannel analyzer (PARC OMA II) was used to accumulate and process the spectra.

A potentiostat constructed in our laboratory was used to roughen the electrode and to carry out the potential experiments. A saturated calomel electrode (SSCE) was used as the reference.

### **Experimental Procedures**

#### Preparation of SERRS-active silver sols

The silver sols were prepared by the method described in the literature [32,33]. Silver nitrate solution (1.0 x 10<sup>-3</sup> M) was brought to the boiling point and a 1% sodium citrate solution was added to the silver nitrate solution. The silver nitrate/citrate solution was heated and stirred continuously for 1 hr. The extinction maximum of the sol was 406 nm.

### Preparation of SERRS-active electrodes

Electrodes used in the SERRS experiments were constructed by sealing flattened silver wire into glass tubing with Torr Seal. The electrode was polished with a three-step polishing sequence in order to achieve a mirror-like finish on the surface. The electrode was first polished with a water slurry of 5.0  $\mu\text{m}$  on a mechanical polishing wheel. The polishing sequence was completed with successively finer particle (0.03  $\mu\text{m}$  and 0.05  $\mu\text{m}$ ) slurries and polishing cloths. To remove excess alumina, the electrode was sonicated in distilled water after each polishing step. Adsorbed organics and surface oxides were removed from the silver surface by applying -2.2 V to the electrode for approximately 30 sec. The electrode was roughened by an oxidation-reduction cycle (ORC) in 0.1  $\text{Na}_2\text{SO}_4$  solution. The potential was stepped from -600 mV to +450 mV and then returned to -600 mV. The total charge passed during the oxidation cycle was approximately 25  $\text{mC}/\text{cm}^2$ .

### RRS and SERRS Experiments

The cyt-c<sub>3</sub> solution was placed in the cell shown in Figure 1. The protein was reduced with  $\text{Na}_2\text{S}_2\text{O}_4$  by titrating the reductant into the protein solution which was purged continuously with  $\text{N}_2$ . The cell was placed at the focal point

of the collection optics and RRS spectra were collected by averaging 50 scans with an integration period of 15 sec per scan.

SERRS spectra were acquired by adding the cyt-c<sub>3</sub> solution to 1.2 ml of sol which was previously placed in the cell. The final concentration of the protein in the sol was 2 μM. The protein was initially reduced with Na<sub>2</sub>S<sub>2</sub>O<sub>4</sub> and then oxidized with the residual oxygen from the N<sub>2</sub> purge. SERRS spectra were collected as the protein was gradually oxidized. The SERRS spectra were obtained by signal averaging 25 scans with a 10 sec per scan integration period. The band frequencies were calibrated against indene as the standard.

The potential experiments were conducted using a SERRS spectroelectrochemical cell constructed in our lab. The protein was adsorbed onto the electrode by immersing it into the protein solution for approximately 15 min. The electrode was placed in the SERRS cell and the potential was stepped at the values indicated in the following section. The electrolyte solution was 85 mM potassium phosphate buffered to a pH of 7.0. The electrode was positioned at the SERRS window and the laser line was directed through the glass onto the silver surface. SERRS spectra were collected as the potential was stepped negative. The spectra were obtained by summing 50 1-sec scans.

**RESULTS AND DISCUSSION****RRS and SERRS Comparison Studies of  
Oxidized and Reduced Cytochrome  $c_3$** 

The absorption properties of cyt- $c_3$  are characterized by a strong Soret band in the high-energy region ( $\approx 410$  nm) and an  $\alpha$  and  $\beta$  band in the low-energy region ( $\approx 510$ - $560$  nm) [12]. Because 514.5 nm excitation is in resonance with the low-frequency  $\beta$  band, this line was used as the radiation source for the Raman experiments. This excitation wavelength is also advantageous because under anaerobic conditions cyt- $c_3$  partially photoreduces when irradiated with shorter wavelengths [34]. Moreover, the Raman frequencies above  $1200$   $\text{cm}^{-1}$  are sensitive to the oxidation, spin, and ligation state of heme-containing proteins [24]. Hence, the RRS and SERRS spectra reported herein were monitored in the  $1200$ - $1700$   $\text{cm}^{-1}$  region.

Figures 2A and 3A depict solution spectra of cyt- $c_3$  in the ferric and ferrous state, respectively. As shown in the figures, specific bands downshift in frequency when cyt- $c_3$  undergoes reduction. These modes include  $1635$ ,  $1619$   $\text{cm}^{-1}$  ( $\nu_{10}$ ),  $1566$ ,  $1540$   $\text{cm}^{-1}$  ( $\nu_{11}$ ),  $1501$ ,  $1492$   $\text{cm}^{-1}$  ( $\nu_3$ ),  $1405$ ,  $1398$   $\text{cm}^{-1}$  ( $\nu_{29}$ ),  $1373$ ,  $1360$   $\text{cm}^{-1}$  ( $\nu_4$ ) and  $1318$ ,  $1316$   $\text{cm}^{-1}$  ( $\nu_{21}$ ). The spin-state markers,  $\nu_{10}$ ,  $\nu_3$ , and  $\nu_2$  ( $1585$   $\text{cm}^{-1}$ ), displayed in

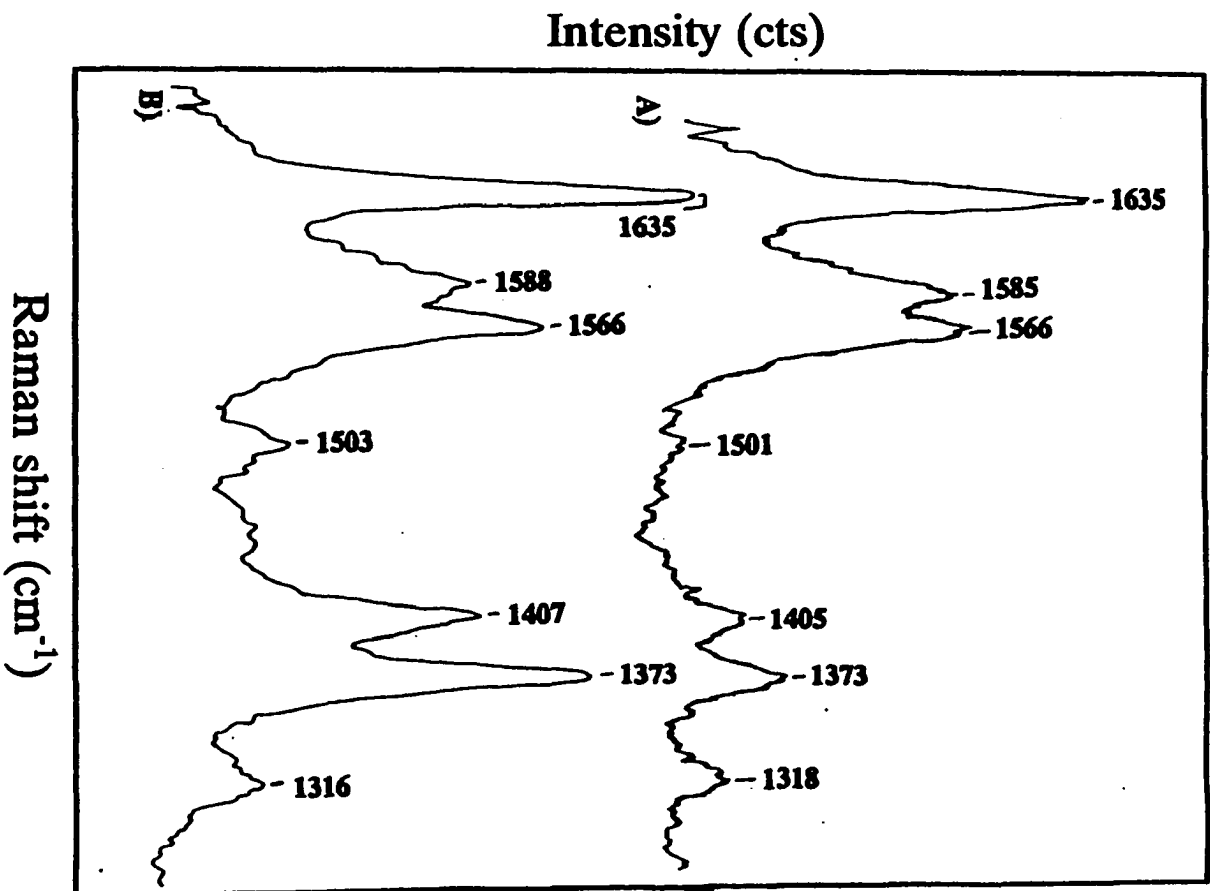


Figure 2. Cyt-c<sub>1</sub> in the oxidized redox state: A) RRS; B) SERRS.

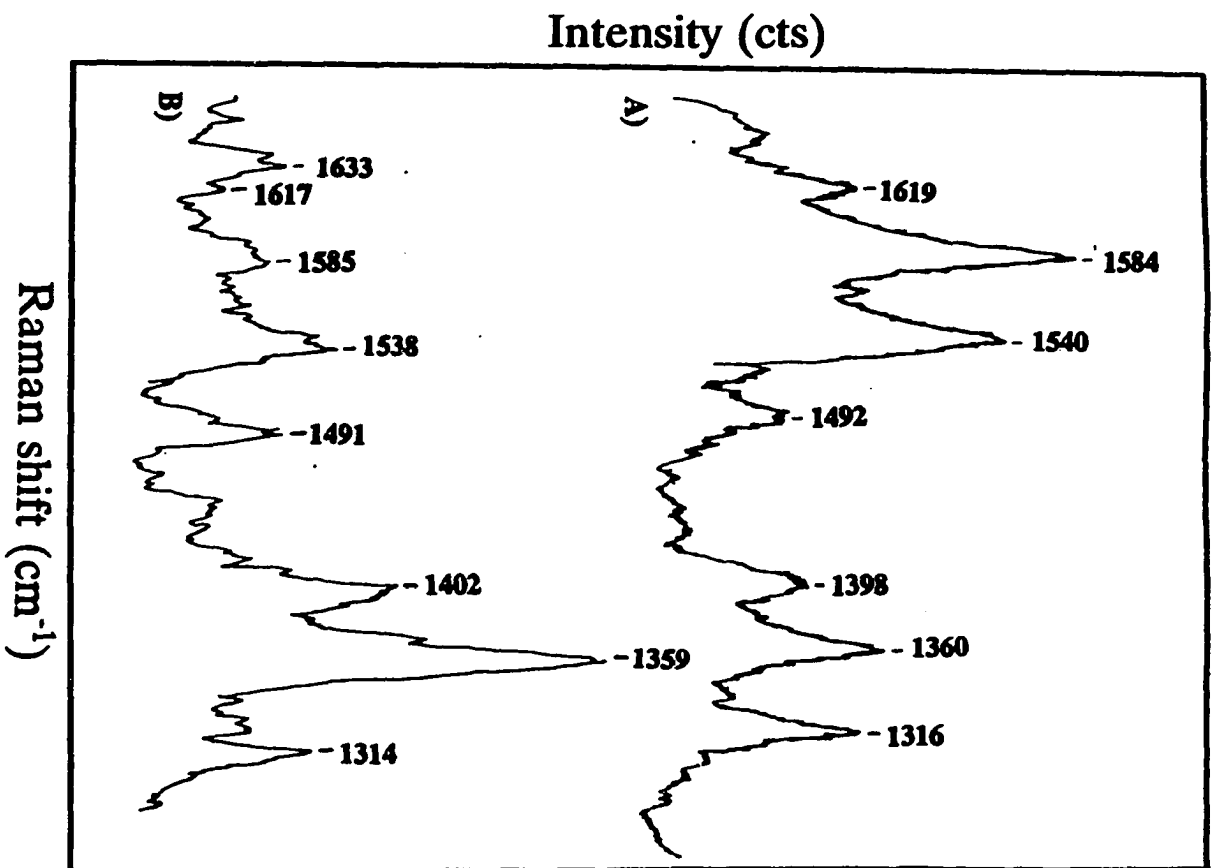


Figure 3. Cyt- $c_3$  in the reduced redox state: A) RRS; B) SRRS.

the RRS spectra are characteristic of a low-spin (LS) six-coordinate heme. Based upon these results, the oxidized and reduced species retain their native structure in solution even with constant laser irradiation.

The SERRS spectra of cyt- $c_3$  in the oxidized (Figure 2B) and reduced (Figure 3B) state show band frequencies comparable to the RRS (Figures 2A and 3A) spectra. The spin-state markers in the SERRS spectra are also indicative of LS 6-coordinate heme. These results indicate that perturbation of the heme environment does not occur when the protein is adsorbed onto a silver sol surface. Thus, a major advantage of SERRS to the application of cyt- $c_3$  is that only 2  $\mu\text{M}$  of the valuable protein is necessary to obtain spectra which are characteristic of the native structure of the protein.

The SERRS data reported in this work do not agree with previously reported SERRS spectra of adsorbed cyt- $c_3$  [35]. The previous spectra are characteristic of a mixed 6-coordinate LS and 5-coordinate HS species. In the previous study as well as in the present study, citrate-reduced silver sols were used as the SERRS-active substrate. However, the sols prepared in the previous investigation produced an absorption maximum at 420 nm whereas the sol used in this work displayed a maximum at 406 nm. Absorption studies have shown that the extinction maximum of sol

suspensions shifts to longer excitation wavelengths when larger particles are produced [36,37]. The adsorption-induced LS to HS conversion observed in the previous study may be caused by the presence of these larger particles. Similar results have been observed for cyt c at sol surfaces composed of larger silver particles. On the other hand, SERRS spectra showed that cyt c exists in a 6-coordinate LS state when the protein is adsorbed onto smaller particles [38].

Although the band frequencies are comparable in the RRS and SERRS spectra, the relative band intensities are different in the two types of spectra of the two redox states. In particular, the SERRS bands at  $1406\text{ cm}^{-1}$  and  $1373\text{ cm}^{-1}$  increase in intensity relative to their magnitude in the RRS spectra. The four hemes contribute equally to the overall spectral intensities of the bands in the RRS spectra. However, the vibrational bands of the heme closest to the SERRS-active substrate undergo greater enhancement as compared to the hemes that are more distant from the surface. In addition, bonds that align parallel with the surface field are selectively enhanced relative to the vibrations that are perpendicular to the field [39]. Based upon SERRS spectra collected as a function of potential, Niki et al. [40] concluded that heme-1 is closest to the substrate surface and is bound through the positively-

charged lysine residues which surround this heme. The authors showed SERRS spectra of only the heme with the most positive redox potential of the four hemes. As monitored by SERRS, the Desulfovibrio vulgaris, Miyazaki and Hildenborough strains, and the Desulfovibrio desulfuricans, Norway strain, are reduced completely at potentials more positive than the voltammetrically determined midpoint potentials when the proteins are adsorbed onto an electrochemically-roughened electrode.

**Investigations of the Intermediate Redox States  
of Cytochrome  $c_3$  using RRS Spectroscopy**

Figure 4 illustrates the RRS spectra of cyt- $c_3$  as a function of  $\text{Na}_2\text{S}_2\text{O}_4$  concentration. The protein was reduced by titrating  $\text{Na}_2\text{S}_2\text{O}_4$  into the protein solution and the corresponding SERRS spectra were obtained. A potential of -620 mV was measured upon complete reduction of the protein. Together with Figures 2A, 3A, and 4, the RRS spectra of cyt- $c_3$  show five distinct reduction states. The bands of the fully oxidized and the fully reduced species (Figures 2A and 3A) are relatively narrow. In contrast, the spectra illustrated in Figures 4A, 4B, and 4C show distinct broadening and overlapping of several redox sensitive bands in the intermediate redox states. As shown in the figure,

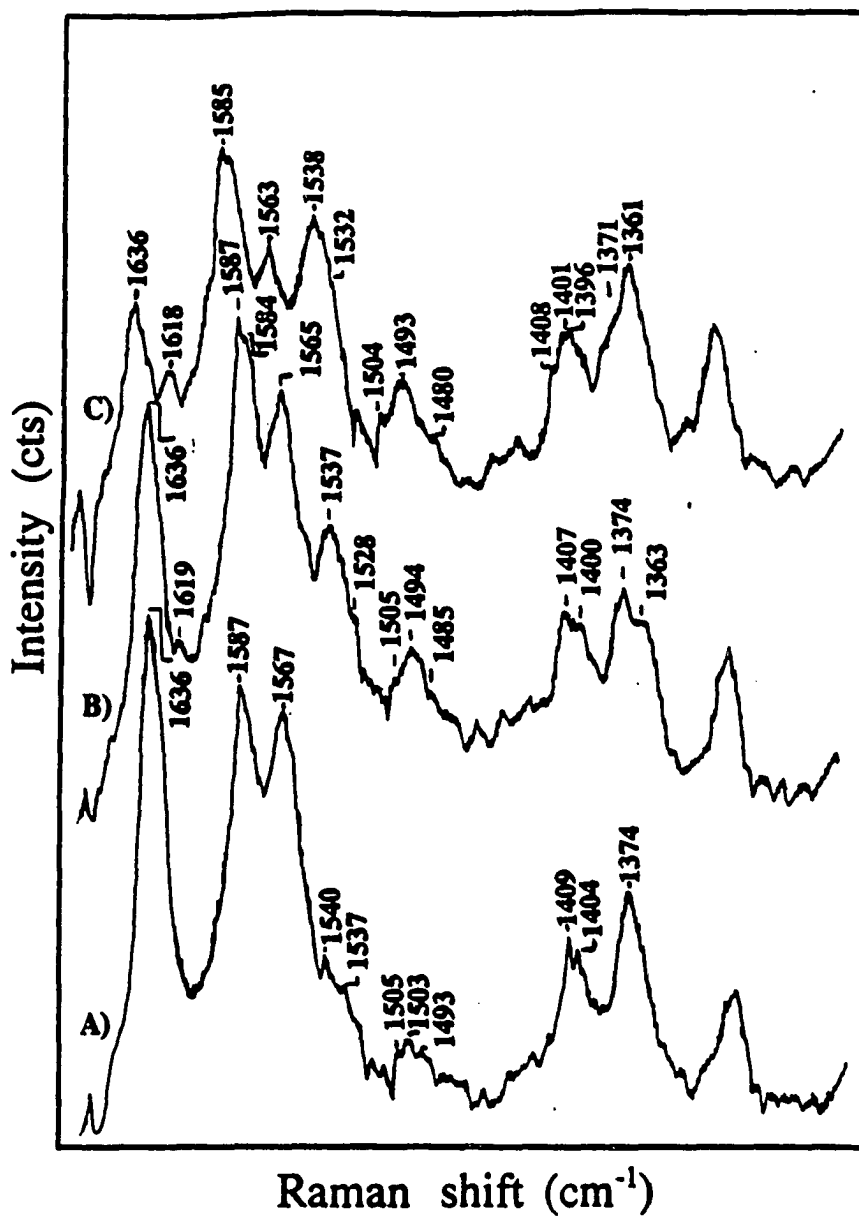


Figure 4. RRS spectra of Cyt-c<sub>3</sub> intermediate redox states: A) state 1; B) state 2; C) state 3.

the  $\nu_4$  develops into two bands,  $1373\text{ cm}^{-1}$  and  $1361\text{ cm}^{-1}$ , as a function of  $\text{Na}_2\text{S}_2\text{O}_4$  concentration. The intensity of the  $1361\text{ cm}^{-1}$  increases and becomes dominant in the fully reduced protein. Resolved structure in the intermediate states is also evident in the  $\nu_3$  at  $1505, 1503, 1493\text{ cm}^{-1}$  (Figure 4A),  $1505, 1494, 1485\text{ cm}^{-1}$  (Figure 4B) and  $1504, 1493, 1480\text{ cm}^{-1}$  (Figure 4C). The  $\nu_3$  mode shifts to  $1492\text{ cm}^{-1}$  upon complete reduction of the protein. With increasing concentrations of reductant, the  $\nu_{11}$  mode is split at  $1567, 1540, 1537\text{ cm}^{-1}$  (Figure 4A),  $1565, 1537, 1528\text{ cm}^{-1}$  (Figure 4B), and  $1538\text{ cm}^{-1}$  (Figure 4C). A broad spectral feature of the  $\nu_{29}$  mode at approximately  $1532\text{ cm}^{-1}$  (Figure 4C) may be attributed to a second unresolved band. In addition, splitting of the  $\nu_{11}$  mode occurs at  $1409, 1404\text{ cm}^{-1}$  (Figure 4A),  $1407, 1400\text{ cm}^{-1}$  (Figure 4B), and  $1408, 1401, 1396\text{ cm}^{-1}$  (Figure 4C). Additional spectral changes with  $\text{Na}_2\text{S}_2\text{O}_4$  titration include the reduction in intensity of  $\nu_{10}$  at  $1636\text{ cm}^{-1}$  and an increase at  $1618\text{ cm}^{-1}$ . The lower overall intensity of the  $\nu_{10}$  band at  $1618\text{ cm}^{-1}$  as compared to the  $1636\text{ cm}^{-1}$  suggests that it is not as strongly in resonance in the reduced state.

Verma et al. [34] reported similar RRS spectral characteristics of cyt- $c_3$  isolated from the Desulfovibrio vulgaris, Miyazaki strain. The authors attributed the five distinct states to a stepwise reduction of each of the

hemes in the biomolecule. Furthermore, the splitting of the bands in the intermediate states was ascribed to direct interactions of the hemes within the protein or to nonequivalent heme environments. The study showed that the intramolecular electron exchange rate is slower than the resonance Raman scattering time. The RRS spectra shown in this study are superpositions of bands arising from the oxidized and the reduced species as compared to an overall time-averaged spectrum. Hence, the RRS spectra monitor the stepwise reduction of each heme. Based upon the results, the intramolecular electron exchange rate of cyt-c<sub>3</sub>, strain NCIMB 8372, is also slower than the RRS scattering times.

#### **Investigations of the Intermediate Redox States using SERRS Spectroscopy**

Figure 5 shows the SERRS spectra of cyt-c<sub>3</sub> adsorbed onto a citrate-reduced sol at various redox potentials. Although the sol/adsorbate was continuously purged with N<sub>2</sub>, the protein oxidized readily on the sol surface. Thus, the SERRS spectra were obtained by first reducing the protein with an excess amount of Na<sub>2</sub>S<sub>2</sub>O<sub>4</sub> reducing agent and monitoring the gradual oxidation of cyt-c<sub>3</sub> by the residual oxygen present in the N<sub>2</sub> purge. Spectra were collected until the protein was fully oxidized.

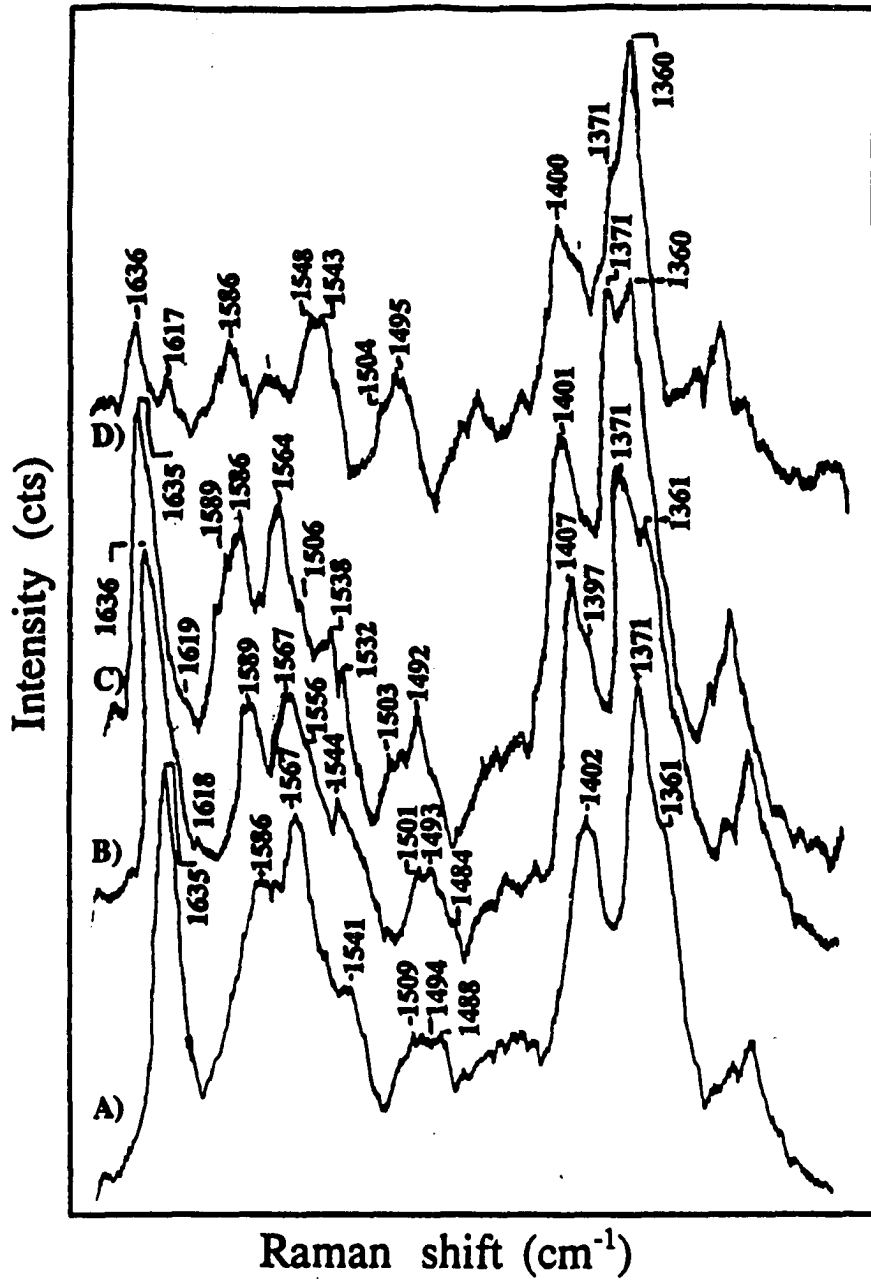
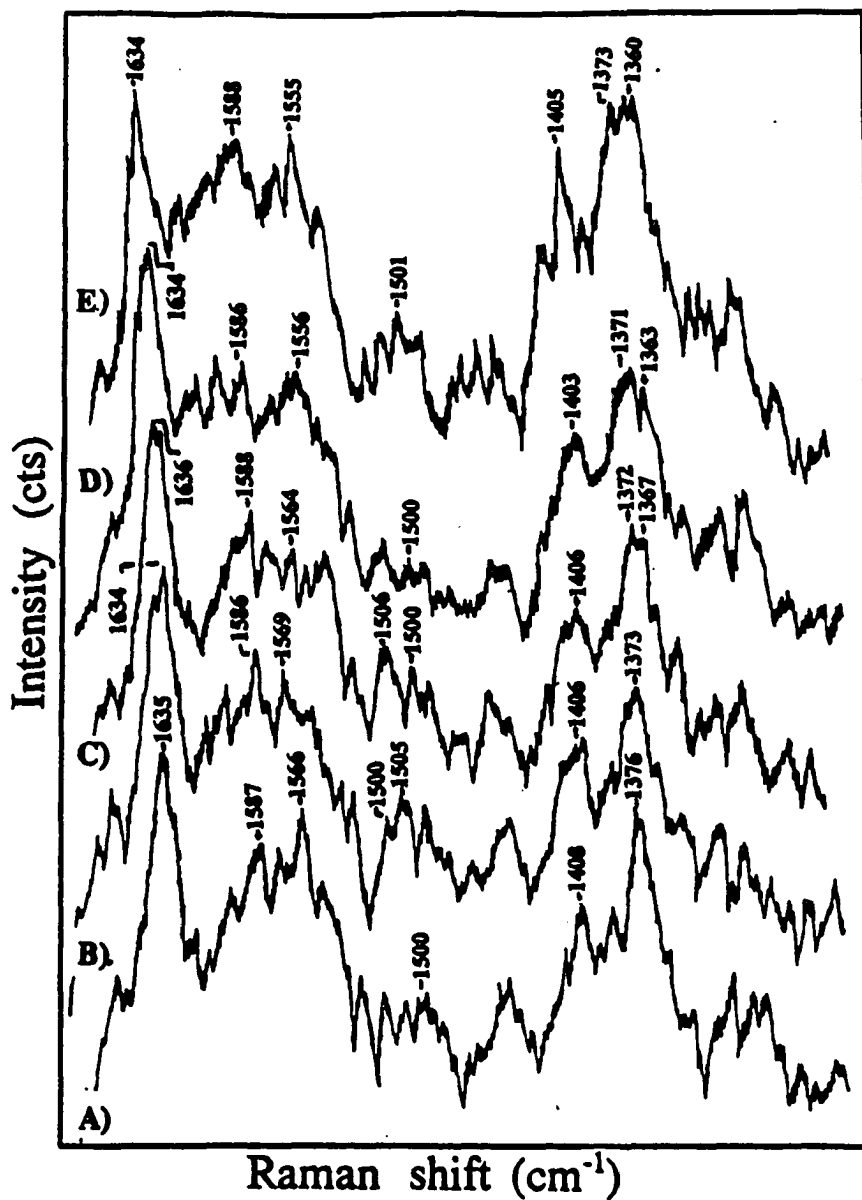
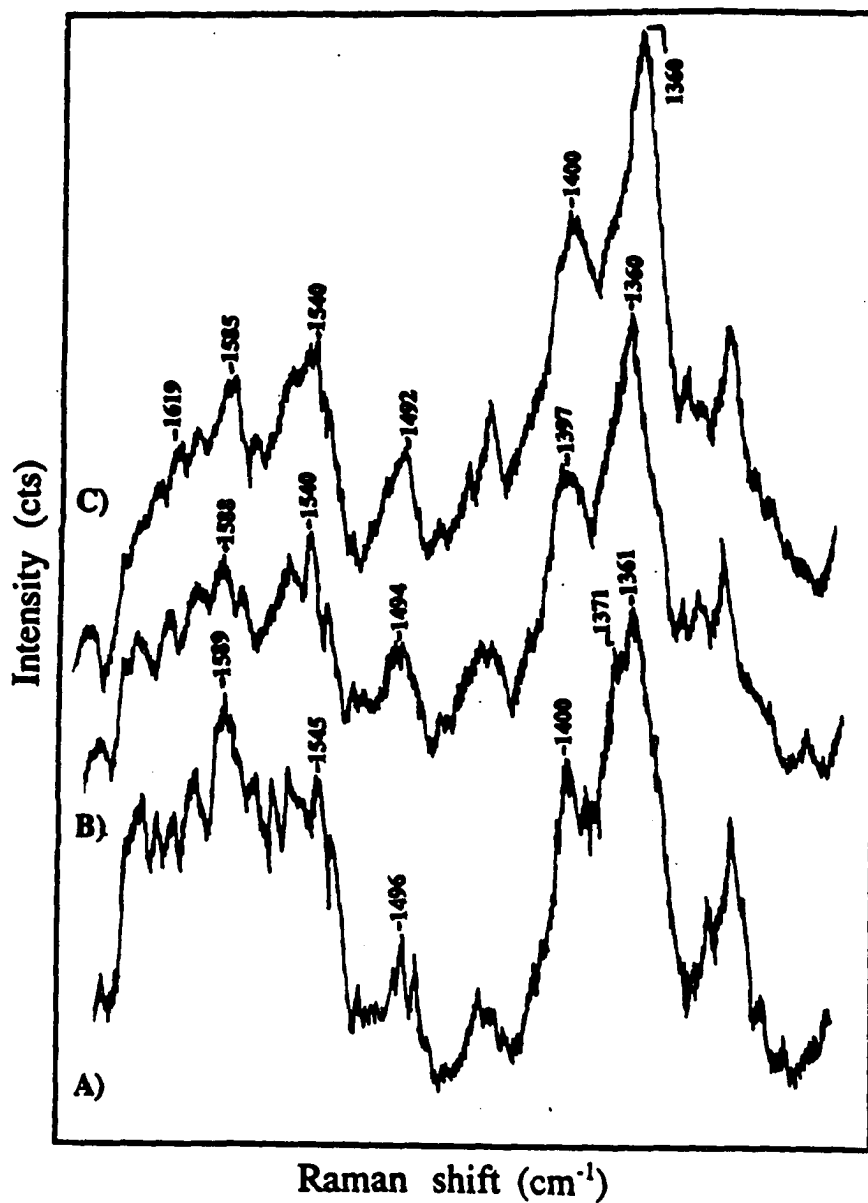


Figure 5. SERRS spectra of Cyt- $c_3$  intermediate redox states. SERRS-active substrate, citrate-reduced sols.

As in the case of the RRS results, the SERRS spectra show several intermediate states (Figures 1B, 2B, and 5). As depicted by Figure 5, distinct changes in the SERRS spectra occurs with oxidation of the protein. Two possible explanations may account for the intermediate reduction states. First, the intermediate states may represent a stepwise oxidation of each heme. However, the heme closest to the SERRS surface is expected to undergo a greater enhancement relative to those more distant from the substrate. Hence, the spectra may be indicative of the partial reduction of the heme adjacent to the substrate. Spectroelectrochemical studies of cyt-c<sub>3</sub> at an electrochemically-roughened silver electrode support the latter proposal. Figures 6 and 7 show SERRS spectra of the protein obtained as a function of potential. As illustrated by the figures, the protein is not as stable at the electrode surface as compared to the sol surface. Although the signal-to-noise ratio is much lower, the oxidation state marker is evident, and the spin-state markers indicate that the native structure of the protein is preserved. The oxidation state marker ( $\nu_4$  at  $1367\text{ cm}^{-1}$ ) of the reduced species starts to appear at  $-300\text{ mV}$  (vs SSCE). As the potential is stepped negative, this band gains intensity until the heme is completely reduced at  $-550\text{ mV}$ . This potential is more positive as compared to that obtained of



**Figure 6.** SERRS spectra of Cyt-c<sub>3</sub> intermediate redox states. SERRS-active substrate, electrochemically-roughened electrode: A) -200 mV; B) -250 mV; C) -300 mV; D) -350 mV; E) -400 mV.



**Figure 7.** SERRS spectra of Cyt-*c*<sub>3</sub> intermediate redox states. SERRS-active substrate, electrochemically-roughened electrode: A) -450 mV; B) -500 mV; C) -550 mV.

the fully reduced species in solution, i.e., -620 mV. The SERRS spectra also indicate that the heme is completely reduced at a potential more positive than the potentials of heme 2, 3, and 4 as determined by cyclic voltammetry and differential pulse voltammetry [29]. As discussed previously, Niki observed similar results and attributed this behavior to the selective enhancement of only the modes corresponding to heme-1 [40].

Although complete reduction of the adsorbed molecule occurs at a redox potential of the most positive heme, the SERRS spectra may reflect contributions from the hemes removed from the surface as well. Figure 5 illustrates splitting of certain bands comparable to those observed in the RRS spectra. In particular, the  $\nu_{11}$ ,  $\nu_3$ , and  $\nu_{29}$  modes are composed of bands with slightly different frequencies. These results cannot be attributed to the partial reduction of the heme closest to the surface. RRS and SERRS studies as a function of potential have shown that cyt  $c$ , which contains only one heme, does not undergo this type of splitting behavior [34,41]. Because the long-range effect of SERRS predicts enhancement of modes separated from the substrate surface, it is quite reasonable to assign the splitting to bands arising from the other three hemes in the protein.

It should be noted that the protein may orient

differently at the electrode surface as compared to the sol surface. The electrode studies indicate that heme-1 is closest to the surface of the substrate; however, the splitting behavior of certain bands is difficult to distinguish because of the low signal-to-noise ratio. At the sol surface, the protein may orient such that one of the other hemes is adjacent to the substrate surface. Investigations concerning the orientation of the protein at different SERRS-active substrates and at various adsorbing potentials are currently being pursued in our lab.

**CONCLUSIONS**

This is the first report of RRS and SERRS spectra of cyt- $c_3$  isolated from the strain Desulfovibrio desulfuricans, NCIMB 8372. The RRS spectra collected during titration with  $\text{Na}_2\text{S}_2\text{O}_4$  show distinct intermediate states similar to those observed for cyt- $c_3$  isolated from the bacterium of the Desulfovibrio vulgaris, Miyazaki strain. The five intermediate states correspond to the stepwise reduction of the hemes in the protein. The RRS results suggest that the electron exchange rate between the hemes is slower than the RRS scattering time.

The SERRS spectra of cyt- $c_3$  at citrate-reduced silver sols and electrochemically-roughened silver electrodes indicate that the environment of the heme is not perturbed upon adsorption. However, the redox behavior of the adsorbed protein is different compared to that observed with RRS. Potential studies performed with the SERRS-active electrode show reduction of the protein occurs at a potential which corresponds to heme-1. These results suggest that the intermediate states shown by the SERRS spectra represent the partial reduction of the heme closest to the surface. On the other hand, the spectra of cyt- $c_3$  at the sol surface depict splitting of certain bands similar to those displayed in the RRS spectra. Hence, the SERRS

spectra may reflect vibrations arising from hemes that are separated from the surface.

**ACKNOWLEDGEMENTS**

The authors are grateful for the support of the National Institutes of Health (GM 35108). We thank Dr. Danli Wang, Dr. Marian T. Stankovich, (University of Minnesota, Minneapolis, MN), Dr. Halina Neujahr, and Lars Eng (Royal Institute of Technology, Stockholm, Sweden) for extracting and purifying the protein and for their insight in the electrochemistry aspect of the study.

## LITERATURE CITED

1. LeGall, J., DerVartanian, D. V., Peck, H. D. Cur. Top. Bioenerg. 1979, 9, 237.
2. Postgate, J. R. Biochem. J. 1954, 56, XI-XII.
3. Dobson, C. M., Hoyle, N. J., Geraldès, C. F., Wright, P. E., Williams, R. J. P., Bruschi, M., LeGall, J. Nature 1974, 249, 425.
4. Ambler, R. P. Biochem. J. 1968, 47, 109.
5. Ambler, R. P., Bruschi, M. LeGall, J. FEBS Lett. 1969, 5, 115.
6. Ambler, R. P., Bruschi, M. LeGall, J. FEBS Lett. 1971, 18, 347.
7. Haser, R., Pierrot, M., Frey, M., Payan, F., Astier, J. P., Bruschi, M., Le Gall, J. Nature (London) 1979, 282, 806.
8. Higuchi, Y., Bando, S., Kusunoki, M., Matsuura, Y., Yasuoka, N., Kakudo, M., Yamanaka, T., Yagi, T., Inokuchi, H. J. Biochem. 1981, 89, 1659.
9. Utsuno, M., Ono, K., Kimura, K., Inokuchi, H., Yagi, T. J. Chem. Phys. 1980, 72, 2264.
10. Yagi, T., Maruyama, K. Biochim. Biophys. Acta 1971, 243, 241.
11. Yagi, T., Honya, M., Tamiya, N. Biochim. Biophys. Acta 1968, 153, 699.

12. Druker, H., Campbell, L. L., Woody, R. W. Biochemistry 1970, 9, 1519.
13. Der Vartanian, D. V., LeGall, J. Biochim. Biophys. Acta 1974, 346.
14. McDonald, C. C., Phillips, W. D., LeGall, J. Biochemistry 1974, 13, 1952.
15. Niki, K., Yagi, T., Inokuchi, H., Kimura, K. J. Electrochem. Soc. 1977, 124, 1889.
16. Niki, K., Kobayashi, Y., Matsuda, H. J. Electroanal. Chem. 1984, 178, 333.
17. Niki, K., Yagi, T., Inokuchi, H. Adv. Chem. Ser. 1983, 201, 199.
18. Sokol, W. F., Evans, D. H., Niki, K., Yagi, T. J. Electroanal. Chem. 1980, 108, 107.
19. Singleton, R., Jr., Campbell, L. L., Hawkridge, F. M. J. Bacteriol. 1979, 140, 893.
20. Bianco, P., Haladjian, H. Electrochim. Acta 1981, 26, 1001.
21. Bianco, P., Haladjian, H. J. Electroanal. Chem. 1982, 137, 367.
22. Eddowes, M. J., Elzanowska, H., Hill, H. A. O. Biochem. Soc. Trans. 1979, 7, 735.
23. Chang, R. K. Ber. Bunsen-Ges. Phys. Chem. 1987, 91, 296.
24. Creighton, J. A. In Surface-Enhanced Raman Scattering,

- Chang, R. K., Furtak, T. E., Eds.; Plenum: New York, 1982; p 315.
25. Weitz, D. A., Garoff, S., Gersten, J. I., Nitzan, A. J. Chem. Phys. 1983, 78, 5324.
  26. Aroca, R., Martin, F. J. Raman Spectrosc. 1985, 16, 156.
  27. Ni, Fan, Cotton, T. M. Anal. Chem. 1986, 58, 3159.
  28. Felton, R. H., Yu, N. T. In The Porphyrins, Dolphin, D., Ed.; Academic Press: New York, 1978, Vol. III, p 347.
  29. Wang, D., Eng, H. L., Stankovich, M. T., Neujahr, H. Y., in press.
  30. Hildebrandt, P., Stockburger, M. In Spectroscopy of Biological Molecules, Alix, A. M. P., Bernard, L., Manfait, M., Eds.; Wiley: New York, 1985; p 25.
  31. Eng, L. H., Neujahr, H. Y. Arch. Microbiol. 1989, 153, 60.
  32. Lee, P. C., Meisiel, D. J. Phys. Chem. 1982, 86, 3391.
  33. Rospendowski, B. M., Ph.D. Thesis, University of Strathclyde, Glasgow, U.K., 1989.
  34. Verma, A. L., Kimura, K., Nakamura, A., Yagi, T., Inokuchi, H., Kitagawa, T. J. Am. Chem. Soc. 1988, 110, 6618.
  35. Verma, A. L., Kimura, K., Yagi, T., Nakamura, A., Inokuchi, H., Kitagawa, T. J. Am. Chem. Soc., in press.

36. Creighton, J. A., Albrecht, M. G., Hester, R. E.,  
Matthew, J. A. D. J. Chem. Soc., Faraday Trans. 2 1979,  
75, 790.
37. Wetzell, H., Gerischer, H. Chem. Phys. Lett. 1980, 76,  
460.
38. Rospendowski, B., Department of Chemistry, Iowa State  
University, unpublished results.
39. Moskovits, M., DiLella, D. P., Maynard, K. J. Langmuir  
1988, 4, 67.
40. Niki, K., Kawasaki, Y., Kimura, Y., Higuchi, Y.,  
Yasuoka, N. Langmuir 1987, 3, 982.
41. Hildebrandt, P., Stockburger, M. In Vibrational Spectra  
and Structure, in press.

**PAPER III SILVER-ISLAND FILMS AS SUBSTRATES FOR ENHANCED  
RAMAN SCATTERING: EFFECT OF DEPOSITION RATE ON  
INTENSITY**

**ABSTRACT**

The relationship between surface-enhanced resonance Raman scattering (SERRS) intensity and the rate of deposition during silver-island film preparation was examined, using zinc tetraphenylporphine (ZnTPP) as the adsorbate. The effect of the deposition rate on the optical properties of the films at specific wavelengths was also analyzed. The data show that the film extinction (the term extinction is used rather than absorption because the spectra have not been corrected for reflection or scattering losses) increases exponentially at 514 nm and 458 nm as the deposition rate is decreased. SERRS intensities also increase exponentially at these two excitation wavelengths with a decrease in the deposition rate. The optical density is linearly related to the SERRS intensity and maximal enhancement is observed for films with the greatest extinction at these excitation wavelengths. In contrast, neither the extinction at 406 nm nor the SERRS scattering intensities resulting from excitation at this wavelength differ substantially.

The surface-enhanced Raman scattering (SERS) intensity and the electronic spectra of 4,4'-bipyridine (BP) adsorbed onto silver films as a function of deposition rate was also examined. The behavior of the nonresonantly-enhanced BP is

comparable to that of the resonantly-enhanced ZnTPP samples.

The effects of the surface morphology, as determined from transmission electron micrographs of the films at various deposition rates, on the corresponding electronic spectra and SERS/SERRS spectra are described.

## INTRODUCTION

Surface-enhanced Raman scattering (SERS) has been studied intensively since Jeanmaire and Van Duyne [1] and Albrecht and Creighton [2] independently demonstrated that Raman scattering intensity is increased 3 to 6 orders of magnitude when a compound is adsorbed on a roughened silver surface. To date, most of the SERS research has focused on elucidating the mechanism(s) of this effect [3-6]. Recently, however, a number of investigations have focused on developing SERS as an analytical tool [7]. Because of the high degree of sensitivity and the structural information that SERS offers, a variety of problems may now be examined by surface vibrational spectroscopy. Applications of SERS to analytical investigations have included the characterization of chemically modified electrodes [8], trace analysis of organic compounds [9-11], in situ observations of charge transfer processes [12,13] and conformational studies of molecules adsorbed onto metal particles [14-16]. SERS has also been recognized as a useful technique for the analysis of biological systems [17,18]. Nonetheless, the general applicability of SERS as an analytical method remains limited because the relationships between the observed scattering intensities and various experimental parameters have not been adequately

characterized in many cases.

One crucial limitation of SERS spectroscopy arises from the need for practical SERS-active substrates. A suitable metal surface must be present to produce strongly enhanced Raman scattering, as previously noted. Experimental results indicate that the magnitude of the enhancement is related to the surface morphology, in accordance with an electromagnetic (EM) enhancement mechanism [3-6]. Theory predicts that the local electromagnetic field is enhanced as a result of propagation of surface plasmon resonances in the metal at appropriate excitation wavelengths. Radiative emission requires a roughened surface. The relationship between scattering intensity and the distance of the adsorbate from the surface, as well as the overall enhancement, is governed by the particle shape and radius of curvature. Thus, an increase in SERS sensitivity can be attained by preparing substrates with optimal surface morphology.

In order for SERS to provide a practical analytical technique, the surface structure of the metal substrate must be reproducible. Experimental conditions that affect the geometry and size of the silver particles must be defined and controlled. Silver-island films as SERS-active substrates have many advantages in this respect. Vapor deposition of a thin film (i.e.,  $<100 \text{ \AA}$ ) of silver onto a

suitable surface produces discontinuous island-like particles that are more stable than sols. As in the case of roughened electrodes and metal sols, the structure of the particles are dependent on several experimental factors, including the substrate material, the temperature of the substrate during and following metal deposition, the thickness of the film and the rate of metal deposition [19]. These conditions are easy to control, and reproducible SERS-active island films can be prepared by maintaining a consistent experimental procedure. Another important consideration is that the degree of particle roughness on the metal-island film surface can be monitored by optical spectroscopy. An intense, broad extinction band that spans the visible region is observed for an aggregated film. Glass et al. [20] showed that with increasing film thicknesses, the band shifts to the red and increases in absorbance. This behavior is due to alterations in the shape, size and packing density of the particles. Sennett and Scott also determined that a maximum occurs in the electronic spectrum of films below a critical thickness of approximately 100 Å [19]. Above this thickness, the particles begin to merge and produce a more continuous film as revealed by transmission electron micrographs. An absorption maximum is no longer apparent for the thicker films [19].

Metal-island film substrates have been used primarily to verify the electromagnetic contribution to SERS by correlating the Raman signals with the optical properties of the film [6,21,22]. Additionally, studies of dyes adsorbed onto silver-island films were conducted to analyze the surface-enhanced resonance Raman scattering (SERRS) response [23,24]. Thin metal films are also ideal substrates for the relationship between surface coverage and SERS or SERRS intensities [25-27].

Although a considerable body of work has been reported concerning the SERS/SERRS mechanisms by using silver-island films as the active substrate, very little research has been directed to development of thin films for analytical purposes. For use of such films in routine analytical investigations, the experimental parameters affecting the surface morphology of the films must be defined so that optimal, reproducible SERS signals are obtained. The goal of this work was, therefore, to examine the effect of deposition rate on the surface morphology and optical properties of silver films and to correlate these properties with the Raman scattering intensity. A resonantly-enhanced molecule, zinc tetraphenylporphine (ZnTPP), and a nonresonantly-enhanced molecule, 4,4'-bipyridine (BP) were used as the analytes to measure the SERRS and SERS response

of the films. The advantage of optimizing the deposition rate for analytical procedures is clearly demonstrated.

**EXPERIMENTAL****Materials and Instrumentation**Materials

Silver used for the preparation of the metal films was 99.99% (AESAR). ZnTPP (Mad River Chemical) and spectroscopic grade acetone (Aldrich Co.) were used as received. The 4,4'-bipyridine (Aldrich Co.) was recrystallized and sublimed prior to use.

Instrumentation

Silver-island films were prepared by vacuum deposition of the metal vapor onto clean glass microscope slides by means of a commercial vacuum system (Edwards High Vacuum, model E306A). The average mass thickness of the film and the rate of silver deposition were measured with a film thickness monitor (Edwards High Vacuum, model FTM4) equipped with a 6 MHz quartz piezoelectric crystal oscillator.

Optical spectra of the silver films and the adsorbate-coated silver films were measured with a Hewlett Packard model 8450A double beam UV-Vis spectrometer.

A transmission electron microscope (TEM) (Phillips 201) was used to determine the surface morphology of the metal substrates. Silver was vapor-deposited under vacuum onto

Formvar-coated 200 mesh copper grids. The metal-coated grids were inspected and photographed with the TEM operated at 60 kV.

Raman spectra were acquired with a Coherent Ar<sup>+</sup> (INNOVA 90-5) or a Kr<sup>+</sup> (INNOVA 100) laser. Plasma lines from the laser emission were eliminated by sending the beam through a premonochromator (Anaspec 300-S). The samples were irradiated with the laser beam at approximately 60° to the surface normal. Raman scatter was collected by using two lenses (Oriel 6236 Model fused silica collection lens and Oriel 6236 focusing lens) in a backscattering geometry. The scattered light was focused onto the entrance slit of a monochromator/spectrograph (Triplemate 1877) fitted with a 1200 grooves/mm grating in the spectrograph stage ( $D^{-1} = 1.4$  nm/mm). The entrance and exit slits were set at 0.500 mm and 0.200 mm, respectively. SERS signals were detected with an intensified silicon diode-array detector (PARC 1420) and processed by a multichannel analyzer (PARC OMA II).

### **Experimental Procedures**

#### **Microscope Slide Pretreatment**

The microscope slides used as substrates for silver films were cut into 1 x 2 cm pieces and placed upright in a Teflon slide holder. Surface contamination was removed by

washing in 3 M KOH/methanol solution for a minimum of 1 h. The slides were next sonicated three times in freshly purified water and stored in deionized water. Prior to the deposition procedure, the glass slides were again rinsed with freshly deionized water and dried at 110 C for a minimum of 20 min. The slides were cooled to approximately 25 C before placement in the vacuum chamber.

#### Silver Film Deposition

The microscope slides were placed in the deposition unit approximately 12 cm directly above a DC molybdenum boat which served as the heating source. The quartz crystal monitor was also positioned 12 cm above the source parallel to the glass slides. The quartz crystal oscillator was calibrated by a coulometric method as described by Fornari et al. [28]. To stabilize the oscillator, thick aluminum and silver films were first deposited on the crystal. The crystal was calibrated by depositing a set of different film thicknesses onto platinum or gold disk electrodes of defined surface areas. The silver thickness values displayed by the monitor were recorded. The electrodes were subjected to thin-layer bulk electrolysis and the film thicknesses coated on the electrodes were calculated. Accurate silver film values were obtained by applying an appropriate correction factor to the monitor if the calibration results proved this

to be necessary. Silver films were deposited onto the substrates at a base pressure of  $<3.0 \times 10^{-6}$  Torr. The metal thickness for all the films was maintained at 50 Å but the deposition rates ranged between 0.02 and 5.00 Å/sec. The deposition rate was controlled by the current passed to the molybdenum boat. Copper grids (200 mesh) for TEM analysis were bonded to the microscope slides and silver was evaporated onto the grids by the same deposition procedure as described above.

#### Adsorption Technique

Analytes were adsorbed onto the thin films by an immersion procedure described previously [29]. The films were submerged in  $10^{-4}$  ZnTPP/acetone or  $10^{-3}$  BP/acetone for 1 min. The solvent evaporated from the substrates as the slides were removed from the solutions. SERS/SERRS spectra were acquired immediately following the dipping procedure.

#### SERS/SERRS Experiments

The samples were positioned at the focal point of the collection optics. Spectra were obtained by averaging 25 scans with an integration period of 1 second per scan. Raman frequency shifts were calibrated with an indene standard.

## RESULTS AND DISCUSSION

### Characterization of Silver-Island Film Surface Morphology

To monitor the surface morphology of metal films as a function of deposition rate, transmission electron micrographs (TEMs) were acquired for 50 Å films prepared with evaporation rates of 0.03, 0.33, and 5.00 Å/sec. A comparison of the surface structure of the films is shown in Figure 1. The micrograph of the film deposited with the slowest rate has a surface composed of distinct, well-separated particles. With increasing evaporation rate, the silver particles are less defined and begin to merge on the glass substrate. The metal film produced with the fastest deposition rate has a nearly continuous structure with very little particle definition. It has been suggested that the shapes and the sizes of the islands are dependent upon the migration of the metal atoms at the surface [30,31]. An independent migration time is associated with each atom as it impinges on the surface. Migration is disrupted if additional atoms arrive in the vicinity during this normal migration time. Consequently, the structure of the film is affected by the arrival rate of the atoms at the substrate. For slowly deposited films, the particles tend to grow in height and are well-separated. Higher deposition rates

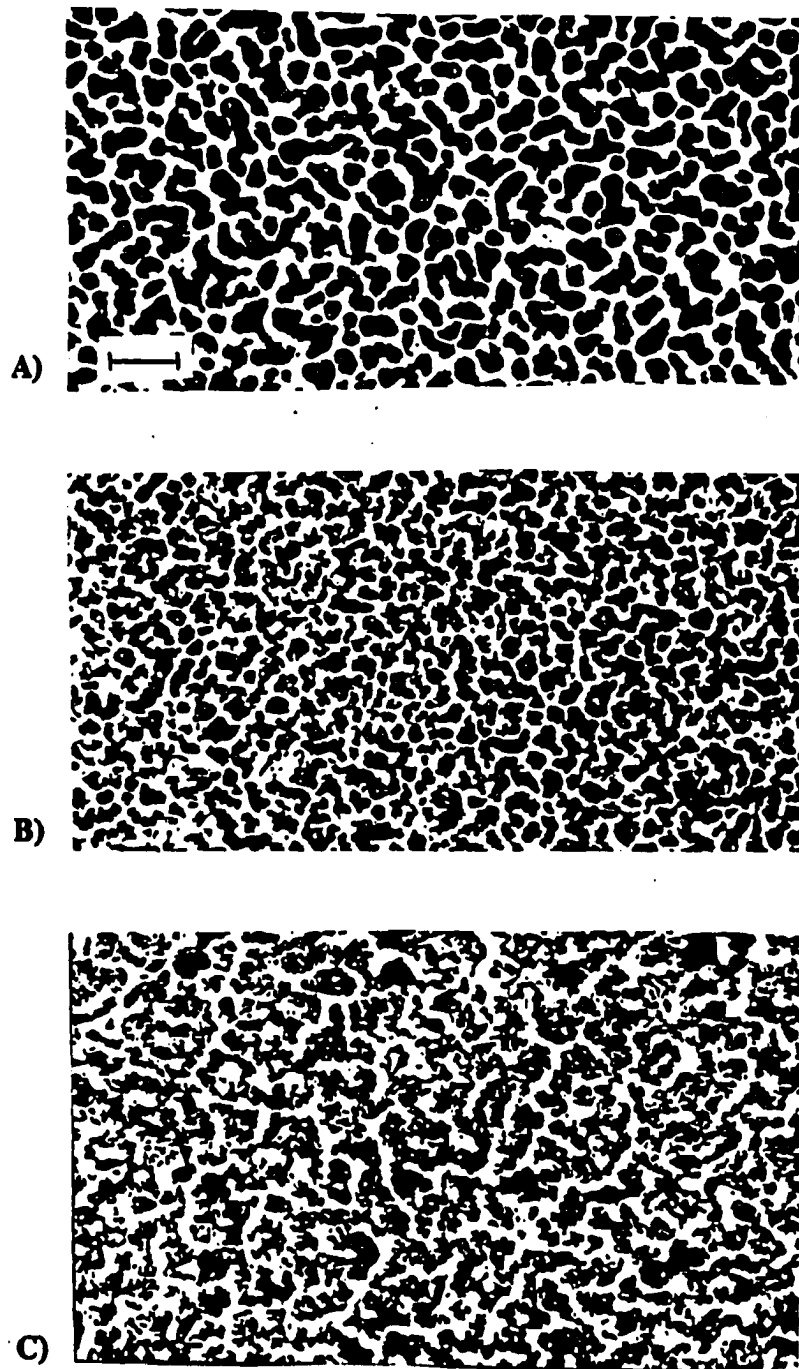


Figure 1. TEM images of 50 Å silver-island films prepared with varying deposition rates: A) 0.03 Å/sec; B) 0.33 Å/sec; C) 5.00 Å/sec. All images were recorded with the same magnification (scale in (A) indicates 1000 Å).

produce aggregates of lesser height and the particles are more interconnected. The TEM data obtained from films of the same silver thickness but different deposition rates are supportive of this conclusion.

Silver-island films reflect different hues ranging from violet to red as the deposition rate is increased. Colors result as differences in optical properties of the substrates as shown in Figure 2. The spectra are characterized by strong, broad extinction bands that shift towards the red region as the rate of deposition is increased. The reported spectra are not corrected for reflection losses and, therefore, the term extinction is used throughout the discussion instead of absorbance. Scattered light was also neglected in this study; however losses due to scattering are negligible for thin silver films [19,21].

The maximum extinction for the film deposited at 0.05 Å/sec occurs at approximately 530 nm. Films prepared at faster deposition rates exhibit decreased extinction at 530 nm and increased extinction at longer wavelengths, indicating a broader distribution of particle sizes and shapes. Other optical properties of the film also vary with deposition rate including the band shapes and relative extinction at specific frequencies. As the rate of deposition is increased the extinction band is broadened.

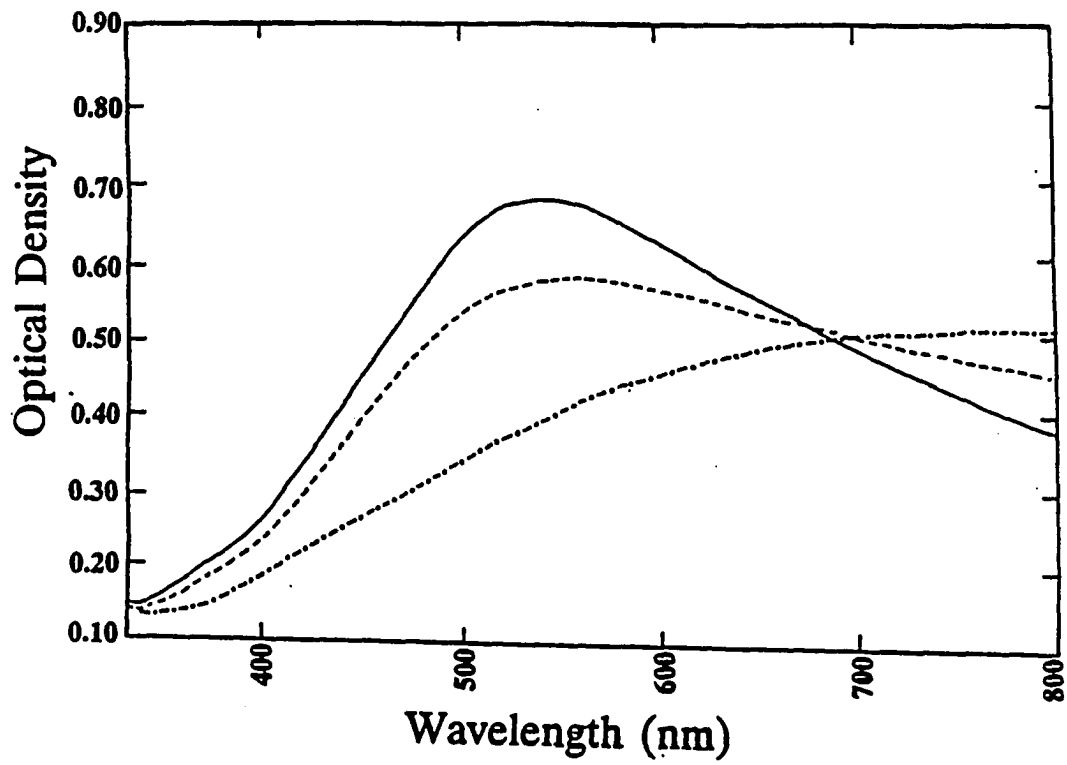


Figure 2. Electronic extinction spectra of 50 Å silver-island films deposited at 0.03 Å/sec (solid line); 0.33 Å/sec (dashed line); and 5.00 Å/sec (dashed/dotted line).

The extinction spectra were acquired from films deposited onto glass substrates and the TEM results were based on silver preparations deposited on Formvar grids. Because the type of substrate affects the surface morphology of the vapor-prepared films, direct comparison of the observed particle structures with the measured optical spectra might be legitimately questioned. However, it has been shown that TEM and optical data for silver films deposited onto glass or Formvar grids were similar [19]. Another variable factor to consider is that the temperature of the glass slides may change as a function of deposition rate. Although the substrate temperature was not monitored during vapor deposition, only a slight change in temperature is expected considering the separation distance, 12 cm, between the source and the substrate. The pressure in the work chamber of the deposition instrument remained fairly constant throughout the depositions suggesting that the temperature did not fluctuate substantially. Small variations in the temperature of the substrate initially at room temperature do not affect the surface morphology of the film. Studies that investigated the morphology of the films as a function of substrate temperature showed that the most pronounced particle changes occurred between 70-300 C [19]. In this study, it is highly improbable that the substrates were heated to these temperatures.

It is well established that the electronic properties of very thin films differ from that of the bulk material [32,33]. The extinction bands observed for island films are attributed to excitation of surface plasmons in the metal. The surface plasmon frequency is governed by the size, shape and interparticle spacing of the aggregates constituting the metal-island structures. Maximal absorption of electromagnetic radiation occurs when the plasmon frequency is coincident with the irradiation frequency, as described by the classical Maxwell-Garnett theory [34] for the optical properties of silver-island films. This theory predicts that the extinction band of a film composed of isolated silver particles should occur in the blue region of the electromagnetic spectrum. However, films deposited at the fastest rate do not display a maximum. Instead, the extinction increases continuously and levels off in the red region of the spectrum. Broadening of maxima results from contact between the individual surface particles, as indicated by the TEM results for the 5.00 Å/sec film. Similar results were observed in previous studies relating the thickness of metal films to their optical properties [19].

In summary, qualitative information relating to the surface morphology of silver-island films prepared with various rates of deposition can be obtained readily from the

optical spectrum. The structure, homogeneity, and distribution of particles is related to the extinction maximum and bandwidth of the film.

### Zinc Tetraphenylporphine Optical/SERRS Investigations

To determine the effects of adsorbed zinc tetraphenylporphine (ZnTPP) on the electronic properties of silver-island films, an extinction spectrum was recorded for a 50 Å film that had been deposited at 0.05 Å/sec. Next, ZnTPP was adsorbed on the film by dipping it into a  $10^{-4}$  M solution of the porphyrin in acetone. The electronic spectra of the bare silver film and the ZnTPP-coated film are shown in Figure 3A. As evident from this figure, the optical properties of the silver film are altered by the presence of the adsorbed compound. The extinction of the ZnTPP-coated silver film is greater and is red-shifted relative to the bare substrate. Structure is also present in the band envelope when ZnTPP is present, with four peaks at approximately 440 nm, 540 nm, 580 nm and 610 nm. The changes in the optical properties of the adsorbate/film system are not due to residual solvent on the film. The extinction maximum of a 50 Å silver-island film submerged in acetone was shifted towards the blue and was decreased in magnitude as a result of the solvent dielectric properties

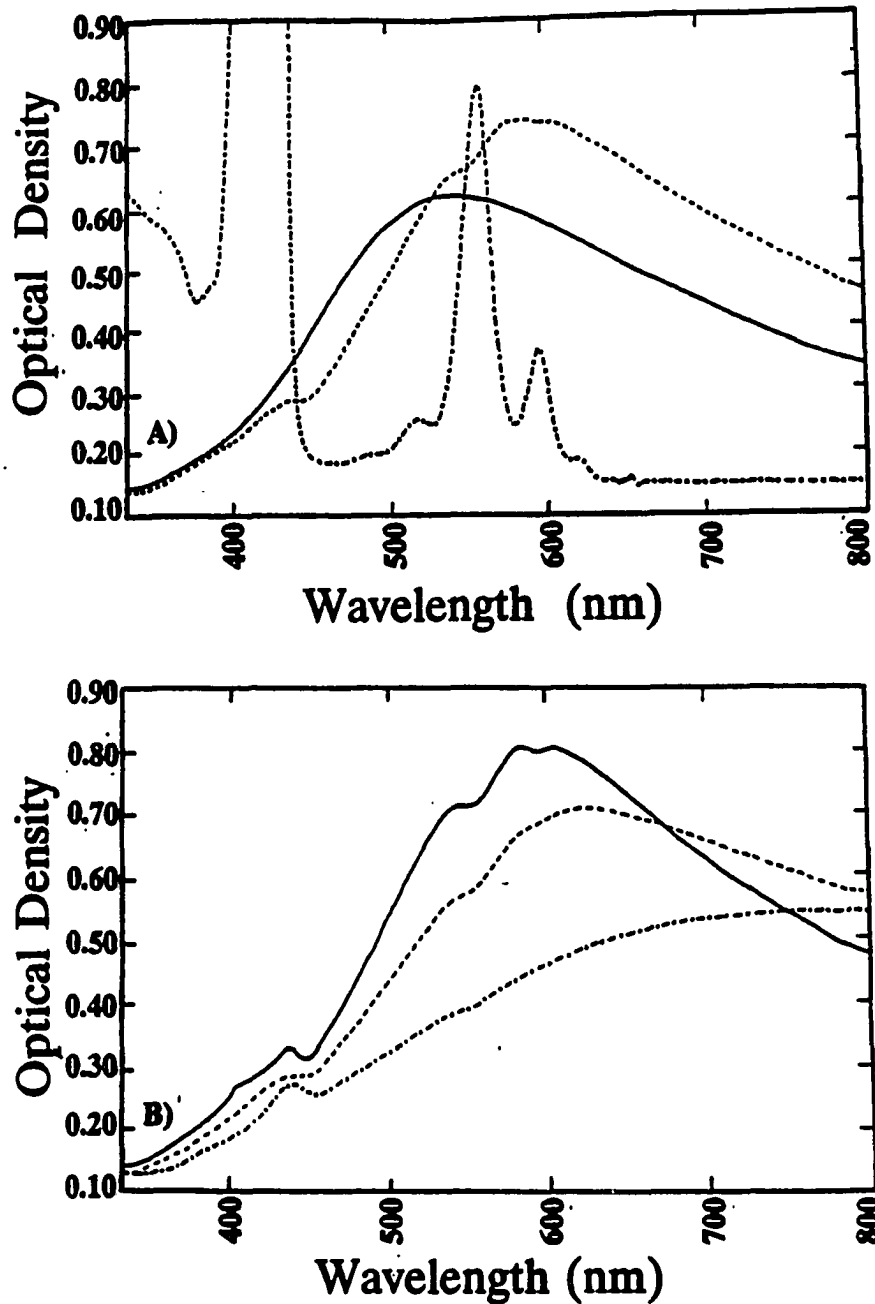


Figure 3. Electronic extinction spectra of 50 Å silver-island films. A) Films deposited at 0.05 Å/sec, uncoated (solid line); coated with ZnTPP (dashed line); and electronic absorption spectrum of  $10^{-5}$  M ZnTPP solution (dashed/dotted line). B) Films deposited at varying rates of silver deposition and coated with ZnTPP: 0.03 Å/sec (solid line); 0.33 Å/sec (dashed line); and 5.00 Å/sec (dashed/dotted line).

[35]. Moreover, the spectrum of the ZnTPP-coated film is not the composite of the silver film and the ZnTPP optical spectrum. The latter is characterized by a strong Soret band near 418 nm (off scale in the figure because of its strong absorbance relative to the Q bands) and Q bands located between 500 and 600 nm. In Figure 3A the dye absorption maxima coincide with minima in the extinction envelope of the ZnTPP/island film.

The structure (depth of minima) in the spectrum of the ZnTPP/film is dependent upon the deposition parameters. Figure 3B shows absorption spectra of films deposited at 0.03, 0.33, and 5.00 Å/sec containing adsorbed ZnTPP. As the rate of silver evaporation is decreased, the splitting within the extinction envelope becomes more distinct. Previous investigators [20] studied the optical properties of rhodamine B/island films as a function of increasing silver film thickness prepared with a constant deposition rate of approximately 2 Å/sec. Their results indicated that the spectrum of the dye-coated film was dependent upon the degree of overlap of the dye spectrum with that of the films. Extensive splitting of the plasmon resonances resulted for films ranging between 7 and 69 Å in thickness. It was concluded that coupling occurs between the adsorbate electronic states with the surface plasmon resonances in the island film. When the film thickness was outside this range

the absorbance overlap with the dye was minimal and the spectra were a composite of the dye and film absorbance. It was also shown that the splitting was affected by the nature of the adsorbate and the surface coverage [36]. Similarly, our films prepared at the fastest deposition rate do not exhibit extensive splitting because the overlap between the absorption bands of the adsorbate and the plasmon resonances of the substrate is minimal. With slower evaporation rates, the overlap is greater and a splitting is observed in the extinction spectrum. The frequency shifts and splitting displayed by the dye-coated metal films are fully rationalized by electromagnetic theory [35,37-39].

In order to determine the relationship between the evaporation rate and the optical spectra of the island film substrates, the optical density of the substrates was correlated with the rate of deposition. Silver films were prepared at different evaporation rates while maintaining all other deposition parameters including the average silver thickness (50 Å) constant. Immediately following the deposition procedure, the films were dipped into a  $10^{-4}$  M solution of ZnTPP for 1 min. The films were removed from solution and an absorption spectrum was recorded. Figure 4 is a plot of optical density at 514 nm as a function of the deposition rate. The solid line was obtained by a least square fit of the experimental data points. As can be seen

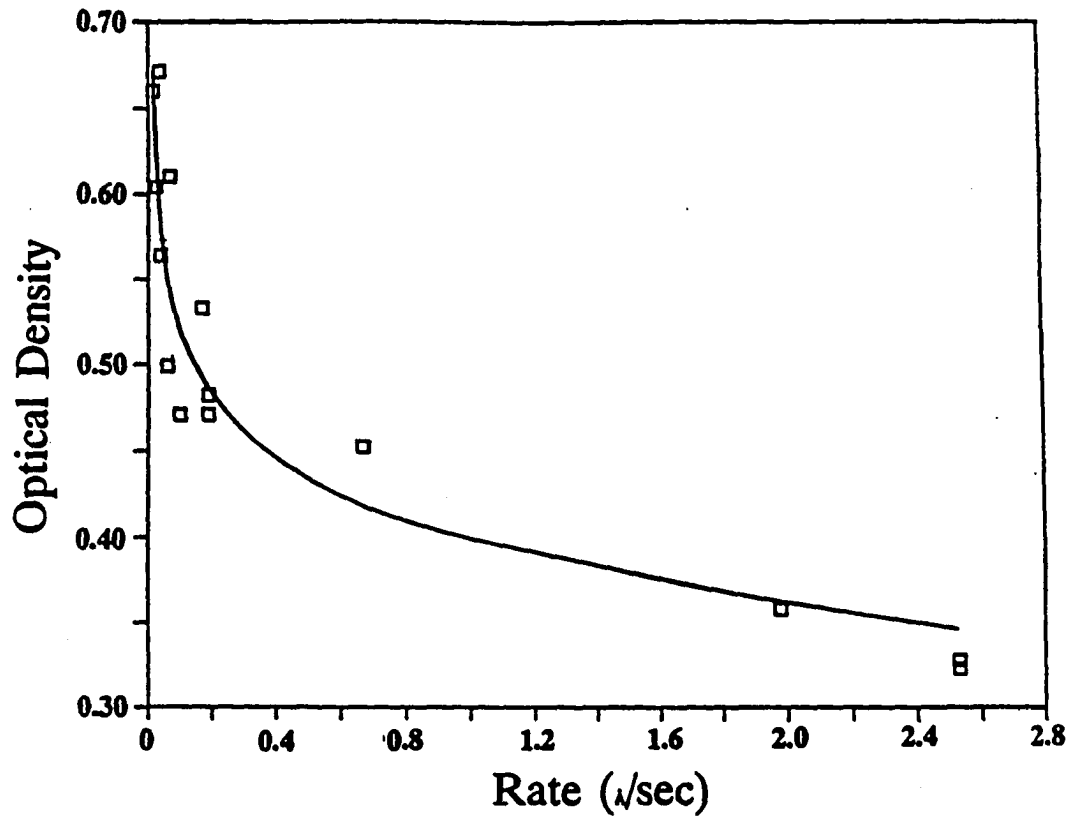


Figure 4. Plot of optical density of 50 Å silver-island film coated with ZnTPP vs rate of silver deposition. Optical density measured at 514 nm.

from the plot, the extinction decreases exponentially with increasing evaporation rates up to 0.6 Å/sec, at which point the extinction decreases only slightly.

The dye-coated films were examined next to determine the effect of the deposition rate on the ZnTPP SERRS intensity. All spectra were acquired with the same slit settings and laser power (50 mW). The 514.5 nm Ar<sup>+</sup> line was chosen as the excitation wavelength for two reasons. First, this laser frequency is coincident with an electronic transition in ZnTPP and produces resonance Raman scattering. Second, the optical properties of the films were correlated with the deposition rates at this wavelength. Figure 5 shows SERRS spectra of ZnTPP adsorbed on films prepared at several deposition rates. In all of the spectra, the band frequencies and relative intensities are the same, but the overall intensity of the spectra differ markedly.

The quantitative relationship between the intensity of the SERRS signals and the rate of evaporation is displayed in Figure 6A. This graph was generated by plotting the magnitude of the ZnTPP 1356 cm<sup>-1</sup> band against the deposition rate for each of the dye-coated films. The data points were fitted to an exponential (solid curve) by using a least squares procedure. The most intense SERRS spectra were observed from ZnTPP on silver films prepared with deposition rates below ca. 0.05 Å/sec while the weakest signals were

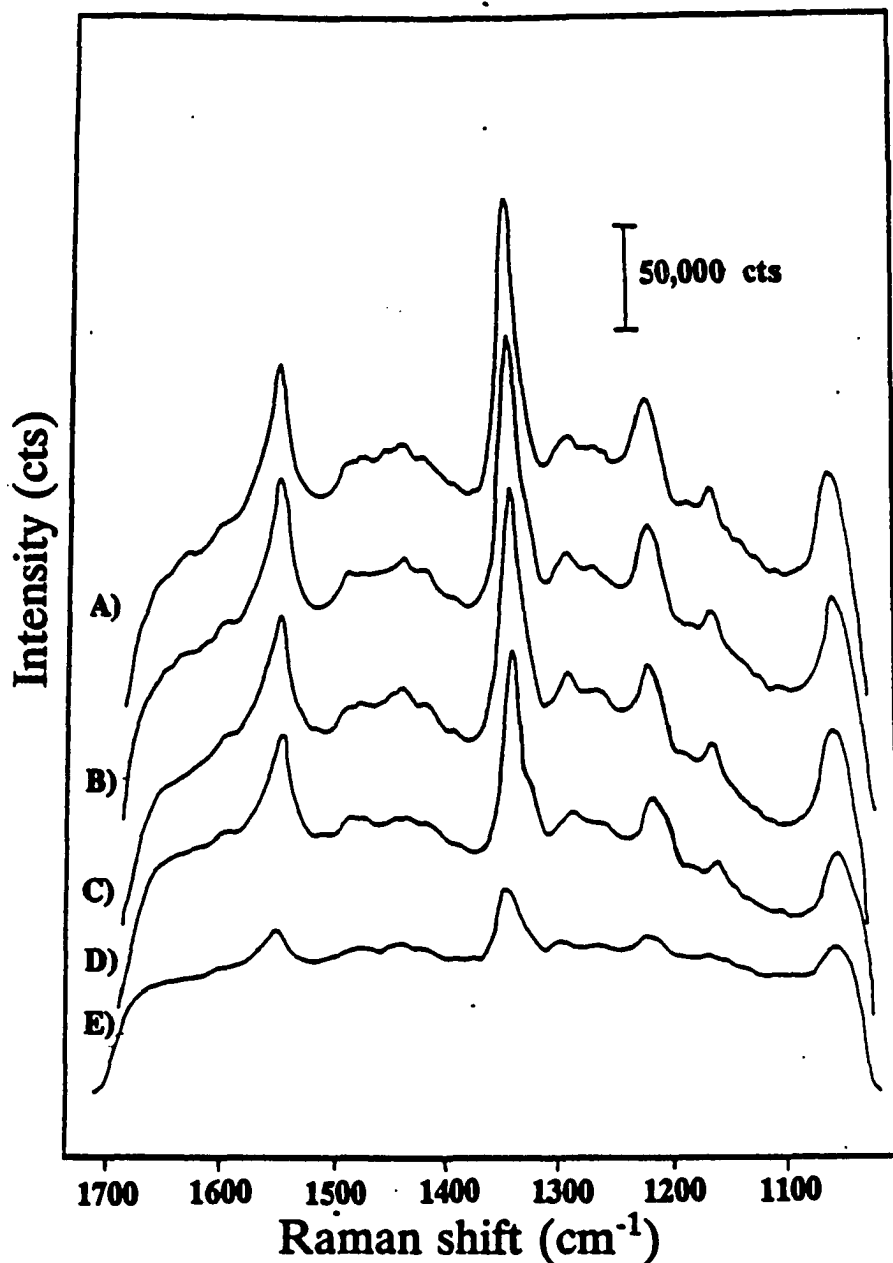


Figure 5. SERRS spectra of ZnTPP adsorbed onto 50 Å silver-island films prepared with varying rates of silver deposition: A) 0.02 Å/sec; B) 0.04 Å/sec; C) 0.07 Å/sec; D) 0.20 Å/sec; E) 2.50 Å/sec. The laser excitation wavelength was 514.5 nm.

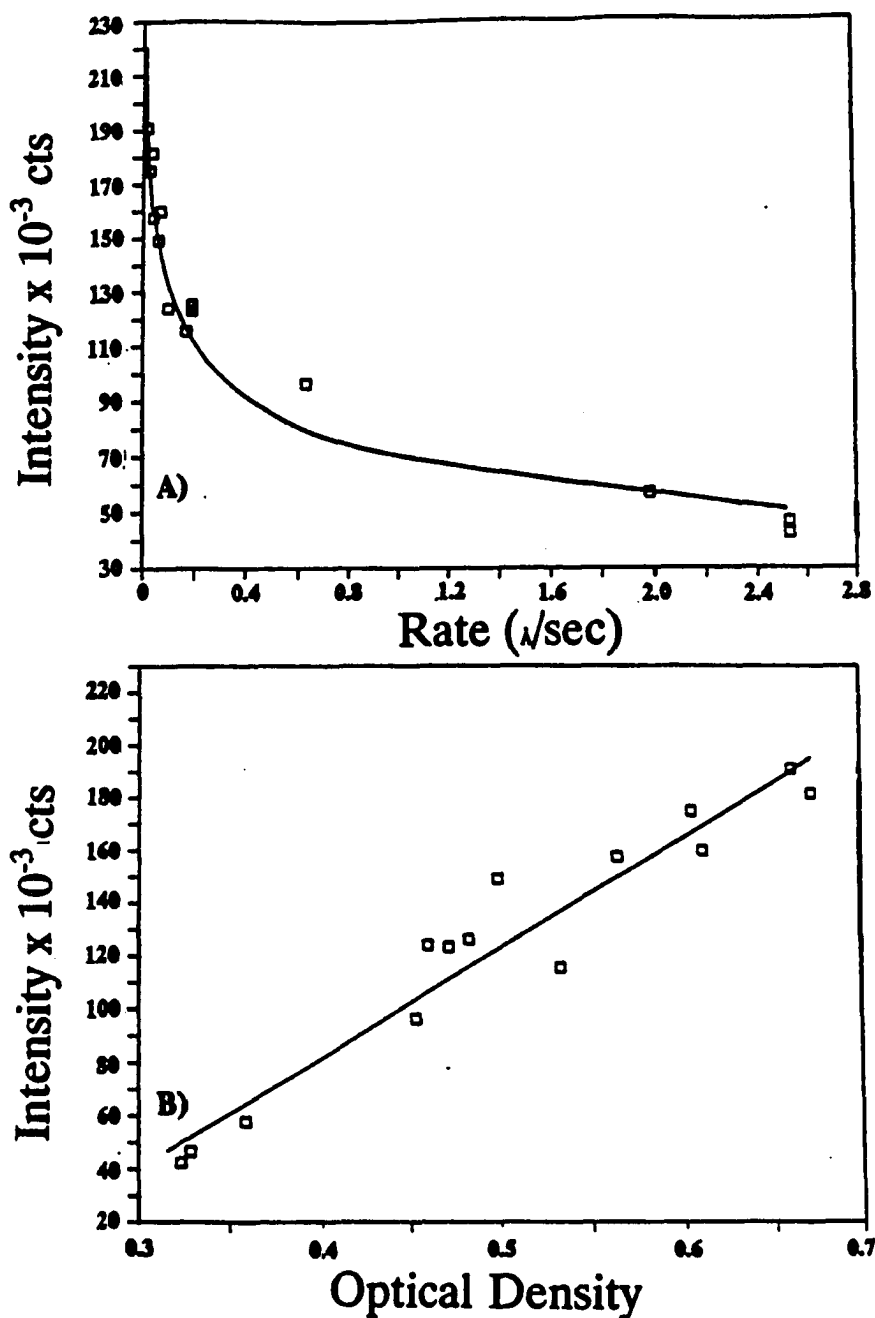


Figure 6. Relationship between SERRS intensity and deposition rate/optical density: A) intensity of the  $1356\text{ cm}^{-1}$  ZnTPP band vs rate of silver deposition; B) intensity of the  $1356\text{ cm}^{-1}$  ZnTPP band vs optical density at  $514\text{ nm}$ . The silver film thickness was  $50\text{ \AA}$  in all cases.

observed from films prepared with deposition rates greater than 2.5 Å/sec.

A comparison of Figure 4 with Figure 6A shows that the exponential relationship between the deposition rate and the extinction properties of the films is similar to that between the deposition rate and the SERRS intensities of ZnTPP. Thus, to substantiate the dependence of the observed SERRS intensities on plasmon excitation, the magnitude of the ZnTPP  $1355\text{ cm}^{-1}$  band intensity is plotted against the film extinction at 514.5 nm in Figure 6B. The positive linear correlation between these two variables is consistent with an EM mechanism for the enhancement process. It is well documented that SERS/SERRS excitation profiles of a number of compounds adsorbed onto thin metal films correlate with the optical spectrum of the adsorbate/film system. As noted above, this response is attributed to surface plasmons generated by the interaction of incident photons with the metal film. The local fields external and internal to the islands are amplified due to the excitation of the plasmons causing the enhancement of the Raman signals and the absorption, respectively. Experimental results verify both qualitatively and quantitatively the interrelationship between the SERS/SERRS effect and the optical properties of the adsorbate/substrate system as predicted from EM theory [22-24,40].

A definite maximum is not observed in the SERRS intensity or extinction plots. However, this type of relationship is not expected for films prepared with varying deposition rates and a constant silver thickness. Because the structure of the particles is dependent upon migration of the atoms incident on the substrate within a given time period, a limiting deposition rate should result, below which slower deposition rates should have no further effect on surface morphology. Consequently, the plots should flatten at very slow evaporation rates in a manner analogous to that observed at rapid deposition rates.

The above results do not imply that slowly deposited films exhibit the most intense SERRS spectra at all excitation wavelengths. Rather, the data indicate that the rate of evaporation must be considered when the particle resonances are affected as characterized by their optical properties. In the above results, the surface plasmon resonance at 514 nm is highly dependent upon the rate of deposition. To examine the effect on the deposition rate of the electronic properties of the films at other excitation wavelengths, spectra were recorded using 457.9 nm and the 406.7 nm excitation. Figure 7 depicts the SERRS spectra obtained from ZnTPP/silver films using 457.9 nm excitation. Although the ZnTPP band frequencies and relative intensities are comparable for films prepared with different deposition

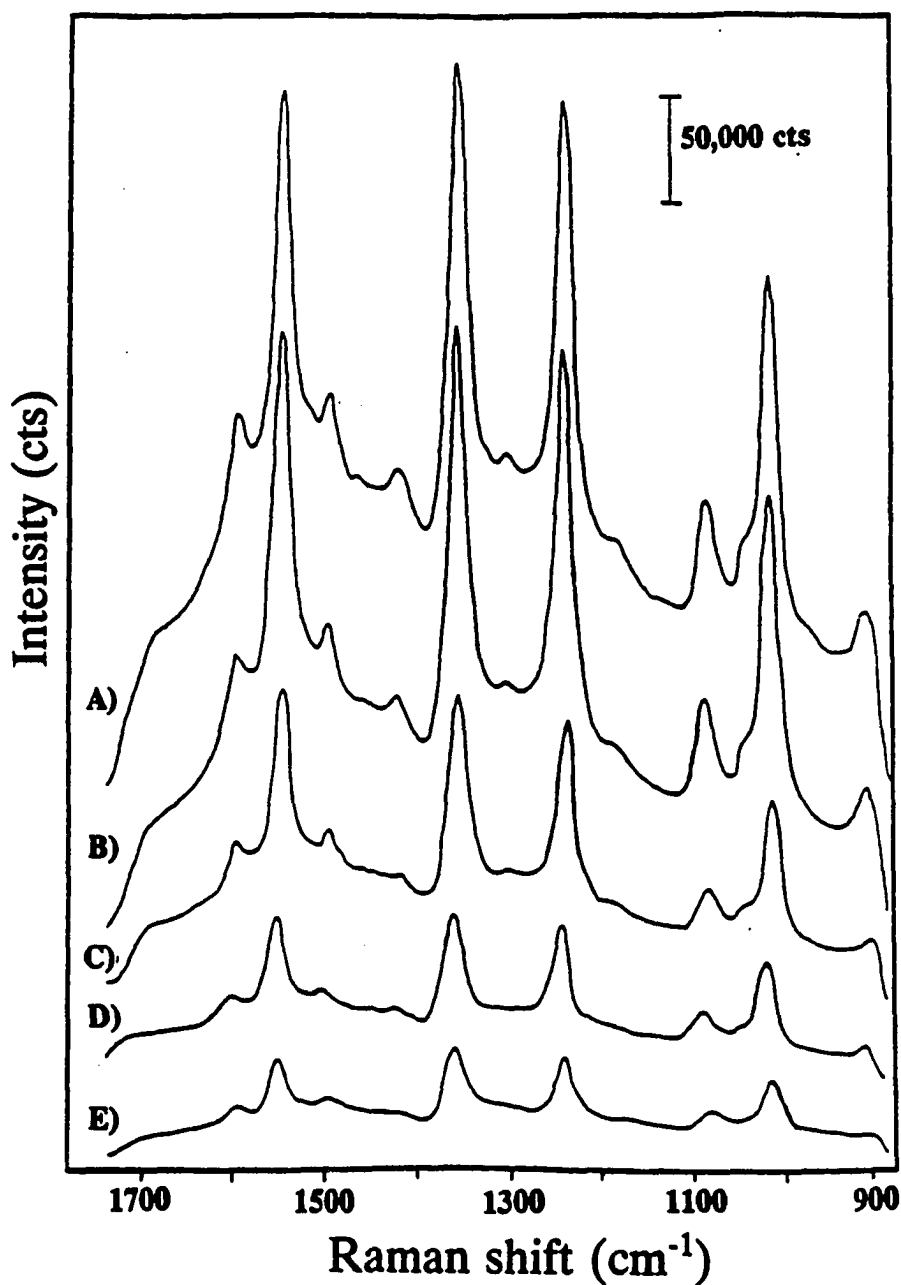


Figure 7. SERRS spectra of ZnTPP adsorbed onto 50 Å silver-island films prepared with varying rates of silver deposition: A) 0.02 Å/sec; B) 0.04 Å/sec; C) 0.08 Å/sec; E) 2.50 Å/sec. The laser excitation wavelength was 457.9 nm.

rates, the SERRS enhancement is strongly affected by the rate of silver evaporation. As with 514.5 nm excitation, a plot of the extinction at 456 nm versus the intensity of the SERRS signals indicates a linear relationship.

In contrast to the results obtained with 514.5 or 457.9 nm excitation, neither the optical properties nor the intensity of SERRS spectra obtained with 406.7 nm excitation varied substantially with changes in the film deposition rate. This latter result suggests that SERRS enhancement is relatively constant because the distribution of particles with plasmon resonances at this wavelength is approximately the same for all of the deposition rates. The magnitude of the enhancement is probably quite small at this wavelength and most of the intensity results from resonance Raman scattering. As can be seen from the absorption spectrum, 406.7 nm is within the intense Soret transition of the porphyrin.

#### **4,4'-Bipyridine Optical/SERS Investigations**

The effect of silver deposition rate on the extinction spectra and the Raman intensity was also investigated for a nonresonantly-enhanced molecule, 4,4'-bipyridine (BP), adsorbed on silver films. Although BP does not have an electronic transition in close proximity to the surface

plasmon resonance of the film, adsorption of BP does affect the optical properties of the metal films, as shown in Figure 8. The solid curve was obtained from a 50 Å film prepared with a deposition rate of 0.04 Å/sec, whereas the dashed curve is the spectrum after BP was adsorbed from a  $10^{-3}$  M acetone solution. In the latter, the extinction maximum is shifted to the red and increased relative to the bare film. No splitting or structure is evident in the envelope in contrast to that observed for ZnTPP/films. The silver film spectrum is changed because of the dielectric properties of the adsorbed BP [35]. When more dilute BP solutions were used in the dipping procedure, the optical response of the film was not as strongly perturbed.

The BP SERS intensity is dependent upon the silver film deposition rate, as evident from Figure 9. As in the case of ZnTPP, the strongest spectrum originates from the film prepared with the slow deposition rate. An exponential relationship between film deposition rate and extinction of the BP/silver film or the SERRS intensity was also observed (data not shown). Figure 10 illustrates the linear relationship between the intensity of the  $1293\text{ cm}^{-1}$  band and the extinction of the BP/silver-island films. Additional SERS and optical studies performed with BP/silver-island films in the 406 nm region showed that the rate of silver

deposition did not greatly influence the intensity of the Raman signals nor the extinction values.

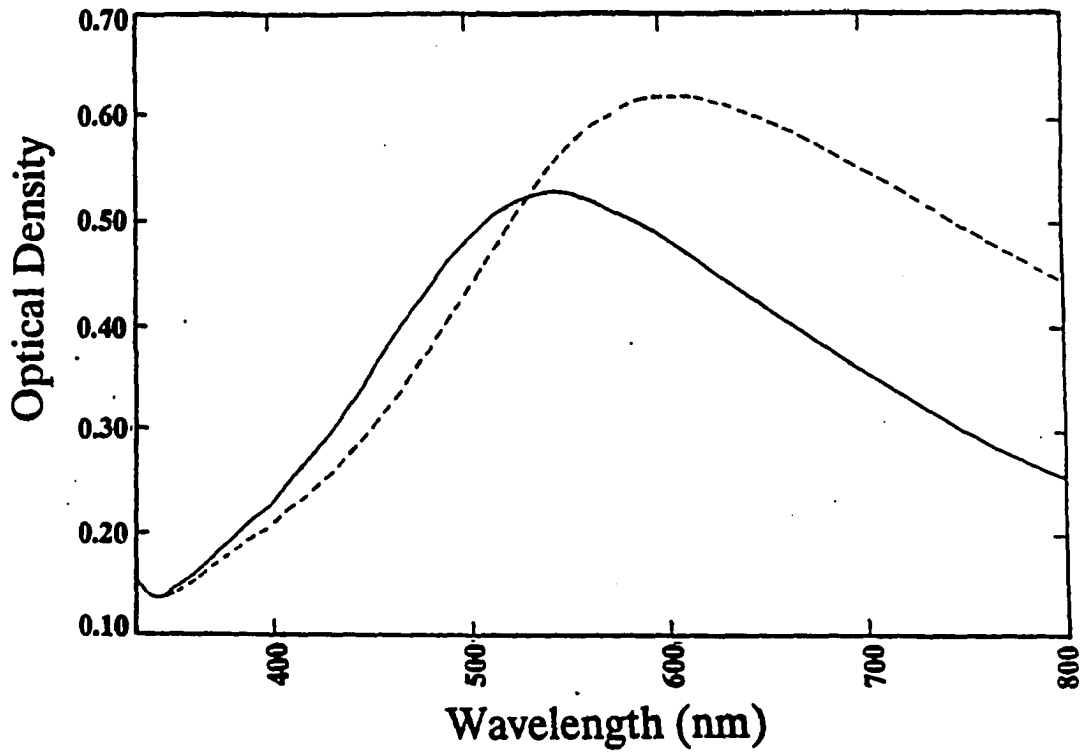


Figure 8. Electronic extinction spectra of 50 Å silver-island films prepared with a rate of silver deposition of 0.04 Å/sec: uncoated (solid line); coated with BP (dashed line).

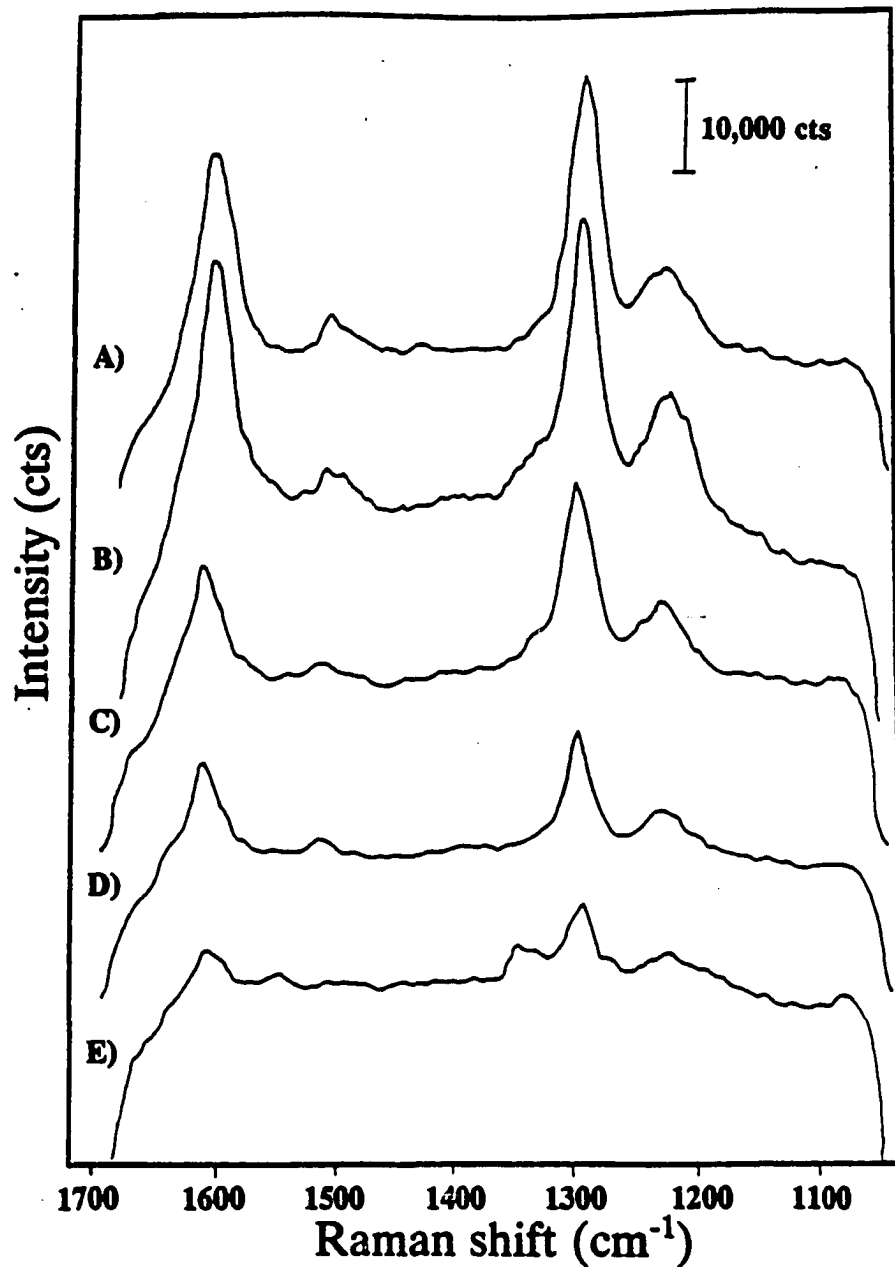


Figure 9. SERRS spectra of BP adsorbed onto 50 Å silver-island films prepared with varying rates of silver deposition: A) 0.05 Å/sec; B) 0.22 Å/sec; C) 0.68 Å/sec; D) 2.00 Å/sec; E) 4.17 Å/sec. The laser excitation wavelength was 514.5 nm.

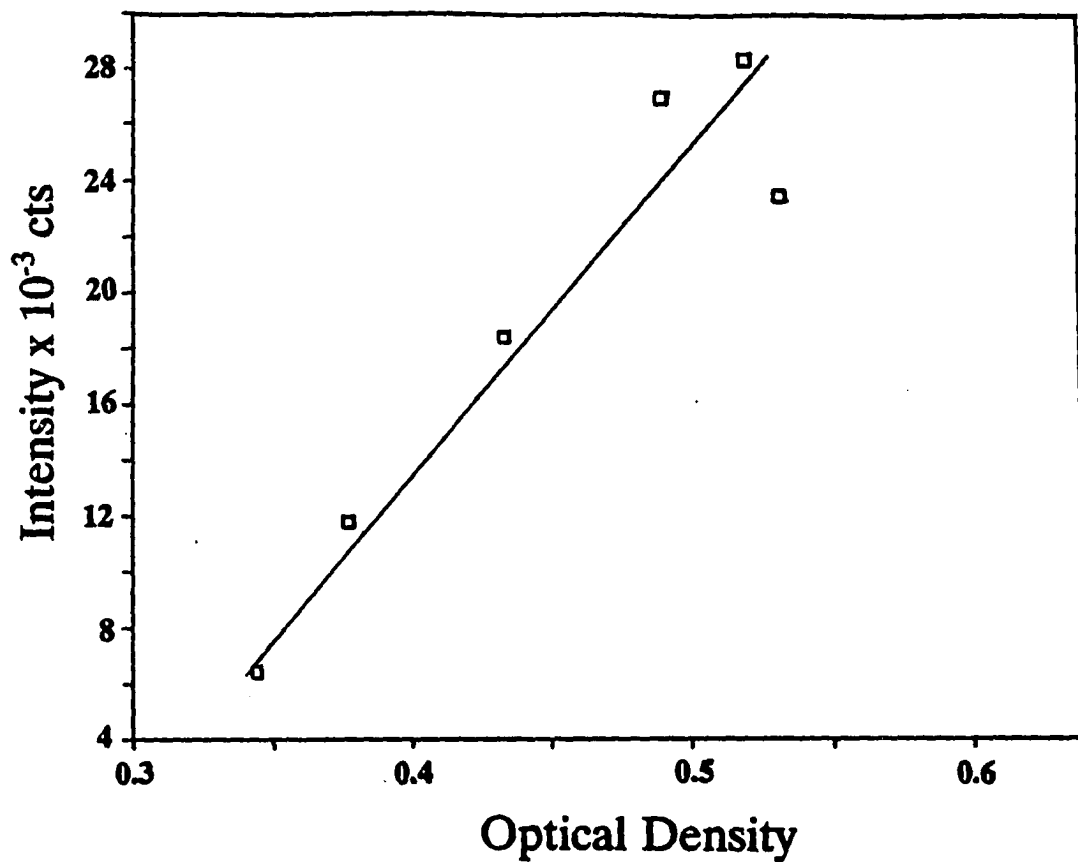


Figure 10. SERS intensity of the 1293 cm<sup>-1</sup> band vs optical density of 50 Å silver-island films at 514 nm. Films were prepared with deposition rates given in Figure 9.

**CONCLUSIONS**

This is the first investigation that quantitatively relates the silver deposition rate, optical properties and SERS/SERRS signals. The results demonstrate that the rate of silver film deposition has the same effect on the optical properties and Raman intensity for both SERS and SERRS. The deposition rate influences the morphology of the particles composing the metal film which, in turn, determines the optical properties of the films and enhancement of the SERS/SERRS signals. In order to prepare silver-island films that elicit optimal and reproducible SERS/SERRS signal intensities, the rate of deposition must be carefully controlled.

**ACKNOWLEDGEMENTS**

The authors are grateful for the support of the National Institutes of Health (GM 35108). Therese M. Cotton is the recipient of a NIEHS Career Development Award (ES10069). We thank Dr. Bernard Rospendowski for his careful reading of the manuscript and his many helpful comments.

## LITERATURE CITED

1. Jeanmaire, D. L., Van Duyne, R. P. J. Electroanal. Chem. 1977, 84, 1.
2. Albrecht, M. G., Creighton, J. A. J. Am. Chem. Soc. 1977, 99, 5215.
3. Chang, R. K., Furtak, T.E., Eds.; Surface-Enhanced Raman Scattering, Plenum: New York, 1982.
4. Otto, A. In Light Scattering in Solids, Cardona, M., Guntherodt, G., Eds.; Springer-Verlag: New York, 1984; Vol. 4, pp 289-418.
5. Van Duyne, R. P. In Chemical and Biological Applications of Lasers, Moore, C. B., Ed.; Academic Press: New York, 1979; Vol. 4, pp 101-185.
6. Wokaun, A. In Solid State Physics, Academic Press: New York, 1984; Vol. 38, pp. 223-294.
7. Garrell, R. Anal. Chem. 1989, 61, 401A.
8. Kaul, B. B., Holt, R. E., Schlegel, V. L., Cotton, T. M. Anal. Chem. 1988, 60, 1580.
9. Enlow, P. D., Buncick, M., Warmack, R. J., Vo-Dinh, T. Anal. Chem. 1986, 58, 1119.
10. Vo-Dinh, T., Hiromato, M. Y. K., Begun, G. M., Moody, R. L. Anal. Chem. 1984, 56, 1667.
11. Tran, C. D. Anal. Chem. 1984, 56, 824.
12. Sandroff, C. J., Hershback, D. R. Langmuir

- 1985, 1, 131.
13. Feng, Q., Cotton, T. M. J. Phys. Chem. 1986, 90, 983.
  14. Chou, Y. C., Liang, N. T., Tse, W. S. J. Physique Coll. 1986, 17, 481.
  15. Koglin, E., Sèquaris, J. -M. J. Physique Coll. 1983, C10, 487.
  16. Sandroff, C. J., Garoff, S., Leung, K. P. Chem. Phys. Lett. 1983, 96, 547.
  17. Ervin, K. M., Koglin, E., Séquaris, J. -M., Valenata, P., Nürnberg, H. W. J. Electroanal. Chem. 1980, 114, 179.
  18. Cotton, T. M. In Spectroscopy of Surfaces, Clark, R. J. H., Hester, R. E., Eds.; John Wiley & Sons: New York, 1988; Vol. 16, pp 91-153.
  19. Sennett, R. S., Scott, G. D. J. Opt. Soc. Am. 1950, 40, 203.
  20. Glass, A. M., Liao, P. F., Bergman, J. G., Olson, D. H. Opt. Lett. 1980, 5, 203.
  21. Bergman, J. G., Chemla, D. S., Liao, P. F., Glass, A. M., Pinczuk, A., Hart, R. M., Olson, D. H. Opt. Lett. 1981, 6, 33.
  22. Weitz, D. A., Garoff, S., Gramila, T. J. Opt. Lett. 1982, 7, 168.
  23. Yamada, H., Nagata, H., Kishike, K. J. J. Phys. Chem. 1986, 90, 818.

24. Weitz, D. A., Garoff, S., Gerstan, J. I., Nitzan, A. J. Chem. Phys. 1983, 78, 5324.
25. Murray, C. A., Bodoff, S. Phys. Review B. 1985, 32, 671.
26. Kim J. -H., Uphaus, R. A., Cotton, T. M., Mobius, D. J. Phys. Chem. 1989, 93, 3713.
27. Zeman, E. J., Carron, K. T., Schatz, G. C., Van Duyne, R. P. J. Chem. Phys. 1987, 87, 4189.
28. Fornari, B., Mattei, G., Pagannone, M. J. Vac. Sci. Technol. A 1988, 6, 167.
29. Garoff, S., Stephens, R. B., Handon, C. D., Granilla, T. J., Sorenson, G. K. Opt. Commun. 1982, 41, 257.
30. Lennard-Jones, J. E. Trans-Faraday Soc. 1932, 28, 333.
31. Appleyard, E. T. S. Proc. Phys. Soc. 1937, 49, 118.
32. Roward, P., Bouquet P. In Progress of Optics, Wolf, E. Ed.; North Holland Publ.: Amsterdam, 1965.
33. McCarthy, S. L. J. Vac. Sci. 1976, 13, 135.
34. Maxwell-Garnett, J. C. Phil. Trans. Roy. Soc. 1904, 203A, 385.
35. Kotter, Z., Nitzan, A. J. Phys. Chem. 1982, 86, 2011.
36. Garoff, S., Weitz, D. A., Gramila, T. J., Hanson, C. D. Opt. Lett. 1981, 6, 245.
37. Craighead, H. G., Glass, A. M. Opt. Lett. 1981, 6, 248.
38. Garoff, S., Stephens, R. B., Hanson, C. D., Sorenson, G. K. Opt. Commun. 1982, 41, 257.

39. Eagen, C. F. Appl. Opt. 1981, 17, 3035.
40. Wetzell, H., Gericher, H. Chem. Phys. Lett. 1980, 76,  
460.

**PAPER IV APPLICATION OF SURFACE-ENHANCED RESONANCE RAMAN  
SCATTERING SPECTROSCOPY TO THE ANALYSIS OF  
COVALENTLY MODIFIED ELECTRODE SURFACES.**

**ABSTRACT**

Surface-enhanced resonance Raman scattering (SERRS) spectroscopy has been applied to the analysis of chemically modified surfaces. The compounds 2,4,6 trinitrobenzene-sulfonic acid (TNBS),  $[\text{Ru}(\text{bpy})_2(\text{i-nic})_2][\text{PF}_6]_2$  (bpy = 2,2'-bipyridyl, i-nic = isonicotinic acid), and 2-[(4-hydroxyphenyl)azo]benzoic acid (HABA) were covalently bonded to a  $\text{SnO}_2$  surface through an aminesilane linking group. Strong SERRS spectra of the covalently bound compounds were obtained following silver deposition (by vacuum or chemical procedures) onto the derivatized  $\text{SnO}_2$  surfaces. The optimal thickness of the overlaid silver film for maximal SERRS effect was determined to be about 50 Å. Under these conditions, it was possible to detect submonolayer (<10% in the case of ruthenium complex) amounts of the chemically bonded species. In the case of HABA derivatized  $\text{SnO}_2$  it was demonstrated that SERRS can provide structural information about the covalently attached species. The technique was also successfully utilized to monitor changes in the SERRS spectrum during in situ electrochemical reduction of the  $\text{NO}_2$  group in TNBS which was covalently attached to the  $\text{SnO}_2$  surface. The advantages and disadvantages of the SERRS technique as applied to the analysis of chemically modified surfaces are discussed.

## INTRODUCTION

Chemically modified electrodes (CMEs) have attracted considerable attention. These devices combine the sensitivity and simplicity of electrochemical procedures with the added specificity imparted by the associated modifying agent. A recent review [1] describes the application of CMEs as analytical tools and the current interest in this area. The potential for novel approaches to the solution of a range of analytical problems through the application of CMEs is considerable. Undoubtedly CMEs will continue to attract widespread interest as new preparative procedures are developed and as new applications are reported.

Concurrent with the development of new types of CMEs, the demand for methods of characterization of these devices has become increasingly important. An "ideal" method should provide information regarding the types and quantities of surface functionalities present, describe the mode and orientation of surface binding, allow in situ analysis of the surface, and provide sufficient sensitivity to observe submonolayers of coverage and their distribution. At present no single surface technique can simultaneously meet all of these requirements. Techniques that have been used to characterize the CMEs include electron microscopy and

various types of spectroscopy, such as UV-vis spectroelectrochemistry, infrared, Raman, fluorescence, X-ray photoelectron spectroscopy (XPS), and Auger electron spectroscopy (AES). Conventional electrochemical techniques such as cyclic voltammetry (CV) and differential pulse voltammetry (DPV) have also been extensively used. Karweik et al. describe the prospects for the successful application of these techniques alone and in combination to the analysis of CMEs [2]. Other techniques that have been applied include photoacoustic and photothermal spectroscopy, reflectance spectroscopy, elemental analysis, secondary-ion mass spectrometry, inelastic tunneling spectroscopy, and radiolabeling. Applications of these techniques are further discussed in a review by Murray [3]. Difficulties associated with the applications of current analytical methods to CMEs include the requirement for ultrahigh vacuum procedures in XPS and AES, the lack of adequate sensitivity in the case of many optical methods, and the inability to perform in situ analysis in many cases.

Surface-enhanced Raman scattering (SERS) and surface-enhanced resonance Raman scattering (SERRS) techniques have several advantages for the analysis of surfaces. These techniques have been shown to provide highly sensitive methods (submonolayer coverages [4]) for the characterization of species adsorbed to metal electrodes

[5], metal colloids [6], metal-island films [7,8], and chemically deposited silver films [9]. Although the enhancement effect has been documented primarily on Ag, Cu, and Au surfaces, SERS/SERRS has been successfully applied to the characterization of other materials following the application of a thin silver overlayer to produce surface enhancement [10]. Very recently Davies *et al.* have extended the SERS technique to sputter-deposited silver on Pt, graphite, alumina, and filter paper [11] and also to the underpotential deposited Hg, Tl, Pb, Pt, and Pd on gold electrodes [12,13]. Two other important advantages, in addition to the excellent sensitivity provided by SERS/SERRS, include the ability to obtain detailed structural information about the surface from the vibrational spectrum and to perform the analysis in situ.

We report herein the first application of SERRS to the analysis of covalently modified SnO<sub>2</sub> electrodes. The covalent attachment of [Ru(bpy)<sub>2</sub>(i-nic)<sub>2</sub>][PF<sub>6</sub>]<sub>2</sub>, 2,4,6-trinitro-benzenesulfonic acid (TNBS), and 2-[(4-hydroxyphenyl)azo]benzoic acid (HABA) was performed by published procedures and the electrodes were coated with a 50 Å thin film of silver, using chemical or vacuum deposition procedures. Optimization of the silver thickness was performed for the Ru complex and the limits of detection were determined. The results demonstrate that the

application of SERRS to the analysis of CMEs offers an additional advantage to those cited above in the simplicity of the experimental method. Other merits and limitations of the technique are discussed further below.

**EXPERIMENTAL****Materials and Preparation of Modified Electrode Surfaces****Materials**

Tin oxide coated glass (PPG Industries) used in the electrode construction was a generous gift from Professor R. W. Murray. [3-[(2-Aminoethyl)amino]propyl]trimethoxysilane (en-silane, Petrarch Systems, Inc.) was vacuum distilled twice and stored under nitrogen. Toluene and tetrahydrofuran (THF) were distilled from sodium benzophenone ketyl and acetonitrile was distilled from calcium hydride under nitrogen. The solvents were degassed by nitrogen bubbling for  $\approx 0.5$  h prior to use. 2,4,6-Trinitrobenzenesulfonic acid (TNBS, Aldrich), [2-(4-hydroxyphenyl)azo]benzoic acid (HABA, Aldrich), and 1,4-dicyclohexylcarbodiimide (DCC, Aldrich) were used without further purification.  $[[\text{Ru}(\text{bpy})_2(\text{i-nic})_2][\text{PF}_6]_2$  (bpy = 2,2'-bipyridyl, i-nic = isonicotinic acid) was prepared as described by Abruna et al. [14]. The silver used in the metal vapor deposition was 99.99% pure and was obtained from D. F. Goldsmith Corp. Silver nitrate was purchased from Mallinckrodt, Inc.

### Electrode Pretreatment

The tin oxide coated glass was cut into  $\approx 0.8$  cm squares. The freshly cut specimens were extracted with heptane to remove any surface contamination. The electrode were next treated with hot concentrated HCL for 4 h followed by copious washing with distilled water and anhydrous ethanol and dried in vacuo before silylation.

### Silylation of SnO<sub>2</sub>

Vacuum-dried pieces of SnO<sub>2</sub>-coated glass were reacted with a 5 % solution of [3-[(2-aminoethyl)amino]-propyl]trimethoxysilane in refluxing dry toluene under a nitrogen atmosphere. The electrodes were dried under vacuum and stored under nitrogen atmosphere until further derivatized by one of the procedures described below.

### Derivatization with TNBS

The silanized electrodes were reacted with a dilute aqueous solution of TNBS (0.5%) for 2 h. The yellow color of the chromophore that is produced upon reaction of TNBS with amines could be seen by visual inspection of the electrodes. The electrodes were washed several times with distilled water over a period of 6 h and air-dried.

### Derivatization with Ru Complex

The silanized electrodes were placed in septa-capped vials and purged with nitrogen. They were washed twice with dry acetonitrile and then reacted with 10 mL of a solution containing 28 mg of  $[\text{Ru}(\text{bpy})_2(\text{i-nic})_2][\text{PF}_6]_2$  of DCC in dry acetonitrile for 24 h at room temperature. After the reaction, the electrodes were washed with several portions of dry acetonitrile and acetone over a period of 24 h to remove any adsorbed, unreacted compound. The derivatized electrodes were dried in a stream of nitrogen gas prior to the SERRS experiments.

### Derivatization with HABA

The silanized  $\text{SnO}_2$  electrodes were allowed to react with a solution of 3.6 mg of HABA and 4.5 mg of DCC in 5 mL of dry THF for 48 h at room temperature. After the reaction, the electrodes were washed six times with THF followed by six washes with acetone over a period of 24 h. The electrodes were dried in a stream of nitrogen prior to the SERRS experiments.

### Silver Deposition

The modified  $\text{SnO}_2$  electrodes were coated with thin films of silver by either vacuum or chemical deposition procedures. In the former, the silver overlayers was

deposited to a thickness of 50 Å at a pressure of  $<1.5 \times 10^{-6}$  Torr and a rate of 0.5-0.8 Å/s. The chemical deposition procedure using Tollen's reagent was performed as described by Ni and Cotton [9]. Tollen's reagent was prepared in a small beaker by adding 10 drops of fresh 5% NaOH to 10 mL of 2% AgNO<sub>3</sub> solution, resulting in a dark brown AgOH precipitate. The precipitate was redissolved by dropwise addition of NH<sub>4</sub>OH. The clear Tollen's reagent was cooled in an ice bath and the TNBS derivatized SnO<sub>2</sub>/en-silane electrode was immersed in the solution. Three milliliters of a 10% D-glucose was added to the solution with careful swirling. The contents were allowed to warm to room temperature and then heated on a water bath (≈55 C) for 1 min, followed by sonication for 1 min, followed by sonication with distilled water, again sonicated in distilled water for 30 sec, and air-dried prior to the SERRS experiment.

### **Characterization of Modified Electrode Surfaces**

#### **Instrumentation**

Vacuum deposition of silver metal vapor was performed by use of a commercial vacuum coating unit (Edwards High Vacuum, Model E306A). Silver film thicknesses were measured by using a film thickness monitor with a quartz

piezoelectric crystal (Edwards High Vacuum, Model FTM4).

The SERRS spectra were obtained by using excitation from either an Ar<sup>+</sup> laser (INNOVA 90-5, Coherent, Inc.) or a Kr<sup>+</sup> laser (INNOVA 100-K3, Coherent, Inc.). The sample was irradiated in the backscattering configuration. The scattered radiation was collected and focused onto the entrance slits of a monochromator/spectrograph (Triplemate 1877). An intensified diode array detector (PARC 1420) was coupled to a multichannel analyzer (PARC OMA II) was used to accumulate and process the spectra. Indene was used for frequency calibration of all spectra.

#### SERRS Experiments

SERRS spectra were obtained by mounting and holding stationary the derivatized electrode containing the silver overlayer at the focal point of the collection optics. The 1200 grooves/mm grating ( $D^{-1} = 1.4 \text{ nm/mm}$ ) was used in the spectrograph stage. Multichannel averaging of 25 scans taken with 1-s integration time was used. No laser-induced degradation was observed.

The SERRS spectra from silver electrodes were obtained by using polycrystalline silver material. These were polished and electrochemically roughened as described previously [15]. Adsorption of the compound of interest was accomplished by placing the roughened electrode into the

solution at the desired adsorbate concentration at room temperature for 10-20 min. The electrode was then removed, rinsed with appropriate solvent, and air-dried. SERRS spectra were recorded as described for the SnO<sub>2</sub> electrodes.

#### Electrochemical Measurements

Electrochemical measurements were made with a BAS-100 electrochemical analyzer (Bioanalytical Systems, Lafayette, IN) by using a three-electrode system and a conventional cell. Square wave voltammetry (SWV) of the [Ru(bpy)<sub>2</sub>(i-nic)<sub>2</sub>][PF<sub>6</sub>]<sub>2</sub> derivatized SnO<sub>2</sub>/en-silane electrode was performed in dry degassed acetonitrile containing 0.1 M tetrabutylammonium perchlorate (TBAP) and a saturated NaCl calomel electrode (SSCE) as the reference electrode. Cyclic voltammetry (CV) and square wave voltammetry of TNBS derivatized SnO<sub>2</sub>/en-silane electrode were performed in 0.1 M Na<sub>2</sub>SO<sub>4</sub> with a Ag/AgCl reference electrode.

## RESULTS AND DISCUSSION

The sequence of reactions involved in the covalent attachment of TNBS, Ru complex, and HABA to the SnO<sub>2</sub> electrode is illustrated in Figure 1. The first step in the sequence, the covalent attachment of alkylamine silane to the SnO<sub>2</sub> electrode, is a well-established procedure [3]. In the second step, one of the three compounds of interest is linked to the alkylamine through various functional groups. TNBS reacts with amine through the sulfonic acid group to produce a yellow-orange chromophore. This reaction has been successfully used in the past for the quantitation of amino groups [16-20]. The second compound, the Ru complex, is amide coupled to the alkylamine-silanized group through the peripheral carboxylic acid groups by using DCC as the coupling agent. This reaction was used successfully in the past to couple the complex to Pt/PtO surfaces [14]. A similar procedure was used to couple the carboxylic acid group of HABA, the third compound used in this study, to the alkylamine-silanized SnO<sub>2</sub> electrode surface.

### Optimization of Silver Overlayer Thickness

To determine the optimum thickness of silver overlayer for SERRS, a range of silver thicknesses with average values

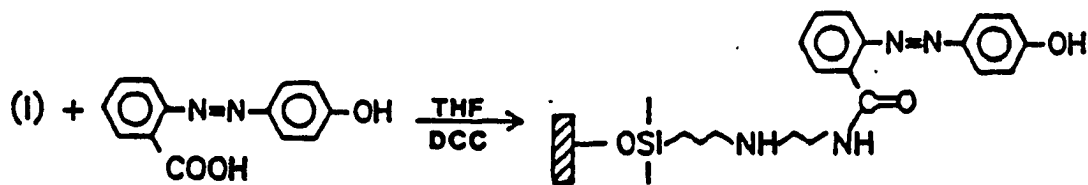
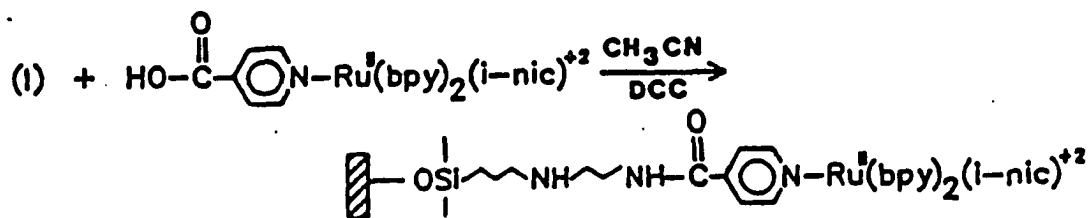
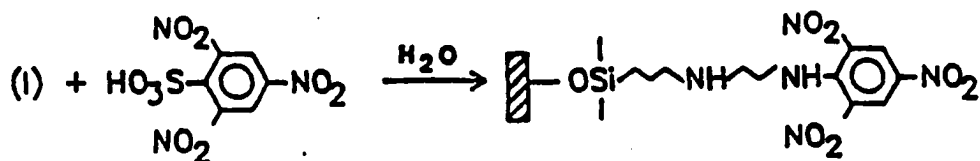
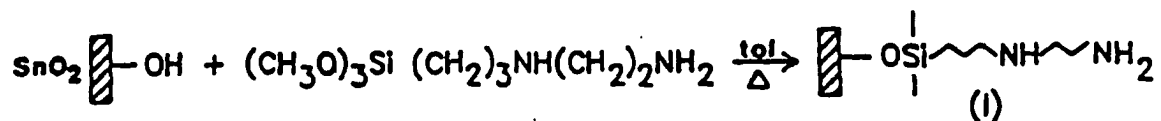


Figure 1. Synthetic schemes for the covalent attachment of TNBS, Ru complex, and HABA to  $\text{SnO}_2$  surfaces.

between 10 Å and 75 Å were deposited onto electrodes that were previously derivatized with Ru complex. The intensity of the 1606-cm<sup>-1</sup> band of the complex is plotted as a function of film thickness in Figure 2. A clear maximum occurs in the curve at ≈50 Å and this thickness gave the most satisfactory results for subsequent SERS/SERRS analysis of all the modified surfaces. It is well established that SERS/SERRS activity produced from vacuum-deposited silver films is highly dependent upon thickness [21-23]. Thin films (<100 Å) form discrete islands which produce efficient enhancement. At thicknesses greater than ≈100 Å, the films become smooth, resulting in the quenching of the plasmon resonance and hence a decrease in the enhancement. Optimal SERS enhancement occurs when the plasmon resonance of the silver islands, which is determined by their size and shape, is coincident with the laser excitation wavelength. In SERRS, additional enhancement is provided by excitation into an absorption band of the compound. These requirements for maximum enhancement have been determined previously for SERRS of Rhodamine 6G by using silver overlayers of varying thicknesses [21]. In the present study, the peak in the curve (Figure 2) occurs at a thickness which probably produces an optimal silver island morphology for maximum enhancement.

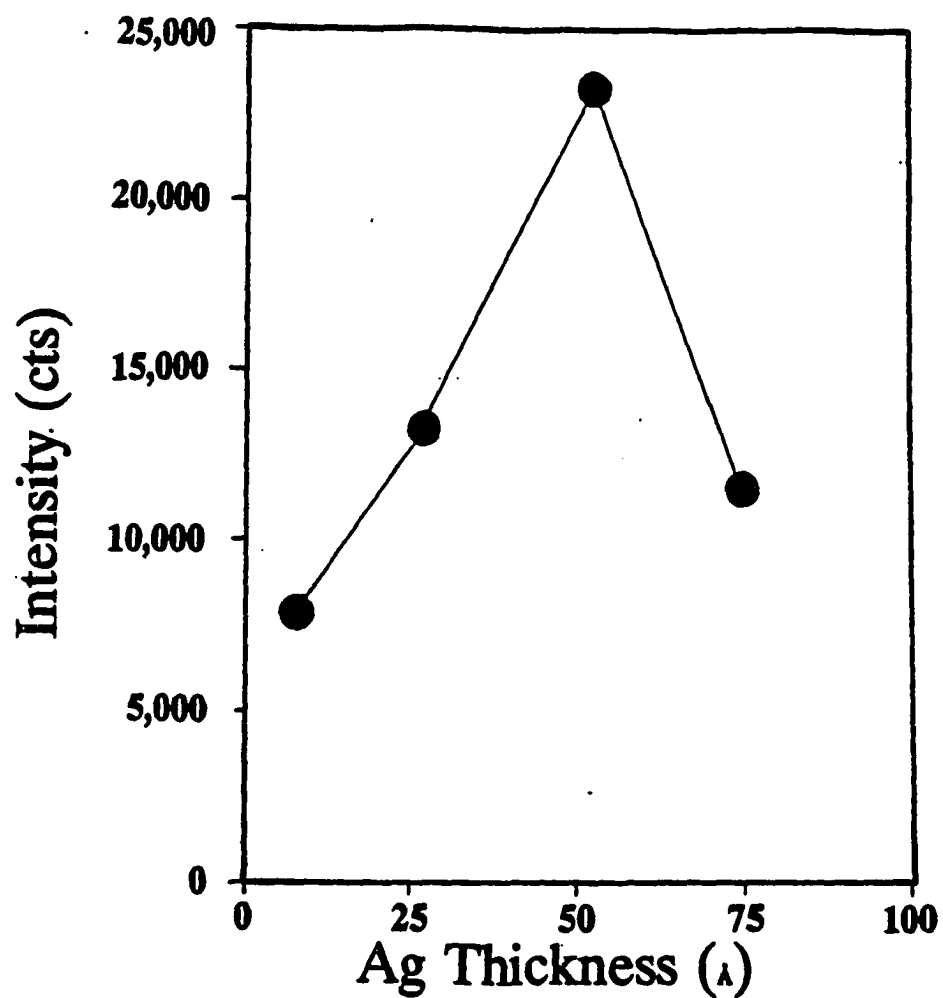
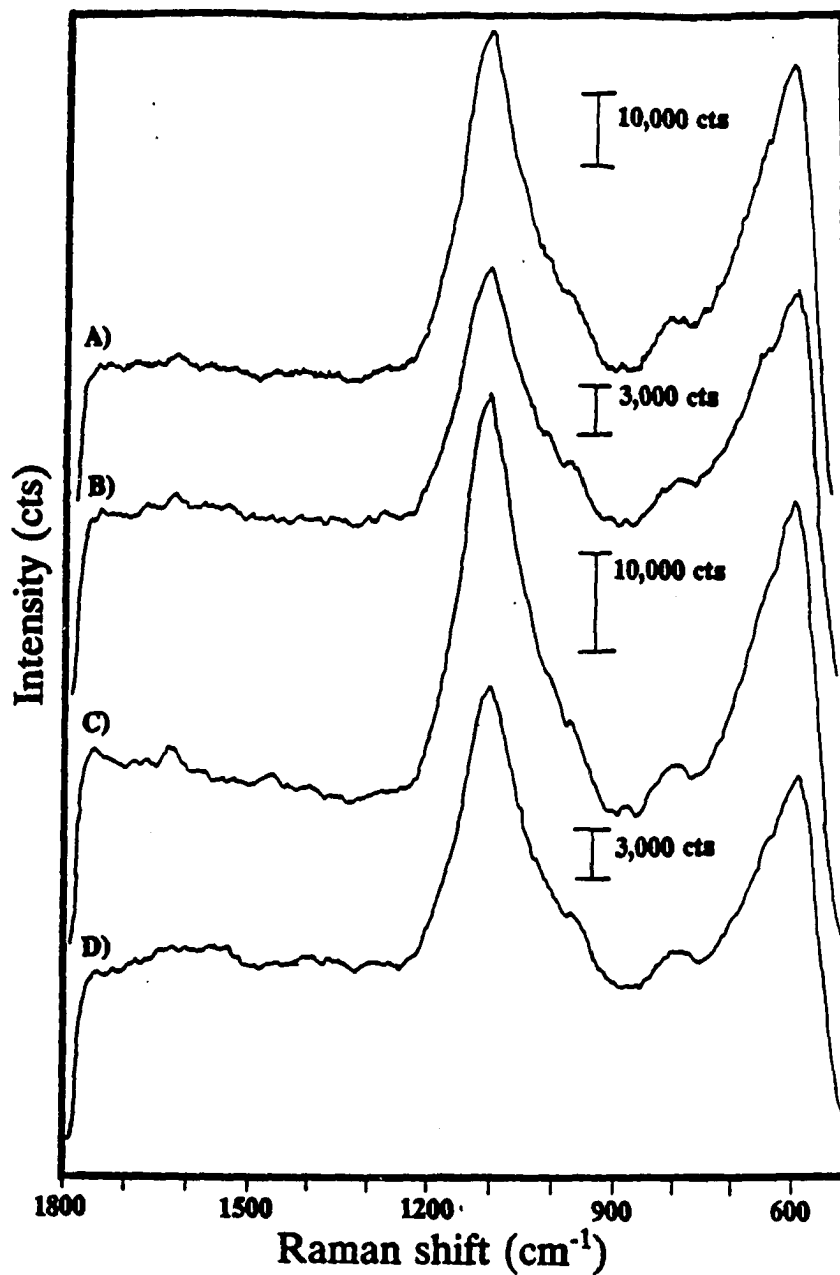


Figure 2. Plot of the SERRS intensity of  $1606\text{ cm}^{-1}$  band of the Ru complex vs silver overlayer film thickness.

## Detection of Covalently Bound Species by SERRS

### Silane-TNBS Attachment

An attempt was made to monitor the first step of the reaction, the attachment of the en-silane group to the SnO<sub>2</sub> to the SnO<sub>2</sub> electrode. Raman spectra of the SnO<sub>2</sub> electrodes with and without covalently attached en-silane are shown in Figure 3. The broad intense features common to these spectra arise from the glass upon which the SnO<sub>2</sub> is coated. These bands are observed with violet laser excitation (413.1 nm) but are absent when 488.0-nm excitation is used. Although SnO<sub>2</sub> has an infrared-active band at 863 cm<sup>-1</sup> [ $\nu(\text{OSnO})$ ] [24], no bands assignable to SnO<sub>2</sub> are observed either with the silver overlayer (Figure 3A) or in the normal Raman spectrum (Figure 3B, no silver overlayer) of the unmodified electrode. Similarly, although neat en-silane is observed to give a strong, characteristic normal Raman spectrum under these conditions (data not shown), no en-silane bands are identifiable in the normal Raman (Figure 3C) or with the silver overlayer (Figure 3D) spectra of the en-silane modified electrode. Other regions of the spectrum where strong Raman bands were observed from the neat en-silane (e.g. 3000-3600 cm<sup>-1</sup>) were also devoid of bands in the spectrum of the en-silane modified electrode. The absence of these bands at the surface concentrations



**Figure 3.** Raman spectra of: A) virgin SnO<sub>2</sub> surface; B) SnO<sub>2</sub> + silver overlayer; C) SnO<sub>2</sub>/en-silane + silver overlayer. Experimental conditions: excitation wavelength, 413.1 nm; laser power, 140 mW.

believed to be present ( $\approx 1$  monolayer) suggests that the scattering cross sections for this species are too small to allow the observation of the spectra above the observed background, even with the additional surface enhancement produced by the silver overlayer. However, when the surface-attached species possesses an electronic absorption band, it is possible to use resonance excitation. Under these conditions, the combined resonance and surface enhancement produces sufficient scattering intensity to allow detection of the SERRS spectrum, as will be demonstrated below.

In order to monitor the first step in the electrode modification scheme, the covalent attachment of the silylamine group, we have reacted the amine groups with TNBS. TNBS offers several advantages as an indicator of amine groups on the electrode surface. First, the reaction of TNBS, with the amine groups produces an intensely absorbing chromophore with an absorption band at 418 nm, whereas the unreacted TNBS is colorless. It is possible to obtain a qualitative estimate of the uniformity of the silanation coverage by visual inspection of the electrode. Second, it is possible to utilize resonance enhancement to discriminate between the TNBS which is covalently attached to the surface and any unreacted TNBS which may be adsorbed noncovalently to the surface. The  $\text{NO}_2$  groups of TNBS

produce strong Raman bands due to their large polarizability and conjugation with the phenyl ring in the molecule. Figure 4A show the SERRS spectrum of the TNBS-aminesilane conjugate (produced by the reaction of TNBS with en-silane in aqueous solution) adsorbed onto a roughened silver electrode. The single most characteristic feature in this spectrum is the intense  $\nu(\text{NO}_2)$  band at  $1330 \text{ cm}^{-1}$ . By comparison, when the TNBS is allowed to react with the silanized  $\text{SnO}_2$  electrode, a uniform yellow color is typically formed on the surface of the electrode and the SERRS spectra shown in parts B and C of Figure 4 are observed following deposition of silver onto the modified surface. Again, the  $\nu(\text{NO}_2)$  band is present in both spectra, albeit at slightly shifted frequencies. This band frequency was previously found to be quite variable in resonance Raman spectra and is very sensitive to both intra- and intermolecular hydrogen bonding [25]. Differences in the hydrogen bonding environment may result from using different silver overlayer deposition methods. Substrates that undergo chemical deposition, which is performed in aqueous solution followed by air-drying of the sample, may retain adsorbed water allowing hydrogen bonding. In contrast, the vacuum deposition of silver at low pressures should remove adsorbed water. Thus, the small shifts in frequencies seen here may result from this difference. No resonance Raman

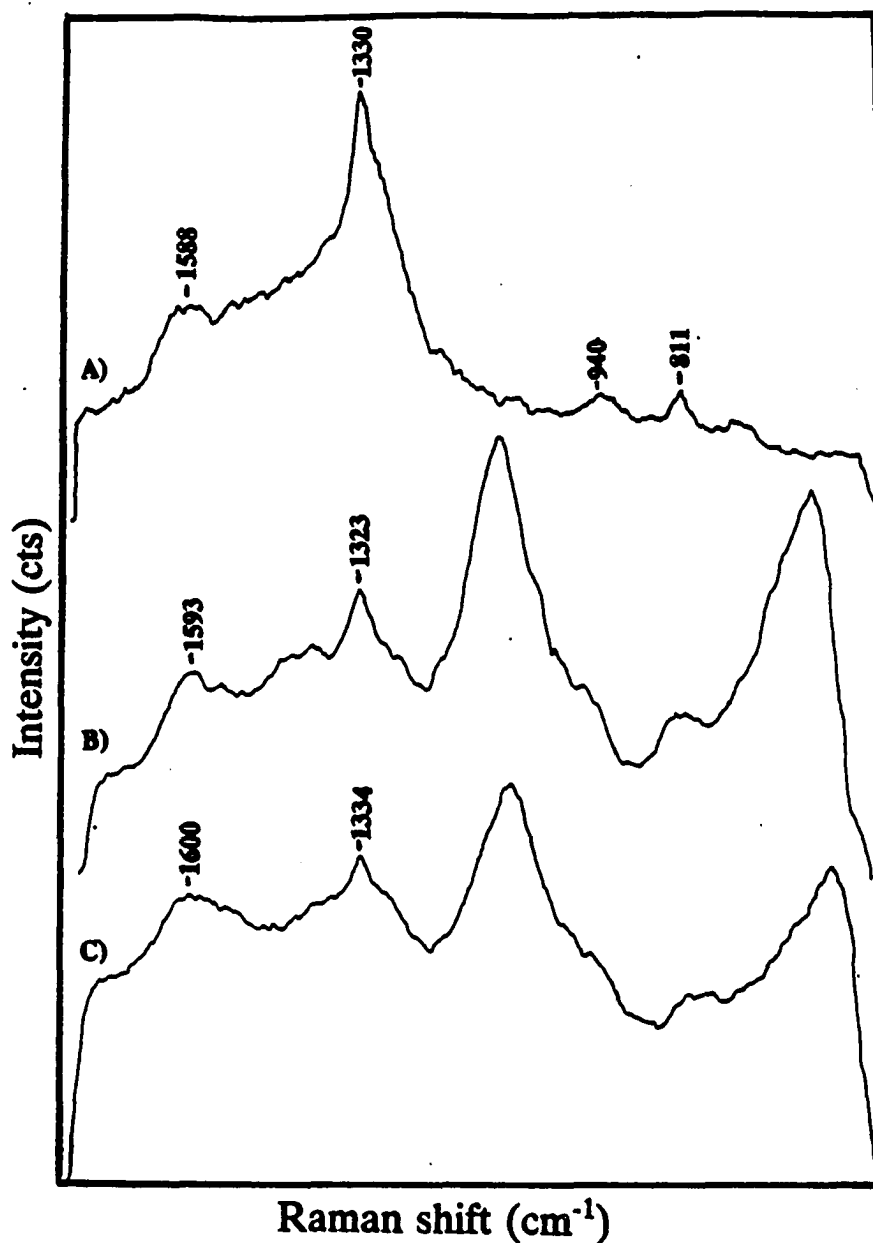


Figure 4. SERRS spectra of: A) en-silane/TNBS conjugate adsorbed onto electrochemically-roughened electrode; B) SnO<sub>2</sub>/en-silane/TNBS + silver overlayer; C) SnO<sub>2</sub>/en-silane/TNBS with a chemically deposited silver overlayer. Experimental conditions: excitation wavelength, 413.1 nm; laser power, 140 mW.

spectrum of the TNBS derivatized electrode was observed due to the presence of a high fluorescence background. However, with the silver overlayer, the high background is quenched and SERRS was observed.

Independent confirmation of the covalent attachment of TNBS to the  $\text{SnO}_2/\text{en-silane}$  electrode was obtained by cyclic voltammetry and square wave voltammetry of the derivatized reversible process occurs in the potential range from +0.0 to -1500 mV with  $E_{pc}$  at -748 mV vs Ag/AgCl. The amount of electroactive material on the electrode surface was estimated by integration of the area under the CV curve. Depending upon whether one or all three of the  $\text{NO}_2$  groups are reduced, the surface coverage is between  $1.3 \times 10^{-10}$  and  $4 \times 10^{-10}$  mol/cm<sup>2</sup>, which corresponds to  $\approx 1$  monolayer coverage [26,27].

An important advantage to the use of SERRS for monitoring surface reactions is the simplicity of the procedure. It is possible to use the chemical procedure previously described [9] to overlayer the sample with silver, as was done to obtain the spectrum shown in Figure 4C. This method provides a simple, inexpensive method for producing SERRS-active samples and is an effective alternative to the more expensive and time-consuming vacuum deposition procedure.

As discussed above, it is possible to detect and

quantitate covalently bound TNBS by visual methods [or UV-vis spectroscopy] and electrochemical techniques. Thus, the need for SERRS analysis might be legitimately questioned. However, neither of these techniques provides structural information nor are they molecularly specific. The broad absorption bands observed in electronic spectroscopy do not define the molecular species present on the surface nor do they provide direct information about the chemical bonding between the reactant and the surface. Electrochemical data can provide quantitative information only. Vibrational spectra, on the other hand, provide "molecular fingerprints" and can yield detailed bonding information from an analysis of band shifts following chemical reactions. In addition, it is possible to monitor electrochemical reactions on the electrode surface and, in some cases, to characterize the reaction products. This latter application is demonstrated for TNBS.

Changes in the SERRS spectrum during the in situ electrochemical reduction of the covalently attached TNBS group were monitored as a function of electrode potential, as shown in Figure 5. As the potential was made, reduction of the major peak at  $1326\text{ cm}^{-1}$  (assigned to  $\nu(\text{NO}_2)$ ) in the spectrum occurs in a region where  $\text{NO}_2$  reduction is also observed by square-wave voltammetry of the modified surface. The lack of reappearance of this peak when the initial

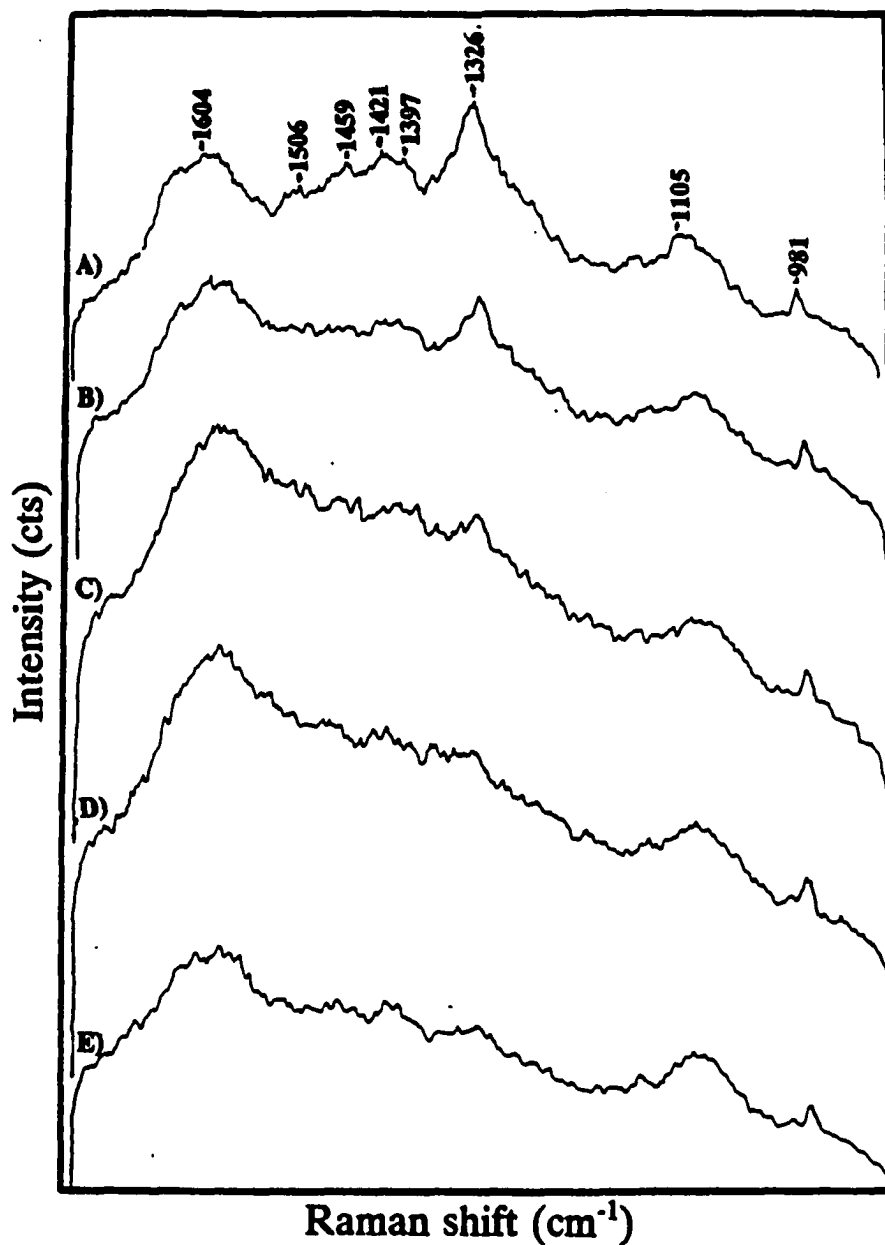


Figure 5. In situ SERRS spectra of  $\text{SnO}_2/\text{en-silane/TNBS}$  electrode at a series of reduction potentials: A) -300 mV; B) -500 mV; C) -600 mV; D) -700 mV. Experimental conditions: excitation wavelength, 413.1 nm; laser power 140 mW.

potential is again applied suggests that the reduction is irreversible, as would be expected for the reduction of the  $\text{NO}_2$  is also observed by square-wave voltammetry of the modified surface. The lack of reappearance of this peak when the initial potential is again applied suggests that the reduction of the  $\text{NO}_2$  moiety, and is consistent with the electrochemical results obtained for this system. The complete loss of the  $\nu(\text{NO}_2)$   $1326 \text{ cm}^{-1}$  suggests that all three of the  $\text{NO}_2$  groups of TNBS are reduced at this potential. The continued presence of low intensity ring stretch modes in the region  $1500\text{--}1600 \text{ cm}^{-1}$  throughout the reduction indicates that the aromatic group is not reduced. This information is not available from the electrochemistry results alone.

#### Ruthenium Complex Attachment

The ruthenium complex chosen for this study produces strong Raman spectra both on a roughened silver electrode (Figure 6A) and in solution (Figure 6B). The band shifts, the changes in relative intensities, of several bands (most notably those arising from ring modes associated with the bipyridyl ligands in the  $1480\text{--}1610\text{-cm}^{-1}$  region), and the increase in overall intensity of the spectrum of the complex adsorbed onto the electrode as compared to in solution are commonly observed in SERS spectra, and the possible origin

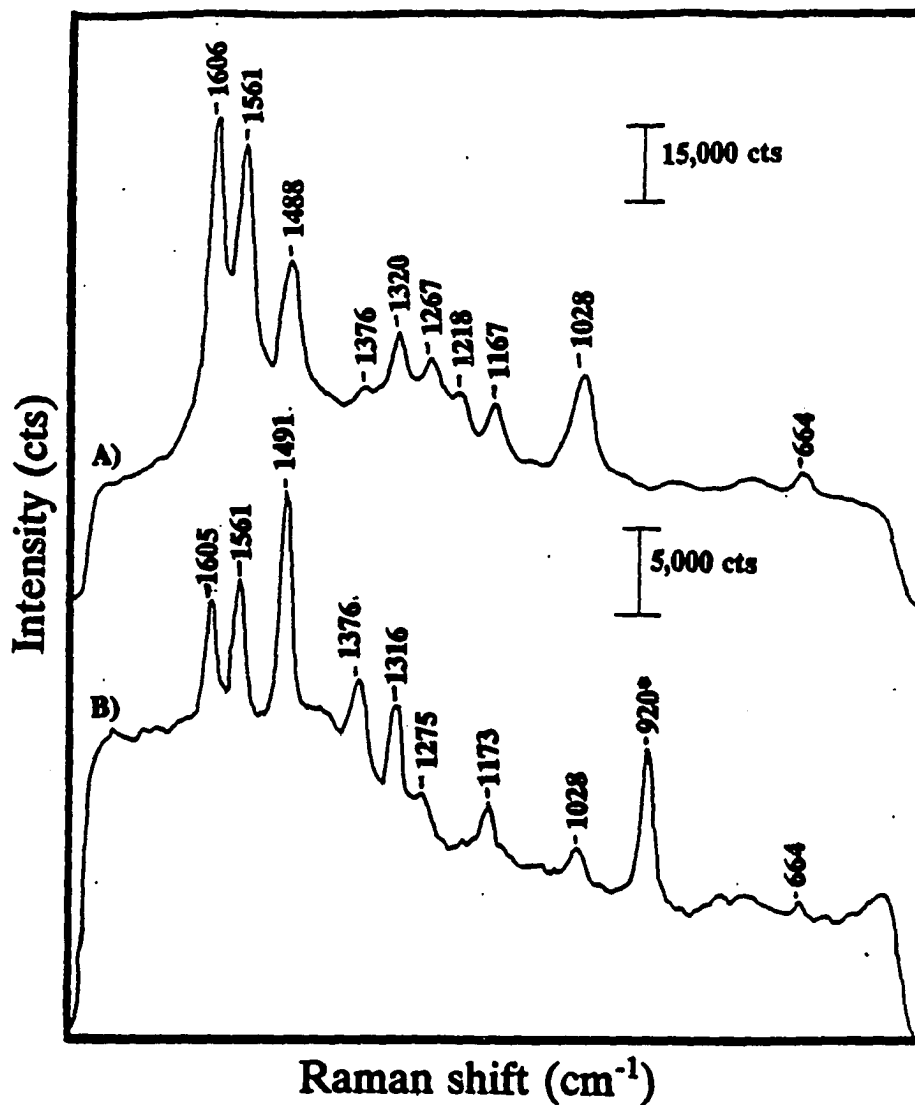


Figure 6. A) SERRS spectra of Ru complex adsorbed onto an electrochemically-roughened electrode; B) RRS of the same complex in acetonitrile solution. Experimental conditions: excitation wavelength, 413.1 nm; laser power, 140 mW.

of these effects have been discussed in the literature [28]. Figure 7A shows the SERRS spectrum of the covalently attached Ru complex on the SnO<sub>2</sub> electrode, following vacuum deposition of 50 Å of silver. The positions and relative intensities of the bands are nearly identical with those in Figure 6A. These results provide confirmation for the successful derivatization of the electrode surface and indicate that the spectrum arises from a SERRS process and not simple resonance enhancement (by comparison to Figure 6B). This is further confirmed by the fact that no spectrum is observed in the absence of a silver overlayer (Figure 7B). To confirm that the Ru complex was covalently attached and not merely adsorbed to the electrode surface, a control was run in which the silanation step was omitted from the reaction sequence. No spectrum was observed or this control following deposition of a silver overlayer (Figure 7C). Independent confirmation of successful derivatization of the electrode surface was also obtained by square-wave voltammetry. As can be seen in Figure 8, the attached Ru complex (without the silver overlayer) oxidizes at approximately +1300 mV vs SSCE. This is close to previously reported redox of +1310 mV [14]. Clearly, the peak current is close to the limit of detection for square-wave voltammetry at this low coverage.

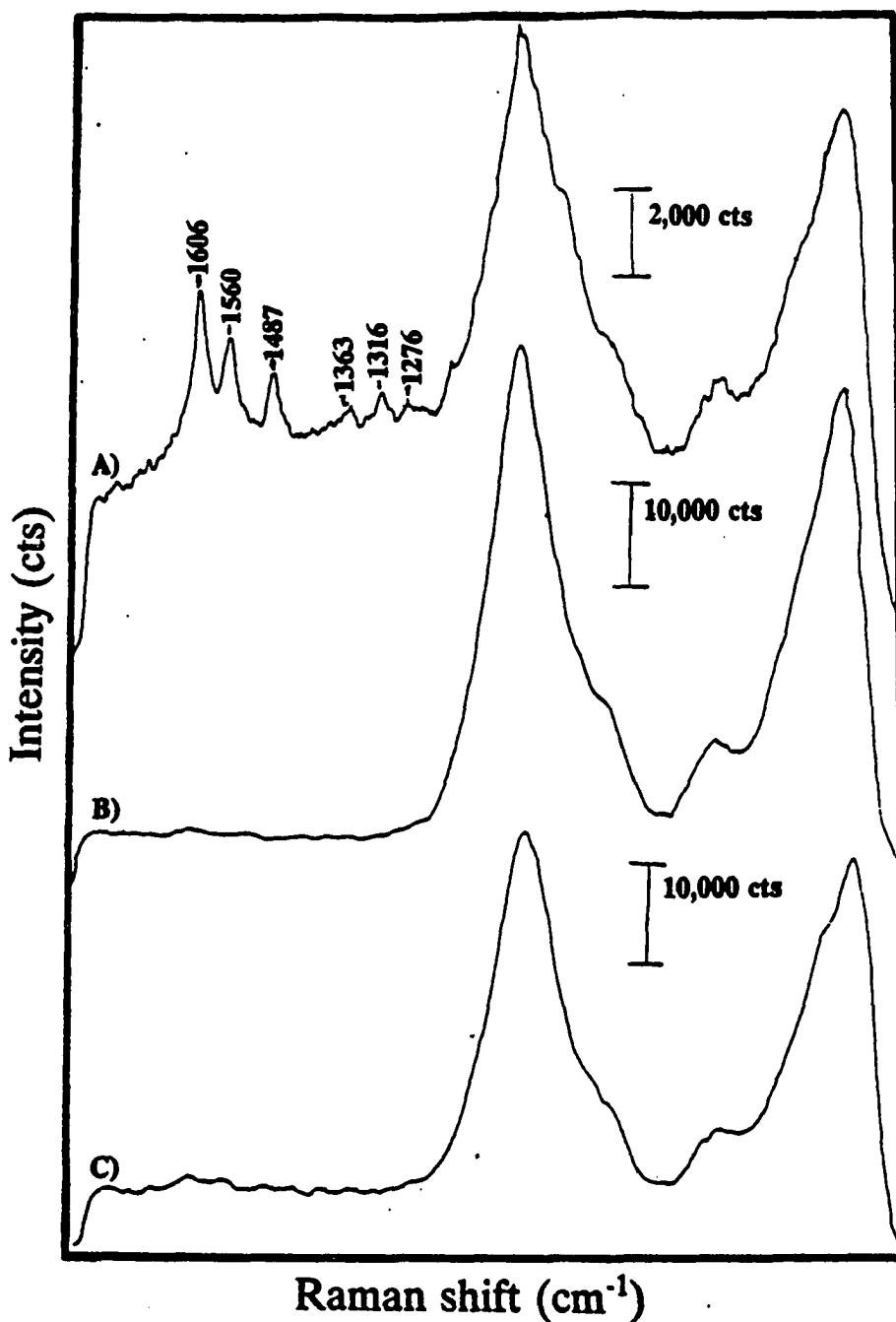


Figure 7. SERRS spectra of Ru complex: A) covalently bonded to SnO<sub>2</sub>/en-silane electrode with a silver overlayer; B) same as (A) without a silver overlayer; C) control reaction without silane linking group. Experimental conditions: excitation wavelength, 413.1 nm; laser power, 140 mW.

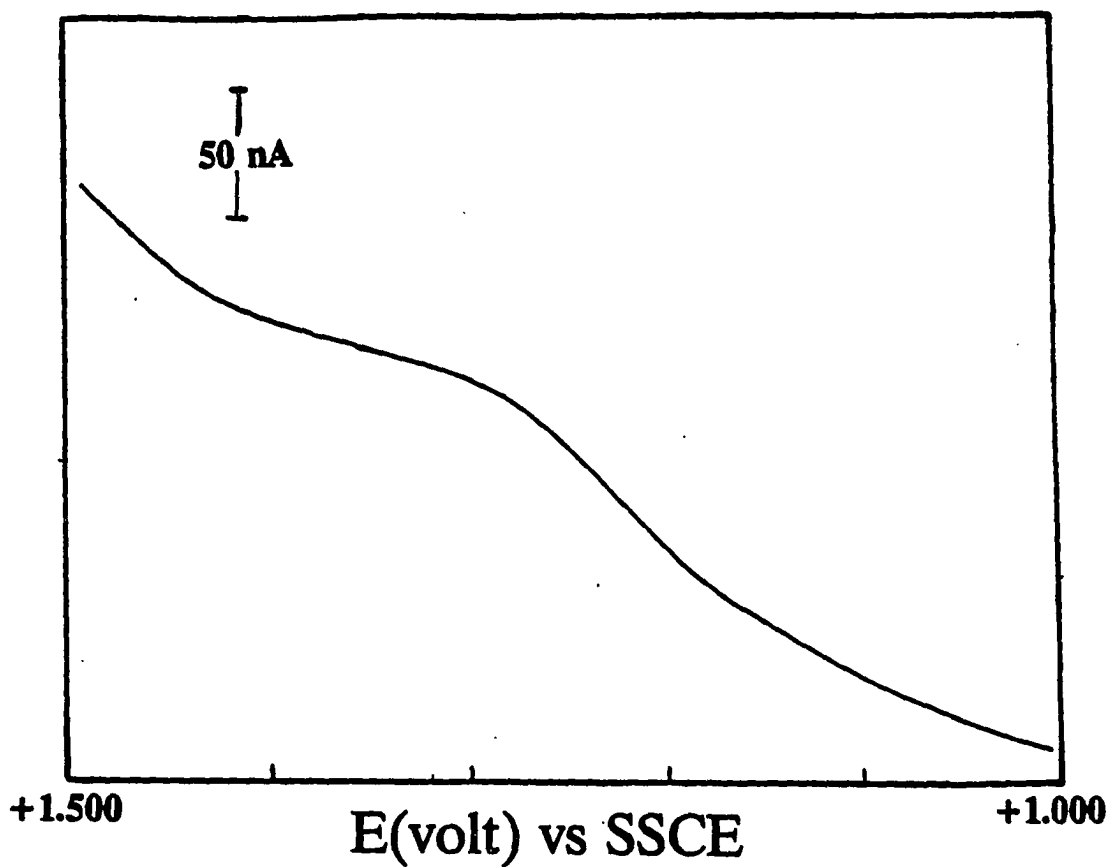
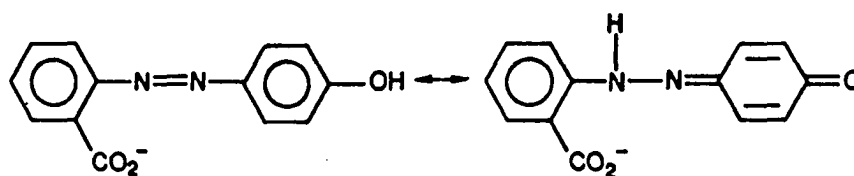


Figure 8. Square-wave voltammetry  $\text{SnO}_2/\text{en-silane}/\text{Ru}$  complex modified electrode in acetonitrile with 0.1 M TBAP as the supporting electrolyte. Experimental conditions: initial potential, +1.00 V; pulse amplitude, 25 mV; frequency, 15 Hz; step voltage, 4 mV.

HABA Attachment

The utility of the SERRS technique for providing structural information regarding covalently attached species is demonstrated in the derivatization of  $\text{SnO}_2$  with HABA. HABA exists in a variety of tautomeric forms at different pH values and these structures have been widely studied by use of resonance Raman methods [29]. Of particular interest is the existence of two tautomers at neutral pH



As shown, it was possible to determine the tautomeric form of the covalently bound HABA from its SERRS spectrum.

The SERRS spectra of adsorbed and covalently attached HABA are shown in parts A and B, respectively. Merlin and Johnson have made detailed assignments of the Raman bands of HABA and its analogues in neutral solution, for both azo and hydrazone tautomers. From a comparison of Figure 9 with these assignments, it can be seen that both tautomers are present when HABA is adsorbed onto the silver surface. This is indicated by the presence of azo bands at 1393 and 1190  $\text{cm}^{-1}$  and the presence of hydrazone bands at 1621, 1606, 1487, 1472, and 1156,  $\text{cm}^{-1}$ . Upon derivatization, however,

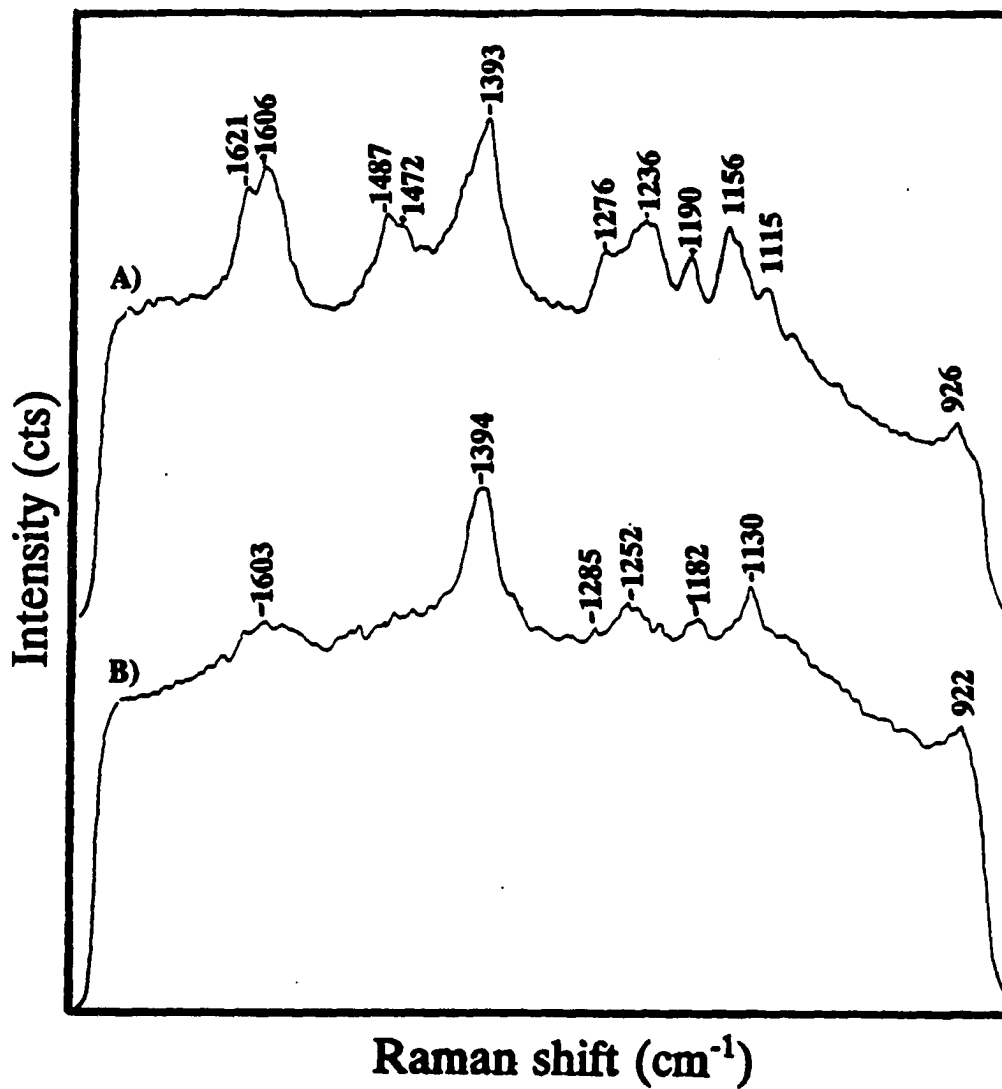


Figure 9. SERRS spectra of HABA: A) adsorbed onto SnO<sub>2</sub> with silver overlayer; B) covalently bonded to SnO<sub>2</sub>/en-silane electrode with a silver overlayer. Experimental conditions: excitation wavelength, 413.1 nm; laser power, 140 mW.

all bands characteristic of the hydrazone tautomer disappear, indicating the presence of only the azo form of the covalently attached HABA.

#### Determination of Detection Limits

To estimate the sensitivity and detection limits of SERRS, the intensity of the Ru complex of varying concentrations were prepared, a known volume was applied to defined areas on glass and SnO<sub>2</sub> surfaces. For this purpose, solutions of the Ru complex of varying concentrations were prepared, a known volume was applied to defined areas on glass and SnO<sub>2</sub> surfaces, and the solvent was allowed to evaporate. Assuming a uniform surface coating of the complex, this procedure produced coverages varying from 10<sup>-13</sup> to 10<sup>-10</sup> mol/cm<sup>2</sup>. Following evaporation of the solvent, a 50 Å silver film was deposited on each surface and the SERRS spectra were measured.

The intensity of the 1606-cm<sup>-1</sup> band is plotted as a function of surface concentration in Figure 10. Two important points should be noted. First, measurable peak intensities were obtained at only 0.1% monolayer coverage (1 x 10<sup>-13</sup> mol/cm<sup>2</sup>) for the compound on both glass and SnO<sub>2</sub>. Second, the sensitivity of SERRS is greater for the glass substrate. The smaller change in signal intensity with

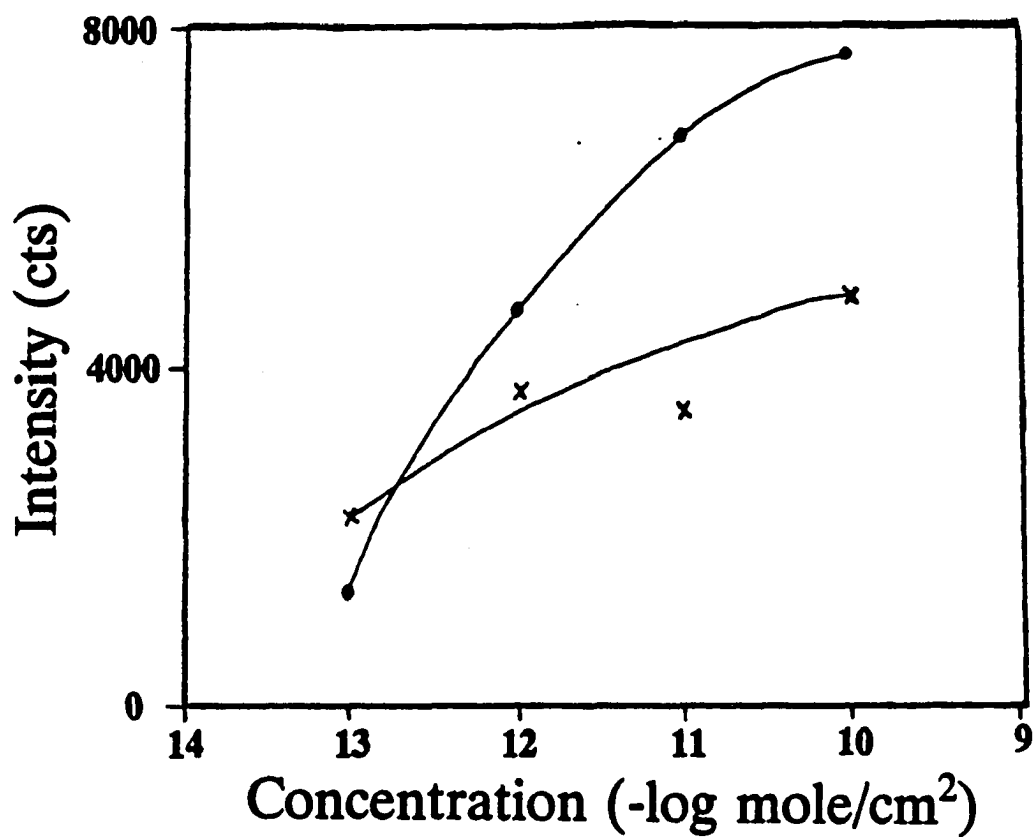


Figure 10. Plot of the SERRS intensity of the  $1606\text{ cm}^{-1}$  band of the Ru complex vs the concentration of the complex on frosted glass (circles) and  $\text{SnO}_2$  (crosses) surfaces.

surface coverage on  $\text{SnO}_2$  is undoubtedly due to the greater inhomogeneity of its surface. Surface roughness leads to pooling of the solution in the valleys or crevices of the surface. Thus, the complex is not distributed evenly over the surface when the solvent evaporates. This was evident from the greater scatter in peak intensities observed at a given surface concentration for the  $\text{SnO}_2$  surface as compared to glass. In spite of the poorer reproducibility on  $\text{SnO}_2$ , some estimate of the surface coverage for the covalently bound Ru complex can be made based upon the peak intensity shown in Figure 7A. A value of about 10% of a monolayer is obtained. This is close to the detection limit for square-wave voltammetry, but as can be seen from Figure 10, it is 2 orders of magnitude higher than that attainable by SERRS.

On the basis of these and previously reported results, it should also be noted that, at best, SERRS can be used as a semiquantitative technique in the submonolayer coverage region. A nonlinear response as a function of surface coverage has been observed for other chromophores [3] as well as nonresonantly-enhanced molecules [31]. In the former [30], the signal intensity was observed to rise rapidly from the detection limit to about 10 mol % and then to decrease somewhat for coverages between 10 and 20 mol %. Above 20 mol %, a much smaller increase in signal intensity was observed. These nonlinear effects may result from

dipole-dipole interactions between the chromophores, as predicted from EM theory [32].

**CONCLUSIONS**

In this study, the first application of SERRS to the analysis of chemically modified SnO<sub>2</sub> surface has been demonstrated. Although the electrode material itself is not SERRS active, the deposition of silver overlayers was used to provide surface enhancement. The advantages of SERRS over other surface-sensitive techniques include the ability to obtain structural information concerning the redox processes of the covalently bound material (as demonstrated in the TNBS study), to detect submonolayer amounts of covalently bound material [as demonstrated in the TNBS study), and to obtain structural information concerning the chemical nature of covalently bound species (as demonstrated in the HABA study). Other important advantages include the ability to perform analysis in situ without the requirement for high vacuum systems (as in XPS, for example). Finally, the analytical procedure is relatively simple in that silver overlayers can be deposited either by a chemical or by vacuum deposition procedure. Only semiquantitative information can be obtained, however, because of the nonlinear SERRS response at submonolayer coverages.

**ACKNOWLEDGEMENTS**

The authors are grateful for the support of the National Institutes of Health (GM 35108). We thank Dr. Bharart Kaul for derivatization of electrodes and Dr. Randy Holt for participating in this research. We also thank Professor R. W. Murray (University of North Carolina, Chapel Hill) for his generous gift of the SnO<sub>2</sub>-coated glass.

## LITERATURE CITED

1. Murray, R. W., Ewing, A. G., Durst, R. A. Anal. Chem. 1987, 59, 379A.
2. Karweik, D. H., Miller, C. W., Porter, M. D., Kuwana, T. In Industrial Applications of Surface Analysis, ACS Symposium Series No. 199, Casper, L. A., Powell, C. M., Eds.; American Chemical Society: Washington, DC, 1982; p 89.
3. Murray, R. W. In Electroanalytical Chemistry, Bard, A. J., Ed.; Marcel Dekker: New York, 1984; Vol. 13, pp 191-368.
4. Sanda, P. N., Demuth, J. E., Tsang, J. C., Warlaumont, J. M. In Surface-Enhanced Raman Scattering, Chang, R. K., Furtak, T. E., Eds.; Plenum: New York, 1982; pp 189-202.
5. Chang, R. K. Ber. Busen-Ges. Phys. Chem. 1987, 91, 296.
6. Creighton, J. A. In Surface-Enhanced Raman Scattering; Chang, R. K., Furtak, T. E. Eds.; Plenum: New York, 1982; pp 315-337.
7. Weitz, D.A., Garoff, S., Gersten, J. I., Nitzan, A. J. Chem. Phys. 1983, 78, 5324.
8. Aroca, R., Martin, F. J. J. Raman Spectrosc. 1985, 16, 156.
9. Ni, Fan, Cotton, T. M. Anal. Chem. 1986, 58, 3159.

10. Kobayashi, Y., Itoh, K. J. Phys. Chem. 1985, 89, 5174.
11. Davies, J. P., Pachuta, S. J., Cooks, R. G., Weaver, M. J. Anal. Chem. 1986, 58, 3159.
12. Leung, L.-W. H., Weaver, M. J. J. Electroanal. Chem. 1987, 217, 367.
13. Leung, L.-W. H., Weaver, M. J. J. Am. Chem. Soc. 1987, 109, 5113.
14. Abruna, H. D., Meyer, T. J., Murray, R. W. Inorg. Chem. 1979, 18, 367.
15. Holt, R. E., Cotton, T. M. J. Am. Chem. Soc. 1987, 109, 1841.
16. Snyder, S. L., Sobocinski, P. Z. Anal. Biochem. 1975, 64, 284.
17. Ernest, M. J., Kim, Ki-Han J. Biol. Chem. 1974, 249, 6770.
18. Oglso, T., Tamura, S., Kato, T., Siglura, M. J. Biochem. (Tokyo) 1974, 76, 147.
19. Shinoda, T., Tsuzukida, Y. J. Biochem. (Tokyo) 1974, 75, 23.
20. Benjamin, D. M., McCormack, J. J., Gump, D. W. Anal. Chem. 1973, 45, 1531.
21. Ritchie, G., Chen, C. Y. In Surface-Enhanced Raman Scattering, Chang, R. K., Furtak, T. E., Eds.; Plenum: New York, 1982; pp 361-378.
22. Ishida, H., Fukuda, H., Katagiri, G., Ishitani, A.

- Appl. Spectrosc. 1986, 40, 322.
23. Cotton, T. M., Schlegel, V. L., Department of Chemistry, University of Nebraska-Lincoln, unpublished results.
  24. Anderson, J. S., Bos, A., Ogden, J. S. J. Chem. Soc. D 1971, 1381.
  25. Kumar, K., Carey, P. R. J. Am. Chem. Soc. 1982, 104, 2742.
  26. Soriaga, M. P., Hubbard, A. T. J. Am. Chem. Soc. 1982, 104, 2742.
  27. Soriaga, M. P., Hubbard, A. T. J. Am. Chem. Soc. 1982. 104, 3937.
  28. Efrima, S. In Modern Aspects of Electrochemistry, Conway, B. E., White, R. E., Bockris, J. O'M., Eds.; Plenum: New York, 1985; Vol. 16, pp 253-369.
  29. Merlin, J. C., Thomas, E. W. Spectrochim. Acta, Part A 1979, 35A, 1243.
  30. Cotton, T. M., Kim, Jae-Ho, Uphaus, R. A., Mobius, D. J. Phys. Chem. 1989, 93, 3713.
  31. Murray, C. A., Bodoff, S. Phys. Rev. Lett. 1984, 52, 2272.
  32. Meitu, H. Prog. Surf. Sci. 1984, 17, 153.

**PAPER V RAMAN MICROPROBE INVESTIGATIONS OF  
RESONANTLY-ENHANCED DYE MOLECULES AT SILVER-ISLAND  
FILMS**

**ABSTRACT**

Surface-enhanced resonance Raman scattering (SERRS) spectra of several dyes adsorbed onto silver-island film substrates were obtained by using a Raman microprobe. The spectra exhibited by the dyes showed well-resolved intense bands. A comparison SERRS study of zinc tetraphenylporphine (ZnTPP) spectra collected by a microsystem and a macrosystem displayed similar bands and relative intensities. The results indicate that the molecule photodegrades when irradiated with the focused laser beam produced by the Raman microscope objectives. The overall spectral intensity decreases with laser irradiation time, but a characteristic spectrum of the dye could be obtained after several seconds with the availability of a diode-array detector. The detection limit for the Raman microprobe was approximately  $10^5$  ZnTPP molecules. The spectra of the dyes, magnesium phthalocyanine, and 1,1'-diethyl-2,2'-cyanine iodide were also observed with SERRS microprobe.

## INTRODUCTION

The successful coupling of Raman spectroscopy with microscopy has allowed acquisition of molecular vibrational information from microsamples. Since its initial development, Raman microprobe spectroscopy has become a well-established method for microanalytical investigations [1-5]. This technique has been applied to the study of a variety of problems, including the detection of defects in optical fibers [6,7], fluid inclusions in geological materials [8], identification of microparticulate materials [9,10], and the structural examination of superconductors [11].

The Raman microprobe directs the laser light onto a small area on a sample by the means of a modified light microscope. The sample is either mounted on a noninterfering substrate, as in the case of particle analysis or the microscopic sample of interest is distributed in a bulk material [11]. The microscope optics tightly focus the excitation line at the sample such that a spatial resolution on the order of 1  $\mu\text{m}$  can be achieved [5]. The scattered photons are collected by the optics and directed into a conventional Raman spectrometer. Thus, the characterization of the chemical components and its surrounding environment of a microsample can be probed by

Raman spectroscopy. Several characteristic features specifically associated with the Raman effect have further made the Raman microprobe particularly adaptable to microsample studies. For example, the examination of a sample is nondestructive, data collection is fairly rapid, and the experiment can be conducted under various conditions, i.e., in situ, under ambient conditions or at varying temperatures, etc.

Recently, surface-enhanced Raman scattering (SERS) spectroscopy and surface-enhanced resonance Raman scattering (SERRS) spectroscopy have developed into suitable techniques for the trace analysis of several aromatic organic compounds [12,13] and for the study of biological systems [14,15]. Although many questions still remain concerning the SERS/SERRS mechanisms, it is currently accepted that the effects involve contributions from both electromagnetic and chemical interactions between an adsorbate/adsorbent system [16-18]. The relative contribution from each mechanism is dependent upon the particular adsorbate/adsorbent system. An important advantage of SERS/SERRS is that these techniques are highly sensitive methods for the characterization of surfaces. It has been documented that the Raman signals exhibited by a molecule are amplified by a factor ranging from  $10^3$  to  $10^7$  when the sample is adsorbed onto a rough metal substrate. The SERS/SERRS enhancement

factor, however, is dependent upon a number of experimental parameters, including the excitation wavelength, the adsorbed species, the type of metal surface, the substrate preparation procedure, and the surface morphology of the substrate. When combined with microscopy, the effects of the experimental conditions on the SERS signal intensities can be monitored. In order to probe the dependence of the pyridine, pyridinium ion, and potassium cyanide SERS signals with potential, Hembree *et al.* [19] developed a spectroelectrochemical cell designed to acquire SERS spectra at an electrochemically-roughened electrode with a Raman microprobe. The microprobe was used to observe the surface particle morphology composing the SERS-active substrate. It was possible to direct the laser line onto specific areas on the substrate surface by using the microscope optics. Additional measurements were performed with the SERS Raman microprobe that entailed the investigation of a gold electroplating process.

Initial SERS studies conducted with the Raman microprobe involved the examination of sulfur oxyanions or tungsten films on vapor deposited silver substrates [20,21]. Van Duyne *et al.* [22] were the first to examine the electrochemical behavior of an aqueous pyridine/electrode model system by combining the SERS technique with the Raman microprobe. The results showed high signal-to-noise SERS

spectra of pyridine adsorbed onto an electrochemically-roughened silver electrode. Detection limits of attomole quantities of pyridine from 1  $\mu\text{m}$  sized sampling areas were obtained. The authors concluded that the spatial resolution of the microprobe coupled with the enhanced Raman scattering of the SERS effect allowed for the low detection limits. Otto *et al.* [23] employed the SERS Raman microprobe to obtain information relating to the orientation of the DNA bases with respect to a surface. Although a low-power He-Ne laser was used as the excitation source, well-resolved, intense SERS spectra were obtained.

Certain limitations restrict the Raman microprobe to the study of more robust molecules. In particular, it is difficult to examine samples that are in resonance with the laser excitation line. Because the microprobe tightly focuses the beam onto the sample, intense illumination results in local heating or decomposition of the molecule. For this reason, resonance Raman spectroscopy (RRS) coupled to microscopy has not been widely employed for microanalytical investigations. In this work, however, we report spectra of resonantly-enhanced molecules adsorbed onto silver-island films obtained with a Raman microprobe. Well-resolved and intense surface-enhanced resonance Raman scattering (SERRS) signals were exhibited by zinc tetraphenylporphine (ZnTPP) by using the 514.5 nm

excitation. Time dependence studies showed some degree of degradation of the SERRS vibrational bands, but a characteristic ZnTPP spectrum could still be obtained after exposure of several sec with laser irradiation. The metal surface may dissipate the thermal energy and/or absorb the energy from the irradiated dye thereby allowing acquisition of SERRS spectra of resonantly-enhanced molecules.

**EXPERIMENTAL****Materials and Instrumentation****Materials**

Zinc tetraphenylporphine (Mad River Chemical), 1,1'-diethyl-2,2'-cyanine iodide (Eastman Kodak) and magnesium phthalocyanine were used as received. Analytical grade acetone (Fisher Scientific) was used without further purification. The silver for the construction of the island films was 99.99% pure (Aesar).

**Instrumentation**

A commercial vacuum coating unit (Edwards High Vacuum, model E306A) was used to vapor deposit silver metal onto glass slides. Silver film thicknesses and deposition rates were measured via a film thickness monitor equipped with a quartz piezoelectric oscillating crystal (Edwards High Vacuum, model FTM4).

The samples were irradiated by using the 514.5 nm excitation from an Ar<sup>+</sup> laser (INNOVA 90-5, Coherent Inc.) and the 647.1 nm excitation from a Kr<sup>+</sup> laser (Coherent INNOVA 100). A research-grade microscope (Spex Micramate) directed and focused the beam onto the samples. The scattered radiation was transmitted into the 10x objective

of the microscope system via a backscattering configuration. The light was collected and focused onto the entrance slit of a monochromator/spectrograph (Spex Triple Spectrometer, model 1877) by the microscope optics. The 1200 grooves/mm grating ( $D^{-1} = 1.4 \text{ nm/mm}$ ) in the spectrograph stage was employed with an exit slit of 0.100 mm or 0.200 mm. A cooled intensified diode-array detector (PARC, model 1421) interfaced to a multichannel analyzer (PARC OMA III) was used to accumulate and process the Raman signals. Indene was used to calibrate the frequencies of the reported spectra.

SERRS spectra obtained from a conventional Raman spectrometer was collected in a backscattering configuration. The scattered radiation was focused directly into the entrance slit by a two lenses collection (Oriel 6236 Model fused silica lens; Oriel 6236 lens). A monochromator/spectrograph (Spex Triplemate, model 1877) dispersed and directed the light into a cooled intensified diode-array (PARC, model 1420). All the reported SERRS spectra were acquired with the 1200 grooves/mm grating ( $D^{-1} = 1.4 \text{ nm/mm}$ ). The exit slit was maintained at 0.200 mm. A multichannel analyzer (PARC OMA III) coupled to the array was used to collect the SERRS data.

## Experimental Procedures

### Microscope Slide Pretreatment and Deposition Experimental Conditions

The silver-island films were deposited onto clean glass slides. Pretreatment of the glass substrates consisted of cutting microscope slides into approximately 2 cm x 1 cm pieces. The slides were cleaned by placing the glass pieces into a 3 M KOH/methanol solution for a minimum of 1 hr. The slides were rinsed with fresh deionized water and sonicated for a minimum of 1 min. This procedure was carried out two additional times. Prior to the deposition procedure, the slides were dried in a oven for 30 min.

The clean glass slides were positioned in the deposition work chamber directly above a molybdenum DC boat source. Silver was deposited onto the slides at a base pressure of  $<2.5 \times 10^{-6}$  Torr. The silver thicknesses and metal deposition rates were maintained at 50 Å or 60 Å and 0.1 Å/sec., respectively, unless otherwise indicated in the discussion section.

### Adsorption Technique

The molecules were adsorbed onto the SERRS-active substrates by a dipping process. This technique involved submerging the films into the adsorbate solution at the

desired concentration for 1 min. The films were removed from the solution and the excess solvent was allowed to evaporate. SERRS spectra were acquired immediately after the films were dipped into the appropriate adsorbate solution.

#### SERRS Experiments

The adsorbate/island film system was placed on the microscope stage at the focal point of the collection optics. The laser excitation line was directed onto the samples and the resulting SERRS spectra were acquired with multichannel averaging of 25 scans or 49 scans with an integration time of 1 sec/scan. Laser power at the sample surface was maintained between 5 mW and 12 mW. The same conditions were used for the macrosystem Raman experiments.

**RESULTS AND DISCUSSION****Raman Microprobe SERRS Studies  
of Zinc Tetraphenylporphine**

Zinc tetraphenylporphine (ZnTPP) was used as the resonantly-enhanced adsorbate because the molecule's electronic spectrum is characterized by an intense B band in the ultraviolet region and Q bands between 500 nm and 600 nm. Several excitations in the visible region can be used to induce the resonance Raman scattering (RRS) effect. For this study, the 514.5 nm excitation was implemented as the radiation source because the molecule absorbs at this frequency. The plasmon resonances of the dye-coated metal particles also coincide with this line [24].

In order to determine if the Raman signals obtained from the dye/silver film surface were solely induced by a resonant enhancement or if contributions from the surface-enhancement phenomenon were involved, the spectra of ZnTPP adsorbed onto a roughened metal surface and a smooth metal surface were compared as shown in Figure 1. Both substrates were prepared by vapor-depositing silver metal onto glass slides under vacuum conditions. However, it has been demonstrated that the shapes and sizes of the silver islands composing the substrate are dependent upon the deposition

experimental parameters [24-27]. For example, thin films below an average thickness of approximately 100 Å are composed of metal islands that are separated from one another. The particles begin to merge together above 100 Å and as the thickness progressively increases, a smooth film is eventually formed. In addition, the metal evaporation rate used during the deposition procedure affects the surface morphology. Slow deposition rates produce aggregated particles that grow in height whereas fast metal evaporation of the metal causes the islands to spread out over the film substrate. The rough substrate was prepared by depositing 50 Å of silver onto the glass slide at a deposition rate of 0.1 Å/sec. To obtain a smooth silver surface, the deposition conditions for the metal thickness and evaporation rate were approximately 1100 Å and 2.5 Å/sec, respectively. The ZnTPP/film systems were positioned on the microscope stage and the scattered radiation was collected with the 10x microscope objective. As depicted in Figure 1B, ZnTPP adsorbed onto the smooth metal surface shows no enhancement. A ZnTPP spectrum also was not obtained from a bare glass slide coated with ZnTPP by using the same dipping procedure and solution concentration described above. The ZnTPP Raman signals shown in Figure 1A are only observed when a rough metal substrate is present. These results suggest that the

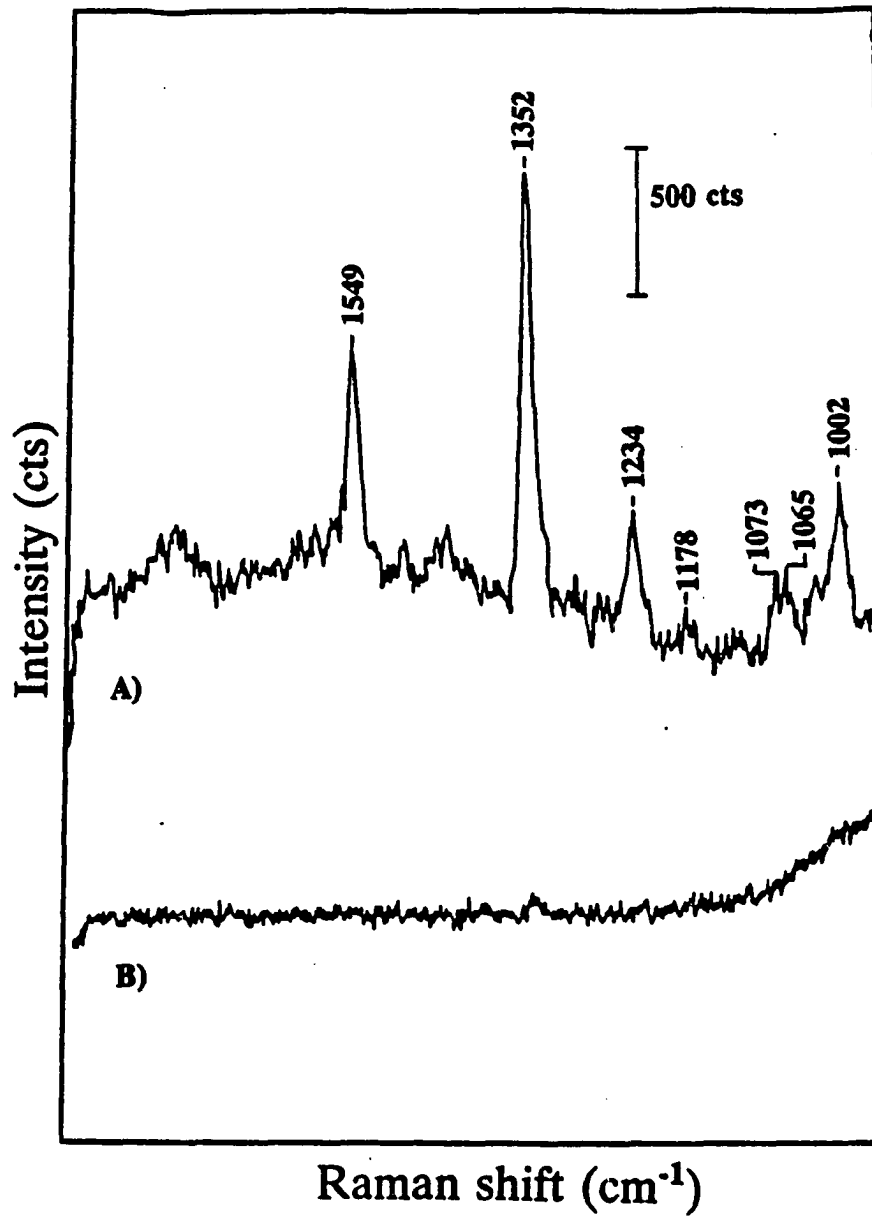


Figure 1. SERRS spectra of ZnTPP adsorbed onto: A) 50 Å silver-island film; B) 1100 Å silver-island film. Experimental conditions: microscope objective, 10x; adsorbing solution, 10<sup>-4</sup> M ZnTPP in acetone; integration time, 1 sec; scans, 25.

scattering is enhanced by an electromagnetic mechanism. A comparison of the ZnTPP resonant Raman scattering (RRS) spectrum with the surface ZnTPP spectrum is another indication that the SERRS electromagnetic mechanism is producing the enhancement. Although the relative band intensities are slightly different, the frequency shifts exhibited in both spectra are similar. It should be noted that this study had to be conducted with an excitation wavelength far from resonance with the molecular transition of the porphyrin, i.e., 457.9 nm. When resonant excitations were employed, ZnTPP signals were not observed because the solution spectrum displayed a fluorescence high background. Hence, the SERRS enhancement factor for this particular molecule was not calculated because a comparison ZnTPP resonant Raman spectrum could not be obtained with the microRaman system.

The ZnTPP spectrum obtained with the Raman microprobe is similar to the spectrum collected by a conventional Raman instrument. Figure 2A and Figure 3A show a comparison between the two spectra acquired with the microRaman and the macroRaman, respectively. The experimental parameters such as the silver thickness, deposition rate, adsorbing solution concentration, number of scans, and the integration time were kept constant for both systems. A comparison of the spectra shows that the relative band intensities and the

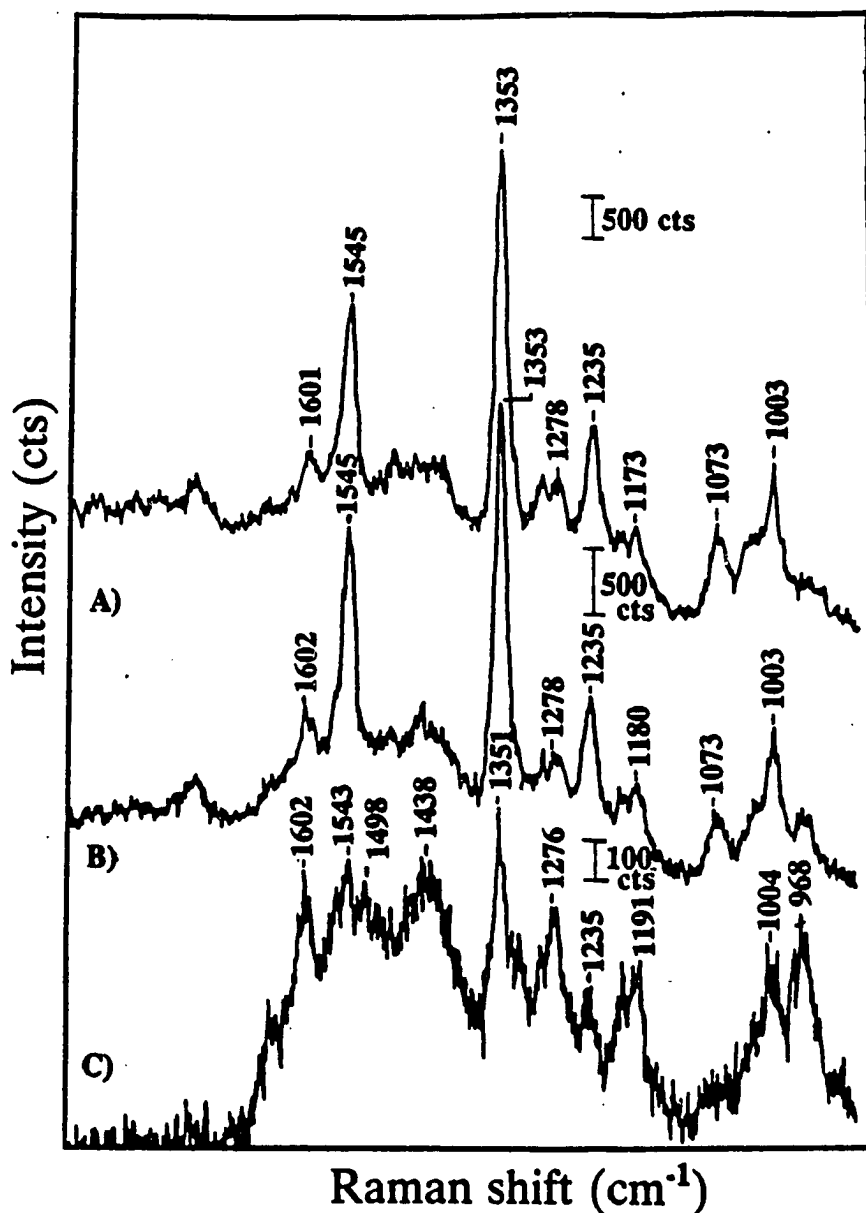


Figure 2. MicroRaman SERRS spectra of ZnTPP adsorbed onto 50 Å silver-island films as a function of ZnTPP adsorbing solution concentration: A)  $10^{-4}$  M; B)  $10^{-5}$  M; C)  $10^{-6}$  M. Experimental conditions: microscope objective, 10x; integration time, 1 sec; scans, 49.

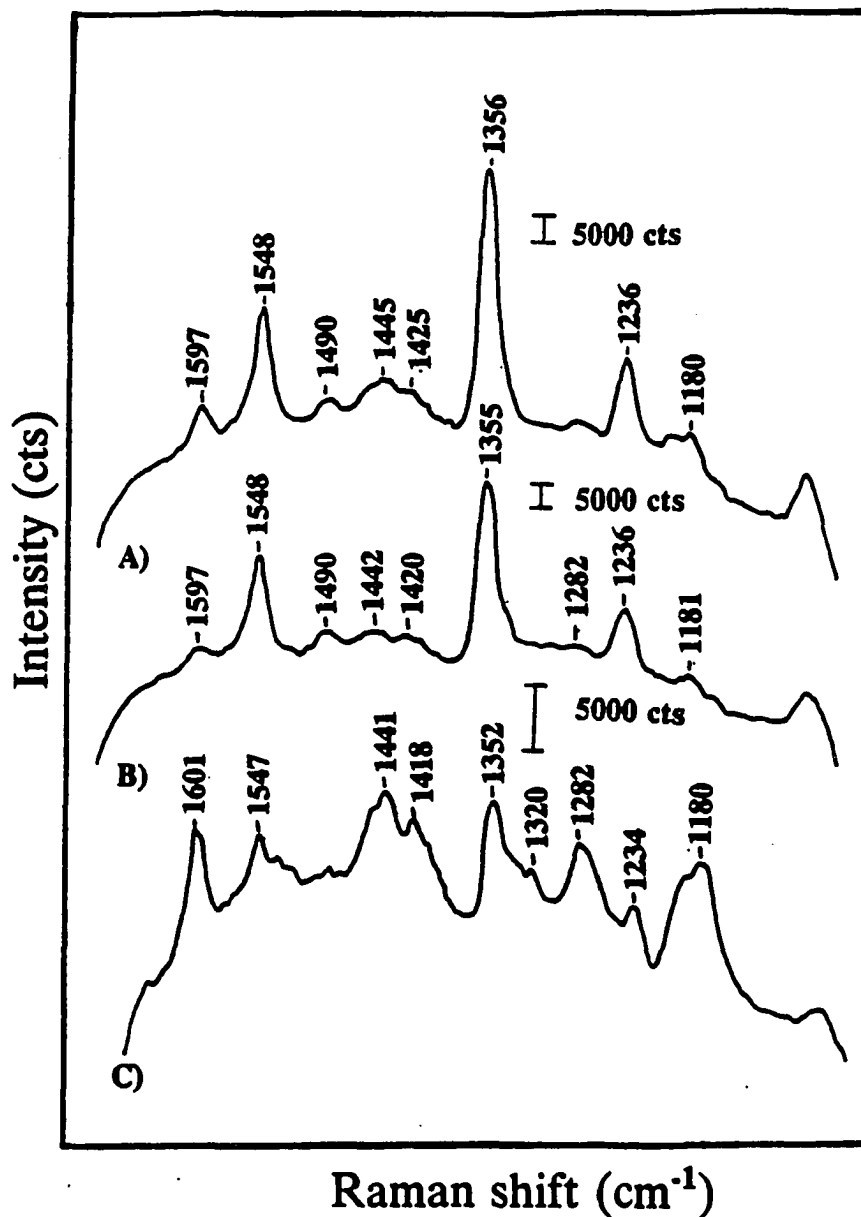


Figure 3. MacroRaman SERRS spectra of ZnTPP adsorbed onto 50 Å silver-island films as a function of ZnTPP adsorbing solution concentration: A)  $10^{-4}$  M; B)  $10^{-5}$  M; C)  $10^{-6}$  M. Experimental conditions: integration time, 1 sec; scans, 49.

frequencies correlate. Although the signal-to-noise ratio is lower in Figure 2A, the bands are sharper and more resolved when the Raman microprobe was used as opposed to the macroRaman. On the other hand, the SERRS signals depicted in Figure 3A were stable with continuous irradiation whereas the spectrum shown in Figure 2A degraded with prolonged laser exposure. These results can be attributed to the power density of the laser on the dye/silver film system. Because the Raman microprobe tightly focuses the excitation line to a fine point, the power density is greater at the sample as compared to the conventional Raman instrument. These observations along with other laser irradiation dependence studies are discussed in greater detail in a following section.

#### Concentration Dependence Studies

Figure 2 also shows SERRS signals displayed by 50 Å silver film systems that were dipped into different concentrations of ZnTPP/acetone adsorbing bulk solutions. Figures 2A, 2B, and 2C correspond to adsorbing ZnTPP bulk solution concentrations of  $1 \times 10^{-4}$  M,  $1 \times 10^{-5}$  M and  $1 \times 10^{-6}$  M, respectively. As shown in this figure, the SERRS frequencies and relative band intensities are comparable for the two higher adsorbing concentrations, but the relative

intensities of the bands obtained from the lowest adsorbing concentrations are significantly different. In particular, the bands at  $1548\text{ cm}^{-1}$ ,  $1352\text{ cm}^{-1}$ , and  $1236\text{ cm}^{-1}$  decrease in enhancement. In order to determine if these differences were caused by a thermal or photo effect resulting from the use of the Raman microprobe, a similar concentration study was performed with a conventional Raman instrument. Figures 3A, 3B, and 3C illustrate the SERRS spectra displayed by the same dye/silver film systems used in the previous investigation but acquired with a macroRaman. Again, the ZnTPP band intensities are similar for the silver films with higher dye surface coverages as indicated in Figures 3A and 3B. However, the spectrum shown in Figure 3C compares to the spectrum of the lowest adsorbing bulk solution obtained with the Raman microprobe. These spectral changes in relative intensities suggest that the molecule reorients at the surface as a function of surface coverage. Zeman *et al.* [28] also reported changes in the relative band intensities for the porphyrin, cobalt phthalocyanine (CoPc) as a function of surface coverage. The authors observed that the enhancement of specific bands inverted when submonolayer to multilayer coverages of CoPc were vapor-deposited onto  $\text{CaF}_2$  roughened silver films. Further studies of the orientation of porphyrins indicated that at high coverages the molecules adsorb in an on-edge configuration with respect to the

surface. On the other hand, with low surface coverages, the porphyrin macrocycle oriented flat relative to the substrate [28].

#### Determination of Detection Limits

The detection limits of the SERRS Raman microprobe were estimated by monitoring the intensity of the ZnTPP signals as a function of surface coverage as shown in Figure 4. To determine the surface coverage, known volumes of varying concentrations of ZnTPP/acetone solutions were delivered to defined areas on 50 Å silver-island films. The coverages that were produced ranged from  $10^{-12}$  mol/cm<sup>2</sup> to  $10^{-10}$  mol/cm<sup>2</sup> assuming a uniform coating of the dye at the substrate surface. SERRS spectra were obtained by using the 40x objective while maintaining a laser irradiation period of 25 sec for each sample. The intensity of the 1356 cm<sup>-1</sup> bands was measured and subsequently normalized with respect to the strongest ZnTPP SERRS signal. The plot of surface concentration vs SERRS intensity depicted in Figure 4 shows that the signal increases with coverages up to a specific point, i.e., approximately  $4 \times 10^{-10}$  mol/cm<sup>2</sup>. At a higher concentration, the enhancement of the band decreases slightly. A nonlinear behavior of the SERRS intensity relative to surface coverages has been reported previously

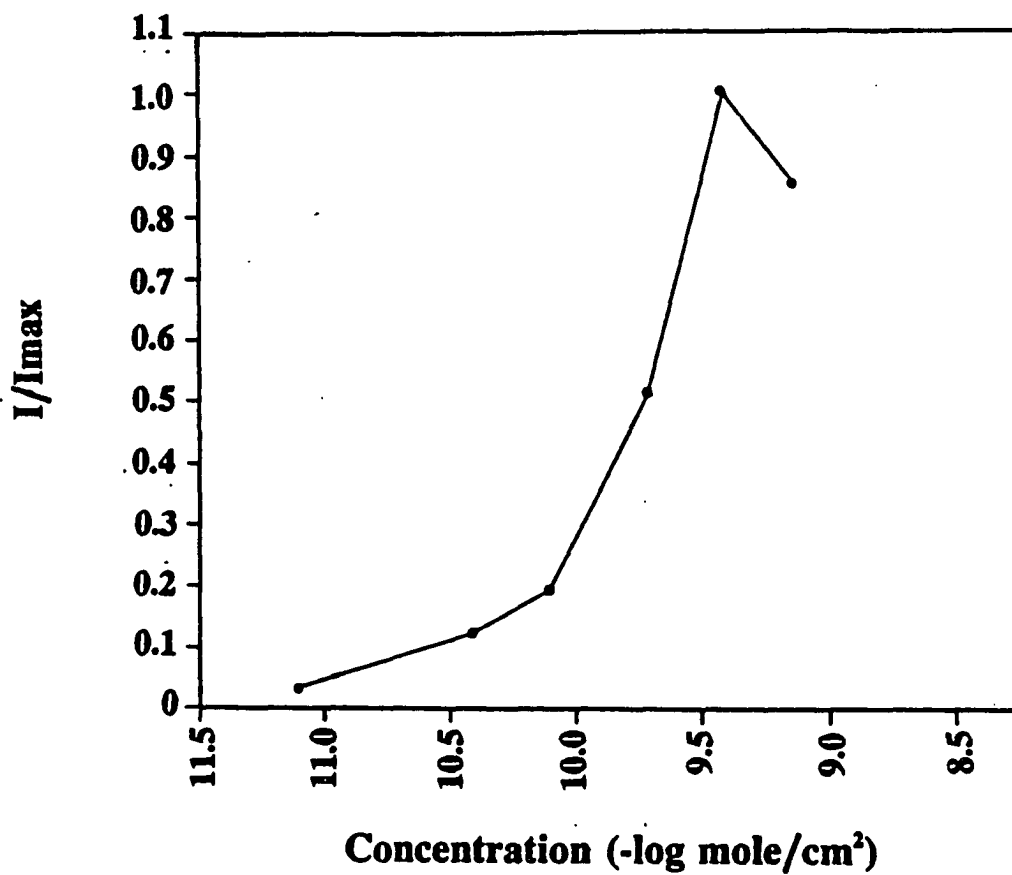


Figure 4. Intensity of the ZnTPP  $1356 \text{ cm}^{-1}$  band vs concentration of adsorbed ZnTPP. Intensities are normalized to maximum SERRS value. Experimental conditions: microscope objective, 10x; integration time, 1 sec; scans 25.

for resonantly-enhanced molecules [29,30]. Kim et al. performed a detailed study regarding the SERRS intensity as a function of surface coverage of a cyanine dye dispersed in a Langmuir-Blodgett lipid matrix and transferred to a silver-island film. According to the authors, the signal intensity increased with surface coverages to approximately 10 mol %, decreased between 10 mol % and 20 mol %, and then slowly increased again above 20 mol %. This nonlinear response was attributed to dipole-dipole interactions of the dye molecules and/or perturbations arising from coverage dependent dielectric properties of the overlayer.

Another important point to note is that measurable signals were obtained at a surface coverage of  $8 \times 10^{-12}$  mol/cm<sup>2</sup>. Furthermore, considering the laser spot size produced on the SERRS-active substrate by the 40x microscope objective, it is calculated that only  $7.3 \times 10^5$  molecules are irradiated. This sampling value was determined via the method described by Siegman [31] and Van Duyne et al. [32]. These calculations take into account the Gaussian spatial distribution of the incident radiation at the sample and the detected scattered light. It was reported by the authors that the Raman microprobe mass detection limits for the nonresonantly-enhanced molecule pyridine were also approximately  $10^5$  molecules. Several experimental factors may be responsible for the comparable detection limits

associated with the nonresonantly-enhanced and the resonantly-enhanced samples. As discussed previously, the intensity of the ZnTPP signals degraded when exposed to continuous laser irradiation whereas pyridine produces a stable SERS spectrum over time. Although the dye/silver film systems were irradiated for only 25 sec, the signals may decrease significantly during this period and affect the calculated detection limit. The limits may be lowered by employing excitation wavelengths that are closer in resonance with the electronic absorption band maximum of the dye, but the photostability of ZnTPP must then be considered. In addition, the SERS study of the non-resonantly-enhanced molecule used a fiber optic coupler to transmit the Raman scattered light which, in turn, may lower the detection limits for the SERS microprobe.

#### **Laser Irradiation Time Dependence Studies**

As discussed above, the relative intensities of the shifts and the frequencies of the bands in the ZnTPP spectra are similar for the spectra collected by the micro and the macro systems. However, signal degradation occurs immediately with the microprobe whereas a stable SERRS spectrum is maintained when the macroRaman instrument is employed. These results can be attributed to the intense

power density of the focused laser in the microprobe system. The diameter of the laser spot at the surface is dependent upon the wavelength of the excitation line and the microscope objectives [33]. In this work, the 514.5 nm was focused to 6  $\mu\text{m}$  and 1  $\mu\text{m}$  for the 10x and 40x objectives, respectively. Therefore, an incident power of only 2 mW produces a peak irradiances at the laser spot center of 8.8 kW/cm<sup>2</sup> with the 10x objective and 320 kW/cm<sup>2</sup> with the 40x objective. These values were calculated via the TEM<sub>00</sub> Gaussian beam distribution treatment given by Siegman [31]. According to this derivation, when the distance of the center of the beam is equivalent to the laser spot size, the peak irradiances drops by 1/e<sup>2</sup>.

Figure 5 illustrates spectra of ZnTPP adsorbed onto a 50 Å silver-island film as a function of continuous laser irradiation exposure time. The data were acquired by directing the laser line through the 10x objective. The surface was irradiated continuously and SERRS spectra were obtained at the specified time intervals indicated in Figure 5. The figure shows that with laser irradiation times ranging from 25 sec to 1525 sec the intensity of the exhibited signals decrease. After a time period of 1525 sec, the signal decayed by a factor of approximately 4. Because the signal-to-noise ratio decreases, certain less intense bands cannot be distinguished from the background as

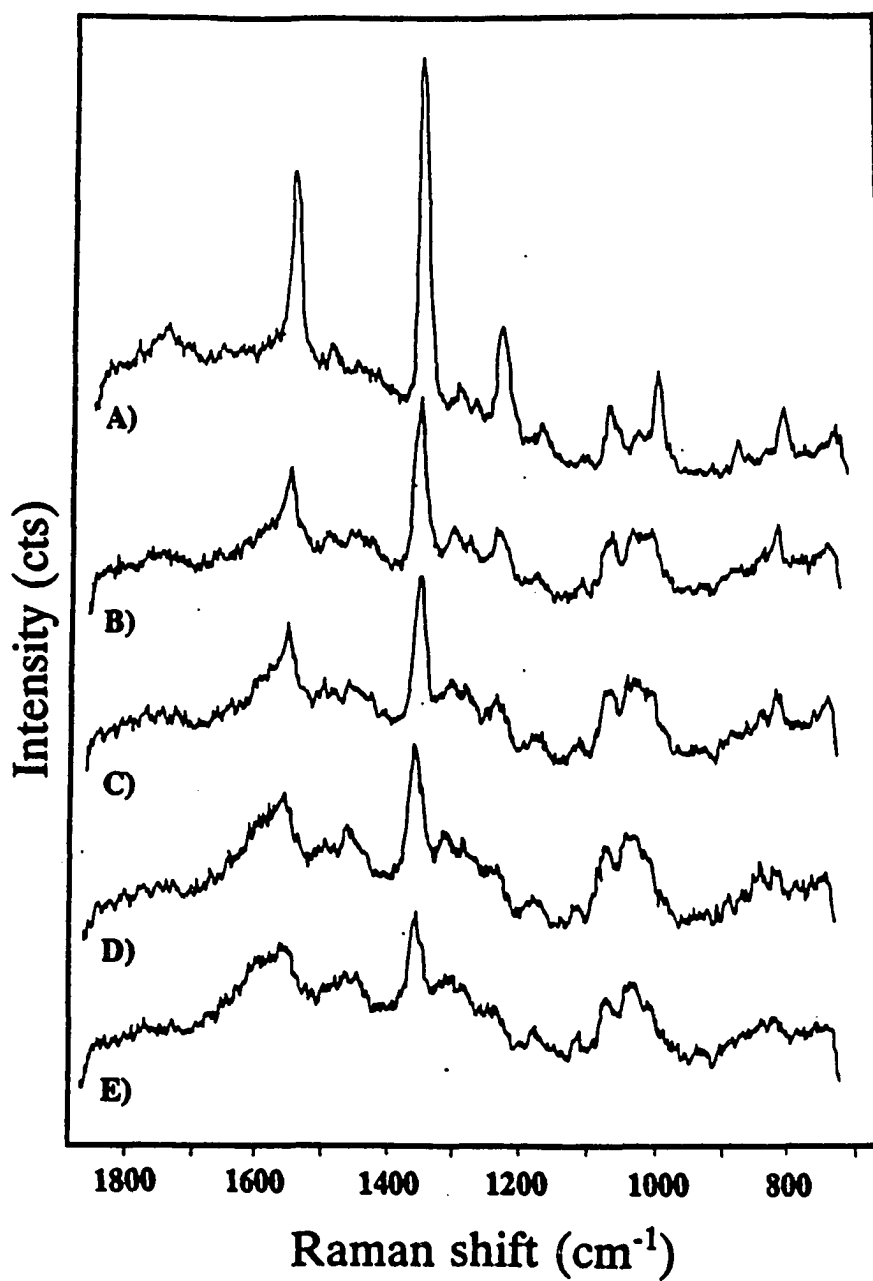


Figure 5. SERS spectra of ZnTPP adsorbed onto 50 Å silver-island films as a function of laser irradiation time: A) 25 sec; B) 2 min 25 sec; C) 5 min 25 sec; D) 15 min 25 sec; E) 25 min 25 sec. Experimental conditions: microscope objective, 10x; integration time, 1 sec; scans, 25.

the exposure time is increased. For example, the  $1234\text{ cm}^{-1}$  frequency is decreased so that after 925 sec it is not discernible from the background noise. In addition, the relative intensities of the band change with continued laser irradiation. The molecule is therefore susceptible to photodamage when exposed to the tightly focused laser line for an extended period of time.

Directing the laser line through the 40x objective onto the ZnTPP/silver-island film system produces bands with greater intensities compared to the 10x objective. Fewer molecules were sampled with the former objective, but the power density at the substrate surface increases significantly which in turn gives rise to greater Raman intensities. The signals measured initially with the 40x objective decrease rapidly with continued irradiation. Figure 6 depicts plots of SERRS intensities vs laser exposure time dependence for the 10x and 40x objectives. The data points were obtained by monitoring the ZnTPP  $1356\text{ cm}^{-1}$  as a function of irradiation time. The experimental

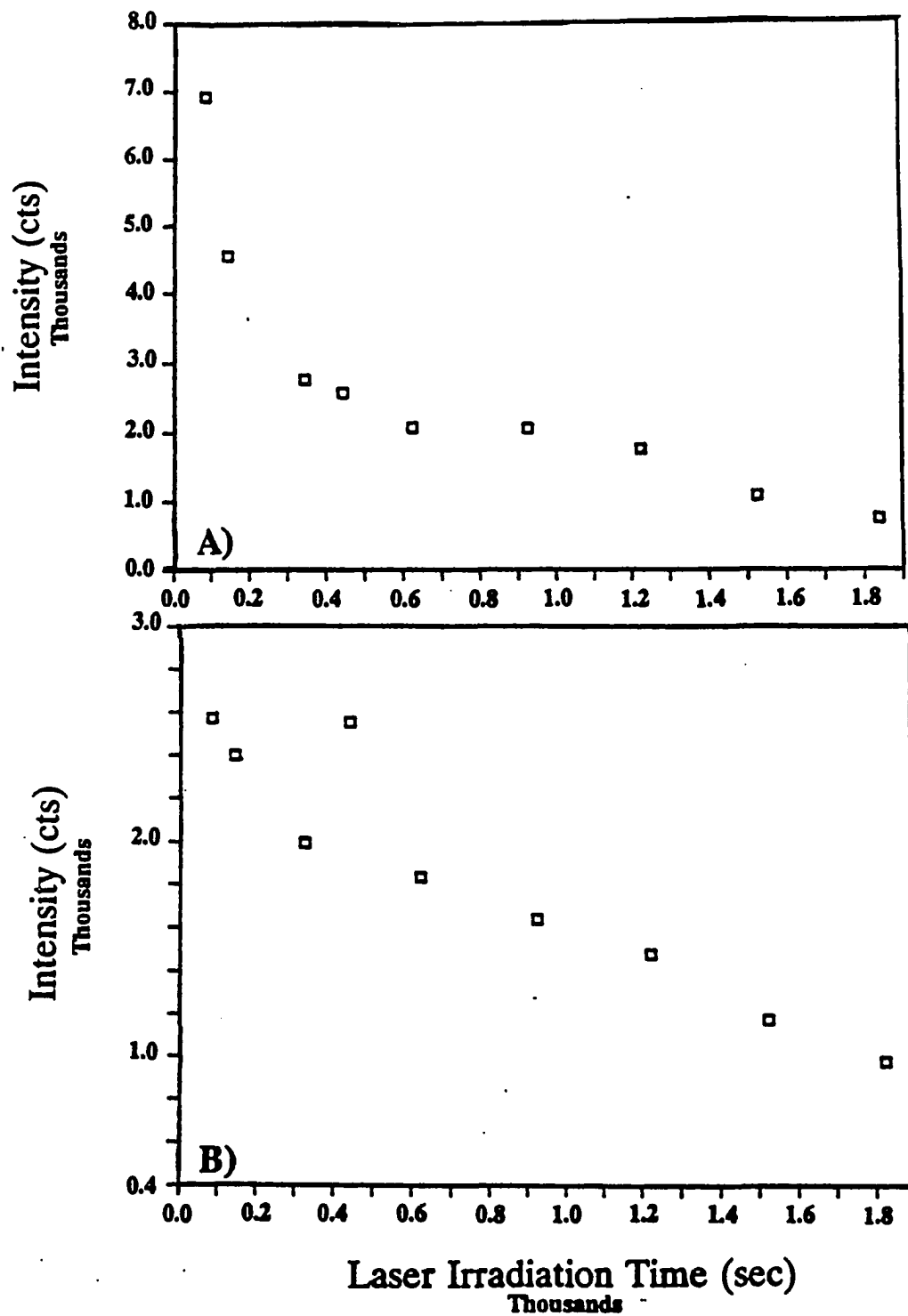


Figure 6. Intensity of the ZnTPP 1356 cm<sup>-1</sup> band vs laser irradiation time: A) 40x microscope objective; B) 10x microscope objective.

conditions for generating the plots were kept constant except for the different objectives which were implemented to focus the laser line onto the sample and to collect the scattered radiation. Figure 6A shows the plot of the intensity of the  $1356\text{ cm}^{-1}$  vs irradiation time for the 40x objective and Figure 6B illustrates the graph generated with the 10x objective. The linear relationship between the SERRS band intensities and the laser irradiation period shown in Figure 6B indicates that the signals steadily decay with time. Alternatively, the exponential curve corresponding to the 40x objective shows that the signals decrease rapidly from 85 sec to 300 sec. With greater exposure periods, the Raman bands display a similar decline in intensity as observed for the plot generated using the 10x objective of the microscope. The photostability of the dye molecules is therefore influenced by the power density of the incident radiation impinging at the ZnTPP/silver film surface. However, a spectrum may be collected in 1 sec by employing a diode-array detector thereby minimizing photodegradation.

**Raman Microprobe SERRS Spectra of Magnesium  
Phthalocyanine and 1,1'-Diethyl-2,2'-Cyanine Iodide**

Other types of dyes were adsorbed onto 50 Å silver-island films and their behavior was monitored with the microsystem. These compounds included magnesium phthalocyanine (MgPc) and 1,1'-diethyl-2,2'-cyanine iodide (DCI). Figure 7 and Figure 8 show the SERRS spectra of DCI and MgPc as a function of laser exposure time. The former dye was irradiated with the 514.5 nm excitation whereas the 647.1 nm excitation served as the incident light source for the collection of the MgPc Raman data. As the figures illustrate, the relative band intensities remain constant with greater exposure periods, but the overall spectral intensity decreases. The DCI molecule behaves much like ZnTPP in that a linear relationship between irradiation time and photodegradation exists. In contrast to ZnTPP and DCI, the signal displayed by the adsorbed MgPc decreased only slightly with continued laser irradiation. These results may be related to the dependence of the laser spot size associated with the longer excitation line. The Gaussian beam theory predicts that the spot size increases when longer wavelength excitation lines are used. Also, the focal spot produced by focusing a Gaussian beam through a lens is directly proportional to the wavelength of the

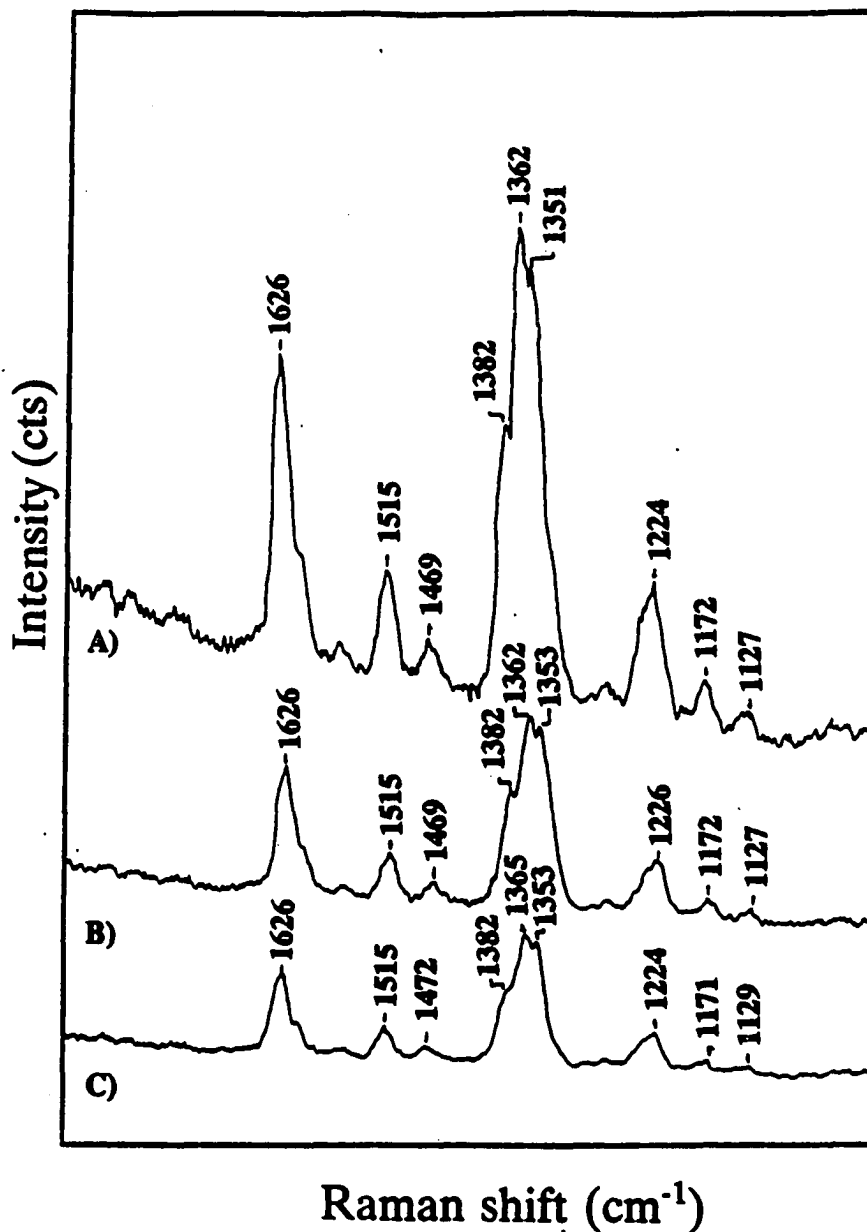


Figure 7. SERRS spectra of DCI adsorbed onto 50 Å silver-island films as a function of laser irradiation time: A) 50 sec; B) 300 sec; C) 600 sec. Experimental conditions: microscope objective, 10x; integration time, 1 sec; scans, 25.

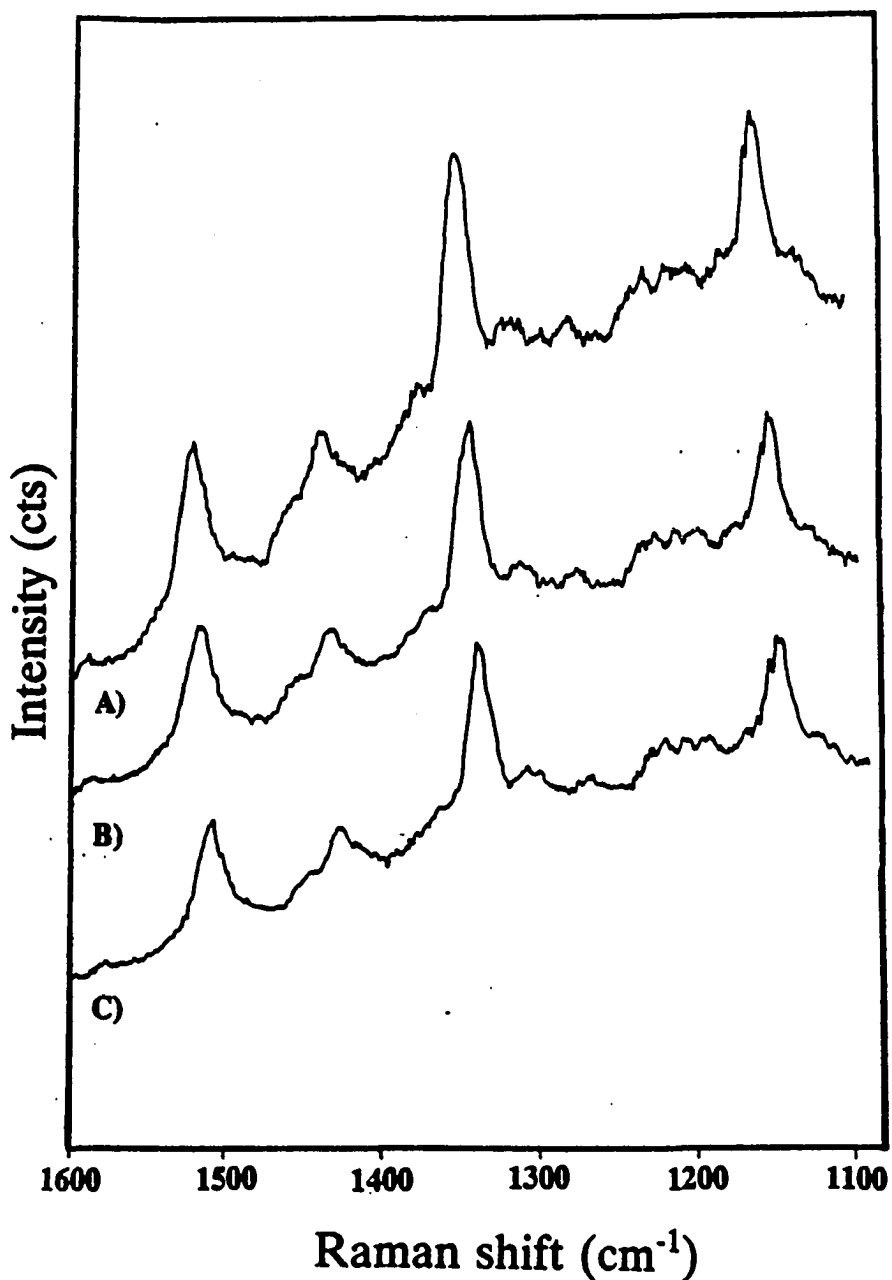


Figure 8. SERRS spectra of MgPc adsorbed onto 50 Å silver-island films as a function of laser irradiation time: A) 25 sec; B) 325 sec; C) 295 sec. Experimental conditions: microscope objective, 10x; integration time, 1 sec; scans, 25.

incident beam [33]. A larger spot size would result with the 647.1 nm line as compared to the 514.5 nm excitation which, in turn, would lower the peak irradiances at the sample surface. In addition, this molecule may be more resilient to the high incident laser power densities as compared to DCI and ZnTPP.

Because of the presence of a high background, RRS solution spectra were not obtained for any of the molecules studied in this work. Raman bands were only observed when a silver surface was present. The metallic surface may contribute to the stabilization of the molecules by absorbing the energy from the irradiated molecules. Yamada et al. [34] showed that greatest SERRS intensities produced by several dyes at silver films are obtained when the maximum absorption band of adsorbed molecules overlaps with the electronic band maxima of the silver films. The authors attributed these results to a stabilization of the intramolecular resonance Raman of the adsorbed dyes. The molecules are stabilized because energy transfer occurs from the dyes to the metal when the absorption bands of the metal and the adsorbed species coincide.

The metal may also dissipates the thermal energy produced by the irradiated molecules and reduce local heating of the samples is reduced. Because silver has a high thermal conductivity,  $4.29 \text{ W cm}^{-1} \text{ K}^{-1}$  [35], the substrate may serve as a "heat sink", thereby allowing Raman

spectra of resonantly-enhanced molecules to be acquired with a focused laser beam.

### CONCLUSIONS

In summary, the data presented in this work demonstrate that Raman signals of resonantly-enhanced molecules can be acquired when the samples are adsorbed on a metallic substrate. The Raman spectral intensities decrease with laser irradiation exposure times but characteristic Raman spectra of the dyes, ZnTPP and DCI, could be obtained in several sec with the use of a diode array detector. On the other hand, the dye, MgPc, did not degrade with continued laser irradiation. The laser line may not be as tightly focused at longer wavelengths. Alternatively, the decrease in spectral intensity as a function of laser irradiation may be dependent upon the nature of the adsorbed sample. It was also shown that less than an attomole of ZnTPP molecules can be detected using a SERRS Raman microprobe.

**ACKNOWLEDGEMENT**

The authors are grateful for the support of the National Institutes of Health (GM 35108). We would like to thank Dr. Randall Holt for his helpful comments and assistance.

## LITERATURE CITED

1. Delhaye, M., Dhamelincourt, P. J. Raman Spectrosc. 1975, 3, 33.
2. Rosasco, G. J., Etz, E. S., Eassatt, W. A. Appl. Spectrosc. 1974, 29, 396.
3. Ishida, H., Ishitani, A. Appl. Spectrosc. 1983, 37, 450.
4. Beattie, I. R. Chem. Soc. Revs. 1975, 4, 107.
5. Gardiner, D. J., Bowden, M., Graves, P. R. Phil. Trans. R. Soc. Lond. A 1986, 320, 295.
6. Mochizuki, K., Namihira, K., Kuwazura, M., Iwamoto, Y. I. J. Quantum Electron. 1984, 20, 694.
7. Bibby, G. W., Ross, J. N. Electron. Lett. 1984, 20 182.
8. Wopenka, B., Pasteris, J. D. Anal. Chem. 1987, 59, 2165.
9. Blaha, J. J., Rosasco, G. J., Etz, E. S. Appl. Spectrosc. 1975, 32, 292.
10. Etz, E. S., Roscasco, G. J., Blaha, J. J. In Environmental Analysis, Ewing, G. W., Ed.; Academic Press: New York, 1977; pp 295-340.
11. Etz, E. S., Wong-Ng, W., Blendell, J. E., Chiang, C. K. In Microbeam Analysis, Newbury, D. E., Ed.; San Francisco Press: San Francisco, 1988; pp 187-192.
12. Vo-Dinh, T., Hiromoto, M. Y. K., Begun, G. M., Moody,

- R. L. Anal. Chem. 1984, 56, 1667.
13. Enlow, P. D., Buncick, M., Warmack, R. J., Vo-Dinh, T. Anal. Chem. 1986, 58, 1119.
  14. Hildebrandt, P., Stockburger, M. In Vibrational Spectra and Structure, in press.
  15. Cotton, T. M. In Spectroscopy of Surfaces, Clark, R. J. H., Hester, R. E., Eds.; John Wiley & Sons: New York, 1988; Vol. 16, pp 91-153.
  16. Van Duyne, R. P. In Chemical and Biochemical Applications of Lasers, Moore, C. B., Ed.; Academic Press: New York, 1979; Vol. 4, p 91.
  17. Chang, R. K., Furtak, T. E., Eds.; Surface-Enhanced Raman Scattering, Plenum: New York, 1982.
  18. Otto, A. In Light Scattering in Solids IV, Cardona, M., Guntherodt, G., Eds.; Springer: New York, 1984; p 289.
  19. Hembree, D. M., Oswald, J. C., Smyrl, N. R. Appl. Spectrosc. 1987, 41, 267.
  20. Ishida, H., Ishitani, A. Appl. Spectrosc. 1983, 37, 450.
  21. Thi, M. P. Chem. Phys. Lett. 1985, 115, 130.
  22. Van Duyne, R. P., Haller, K., Altkorn, R. I. Chem. Phys. Lett. 1986, 126, 190.
  23. Otto, C., van den Tweel, T. T. J., De mul, F. F. M., Greve, J. Raman Spectrosc. 1986, 17, 289.
  24. Schlegel, V. L., Cotton, T. M., Department of

Chemistry, Iowa State University, in press.

25. Sennett, R. S., Scott, G. D. J. Opt. Soc. Am. 1950, 40, 203.
26. Bergman, J. G., Chemla, D. S., Liao, P. F., Glass, A. M., Pinczuk, A., Hart, R. M., Olson, D. H. Opt. Lett. 1981, 6, 33.
27. Weitz, D.A., Garoff, S., Gramila, T. J. Opt. Lett. 1982, 7, 168.
28. Zeman, E. J., Carron, K. T., Schatz, G. C., Van Duyne, R. P. J. Chem. Phys. 1987, 87, 4189.
29. Kaul, B. B., Holt, R. E., Schlegel, V. L., Cotton, T. M. Anal. Chem. 1988, 60, 1580.
30. Kim, J. -H., Cotton, T. M., Uphaus, R. A., Möbius, D. J. Phys. Chem. 1989, 93, 9713.
31. Siegman, A. E., Ed., In Introduction to Lasers and Masers, McGraw-Hill: New York, 1971; ch. 8.
32. Van Duyne, R. P., Haller, K. L., Altkorn, R. I. Chem. Phys. Lett. 1986, 126, 192.
33. Young, M. In Optics and Lasers, Tamir, T., Ed.; Springer-Verlag: New York, 1984; Vol.5, ch. 7.
34. Yamada, H., Nagata, H., Kishibe, K. J. Phys. Chem. 1986, 90, 818.
35. Kittle, C., Ed., In Introduction to Solid State Physics, McGraw-Hill: London, 1977.

### CONCLUDING REMARKS

Surface-enhanced resonance Raman scattering spectroscopy is a powerful technique for biological and analytical investigations. However, SERRS is only applicable to these studies when the optimal experimental conditions are defined and controlled. As presented in this work, the types of SERRS-active surfaces as well as their preparation procedures affect the frequencies, relative band intensities, and overall spectral intensity of the resulting Raman spectra.

Biological samples are particularly sensitive to the experimental parameters required for the preparation of SERRS-active substrates. The studies of heme-containing presented herein show that the native structure of the adsorbed biomolecules can be retained by optimizing the appropriate adsorption conditions. Future applications of SERRS to various biological systems appears to be entirely feasible based on the reported results. Once the necessary adsorption parameters are established, the biological activity of the protein and its structure can be examined with SERRS. The substrate also can be used to mimic a biological membrane. By initially depositing a lipid layer onto the surface, membrane interactions of the adsorbed protein can be monitored.

The SERRS intensity is further dependent upon the preparation procedure of silver-island films. Specifically, the morphology of the surface particles, and consequently, the intensity of the SERRS signals are affected by the rate of deposition. Previous SERRS/SERS experiments using metal films as the active substrate, the evaporation rate was not optimized. This is the only investigation that has examined the effects of the rate of silver deposition on the SERRS/SERS intensity. However, several experimental parameters of metal films have not yet been fully characterized, including metal thickness and substrate temperature. In addition, the effects of preparation procedures of metal films such as gold and copper on SERRS/SERS have not yet been determined. By optimizing these conditions, metal-island films can be used successfully for various analytical applications as shown by the Raman microprobe studies of resonantly-enhanced molecules and by the covalently modified electrode investigations presented in this work.

## LITERATURE CITED

1. Fleischmann, M., Hendra, P. J., McQuillan, A. J. J. Chem. Soc., Chem. Commun. 1973, 80.
2. Fleischmann, M., Hendra, P. J., McQuillan, A. J. Chem. Phys. Lett. 1974, 26, 163.
3. Jeanmaire, D. L., Van Duyne, R. P. J. Electroanal. Chem. 1977, 84, 1.
4. Albrecht, M. G., Creighton, J. A. J. Am. Chem. Soc. 1977, 99, 5215.
5. Billman, J., Kovacs, G., Otto, A. Surf. Sci. 1980, 92, 153.
6. Bergman, J. G., Heritage, J. P., Pinczuk, A., Worlock, J. M., McFee, J. H. Chem. Phys. Lett. 1979, 68, 412.
7. Van Duyne, R. P. In Chemical and Biochemical Applications of Lasers, Moore, C. B., Ed.; Academic Press: New York, 1979; Vol. 4, p 101.
8. Chang, R. K., and Furtak, T. E., Eds.; Surface-Enhanced Raman Scattering, Plenum: New York, 1984; p 289.
9. Otto, A. In Light Scattering in Solids IV, Cardona, M., Guntherodt, G., Eds.; Springer-Verlag: New York, 1984; p 289.
10. Wokaun, A. Solid State Phys. 1984, 38, 223.
11. Metiu, H., Das, P. Annu. Rev. Phys. Chem. 1984, 38, 223.

12. Creighton, J. A. In Spectroscopy of Surfaces, Clark, J. H., Hester, R. E., Eds.; John Wiley & Sons Ltd: New York, 1988; Vol. 16.
13. Moskovits, M. Rev. Mod. Phys. 1985, 57, 783.
14. Moskovits, M. J. Chem. Phys. 1978, 69, 4159.
15. McCall, S. L., Platzman, P. M., Wolff, P. A. Phys. Lett. A 1980, 77A, 381.
16. Ferrell, T. L., Callcott, T. A., Warmack, R. J. J. Am. Sci. 1985, 73, 344.
17. Aroca, R., Fernando, M. J. Raman Spectrosc. 1985, 16, 156.
18. Kerker, M., Wang, D. -S., Chew, H. Appl. Optics 1980, 19, 4159.
19. Barber, P. W., Chang, R. K., Massoudi, H. Phys. Rev. Lett. 1983, 50, 997.
20. Bergman, J. G., Liao, P. F., Chemla, D. S., Wokaun, A., Melugailis, J., Hawryluk, A. M., Economou, N. P. Chem. Phys. Lett. 1981, 82, 355.
21. Zeman, E. J., Schatz, G. C. J. Phys. Chem. 1987, 91, 634.
22. Wang, D. -S., Kerker, M. Phys. Rev. 1981, B24, 1777.
23. Kotler, Z., Nitzan, A. J. Chem. Phys. 1982, 86, 2011.
24. Weitz, D. A., Garoff, S., Gramila, T. J. Opt. Soc. of Am. 1981, 6, 33.
25. Gersten, J. I., Birke, R. L., Lombardi, J. R. Phys.

- Rev. Lett. 1979, 43, 143.
26. Otto, A., Billman, J., Eickmans, J., Erturk, U.,  
Pettenkofer, C. Surf. Sci. 1984, 138, 319.
27. Pettinger, B., Wenning, J. Kolb, D. M. Ber. Bunsenges.  
Phys. Chem. 1978, 82, 1136.
28. Abe, H., Manzel, K., Schulze, W., Moskovits, M.,  
DiLella, D. P. J. Chem. Phys. 1981, 74, 792.
29. Cotton, T. M., Schultz, S. G., Van Duyne, R. P. J. Am.  
Chem. Soc. 1980, 102, 7962; 1980, 104, 6528.
30. Cotton, T. M., Timovich, R., Cork, M. S. FEBS Lett.  
1981, 133, 39.
31. Itabashi, M., Kato, K., Itoh, K. Chem. Phys. Lett.  
1983, 97, 528.
32. Hagen, G., Simic Glavaski, B., Yeager, E. J.  
Electroanal. Chem. 1978, 88, 269.
33. Weitz, D. A., Garoff, S., Gersten, J. I., Nitzan, A. J.  
Chem. Phys. 1983, 78, 5324.
34. Kotler, Z., Nitzan, A. J. Phys. Chem. 1982, 86, 2011.
35. Zeman, E. J., Carron, K. T., Schatz, G. C., Van Duyne,  
R. P. J. Chem. Phys. 1987, 87, 4189.
36. Siiman, O., Lepp, A., Kerker, M. J. Phys. Chem. 1983,  
87, 5319.
37. Stacey, A. M., Van Duyne, R. P. Chem. Phys. Lett. 1983,  
102, 365.
38. Bachackashvilli, A., Efrima, S., Katz, B., Priel, Z.

- Chem. Phys. Lett. 1983, 94, 571.
39. Seki, H. J. J. Elec. Spectrosc. Rel. Phenom. 1986, 39, 289.
  40. Pockrand, I. Chem. Phys. Lett. 1982, 85, 37.
  41. Schulze, W., Breithaupt, B., Charlé, B., Kloss, U. Ber. Bunsenges. Phys. Chem. 1984, 88, 308.
  42. Lunk, P. A., Tevault, D. E., Smardzewski, R. R. J. Phys. Chem. 1984, 88, 1731.
  43. Lopez-Rios, T., Pettenkofer, C., Pockrand, I., Otto, A. Surf. Sci. 1982, 121, 541.
  44. Krasser, W., Renouprez, A. J. J. Raman Spectrosc. 1981, 11, 425.
  45. Yamada, H., Yamamoto, Y., Tani, N. Chem. Phys. Lett. 1982, 86, 397.
  46. Loo, B. H. Solid State Commun. 1982, 43, 349.
  47. Fleischmann, M., Graves, P. R., Hill, I. R., Robinson, J. Chem. Phys. Lett. 1983, 95, 322.
  48. Krasser, W., Renouprez, A. J. Solid State Commun. 1982, 41, 231.
  49. Schultz, S. G., Janik-Czachor, M., Van Duyne, R. P. Surf. Sci. 1981, 104, 419.
  50. Rowe, J. E., Shank, C. V., Zwemer, D. A., Murray, C. A. Phys. Rev. Lett. 1980, 44, 1770.
  51. Burstein, E., Chen, C. Y., Murphy, W. R., Eds.; Proc

- 7<sup>th</sup> Intern Conf. Raman Spectroscopy, Ottawa, 1980; p.  
346.
52. Jiang, X., Campion, A. Chem. Phys. Lett. 1987, 140, 95.
53. Chang, R. K., Laube, R. L. CRC Crit. Rev. Solid State Mater. Sci. 1984, 12, 1.
54. Macomber, S. H. J., Furtak, T. E., Devine, T. M. Chem. Phys. Lett. 1982, 90, 439.
55. Chen, T. T., Von Raben, K. U., Owen, J. F., Chang, R. K., Laube, B. L. Chem. Phys. Lett. 1982, 91, 494.
56. Barz, F., Gordan II, J. G., Philpott, M. R., Weaver, M. J. Chem. Phys. Lett. 1982, 91, 291.
57. Devine, T. M., Furtak, T. E., Macomber, S. H. J. Electroanal. Chem. 1984, 164, 299.
58. Barz, F., Gordan II, J. G., Philpott, M. R., Weaver, M. J. Chem. Phys. Lett. 1983, 94,
59. Moskovitz, M., DiLella, D. Chem. Phys. Lett. 1980, 73, 500.
60. Wood, T. H., Klein, M. V. Solid State Commun. 1980, 35, 263.
61. Dornhaus, R., Long, M. B., Benner, R. E., Chang, R. K. Surf. Sci. 1980, 93, 240.
62. Gold, H. S., Buck, R. P. J. Raman Spectrosc. 1979, 8, 323.
63. Otto, A. Surf. Sci. 1978, 75, L392.
64. Pettinger, B., Wenning, J., Wetzels, H. J. Chem. Phys.

- Lett. 1980, 70, 49.
65. Chang, R. K. Ber. Bunsenges. Phys. Chem. 1987, 91, 296.
66. Creighton, J. A., Blatchford, C. G., Albrecht, M. G. J. Chem. Soc., Faraday Trans. 2 1979, 75, 790.
67. Wetzal, H., Gerischer, H. Chem. Phys. Lett. 1980, 76, 460.
68. Kerker, M. J. Colloid and Interface Sci. 1985, 105, 297.
69. Lee, P. C. Meisel, D. Chem. Phys. Lett. 1983, 99, 262.
70. Heard, S. M., Grieser, F., Barraclough, C. G. Chem. Phys. Lett. 1983, 99, 154.
71. Laserna, J., Torres, E., Winefordner, J. Anal. Chim. Acta 1987, 200, 469.
72. Soper, A. S., Kuwana, T. Appl. Spectrosc. 1989, 43, 1180.
73. Siiman, O., Bumm, L. A., Callaghan, R., Blatchford, C. G., Kerker, M. J. Phys. Chem. 1983, 87, 1014.
74. Blatchford, C. G., Campbell, J. R., Crieghton, J. A. Surface Sci. 1982, 87, 435.
75. Blatchford, C. B., Siiman, O., Kerker, M. J. Phys. Chem. 1983, 87, 2503.
76. Tran, C. Anal. Chem. 1984, 56, 824.
77. Tran, C. J. Chromatogr. 1984, 432.
78. Laserna, J., Campiglia, A., Winefordner, J. Anal. Chim. Acta 1988, 208, 21.

79. Séquaris, J., Koglin, E. Anal. Chem. 1987, 59, 527.
80. Wang, D. S., Kerker, M. Phys. Rev. B 1981, 24, 1777.
81. Blatchford, C. G., Campbell, J. R., Creighton, I. A. Surf. Sci 1981, 108, 411.
82. Creighton, J. A., Alvarez, M. S., Weitz, D. A., Garoff, S., Kim, M. W. J. Phys. Chem. 1983, 87, 4793.
83. Torres, E., Winefordner, J. Anal. Chem. 1987, 59, 1626.
84. Freeman, R., Hammaker, R., Fateley, W. Appl. Spectrosc. 1988, 42, 456.
85. Berthod, A., Laserna, J., Winefordner, J. Appl. Spectrosc. 1988, 42, 1137.
86. Laserna, J., Berthod, A., Winefordner, J. Talanta 1988, 34, 745.
87. Kwon, C. K., Kim, S. M., Kim, K. J. Raman Spectrosc. 1989, 20, 575.
88. Sandroff, C. J., King, Jr., H. E., Herschbach, D. R. J. Phys. Chem. 1984, 88, 5647.
89. Murray, C. A., Bodoff, S. Phys. Rev. B 1985, 32, 671.
90. Wietz, D. A., Garoff, S., Gramila, T. J. Opt. Lett. 1982, 7, 168.
91. Liao, P. F., Bergman, J. G., Chemla, D. S., Wokaun, A., Melngailis, J., Hawryluk, A. M., Economou, N. P. Chem. Phys. Lett. 1981, 82, 355.
92. Bergman, J. G., Chemlas, D. S. Liao, P. F., Glass, A. M., Pinczuk, A., Hart, R.M., Olson, D. H. Opt. Lett.

- 1981, 33, 6.
93. Wood, T. H., Klein, M. V. J. Vac. Sci. Technol. 1979, 16, 459.
94. Wood, T. H., Klein, M. V. Solid State Commun. 1980, 35, 263.
95. Chen, C. Y., Davoli, I., Ritchie, G., Burstein, E. Surf. Sci. 1980, 101, 363.
96. Sennett, R. S., Scott, G. D. J. Opt. Soc. Am. 1950, 40, 203.
97. Pockrand, I., Otto, A. Solid State Commun. 1981, 38, 263.
98. Murray, C., Allara, D. J. Chem. Phys. 1982, 76, 1290.
99. Vo-Dinh, T., Hiromoto, Y. K., Begun, G. M., Moody, R. L. Anal. Chem. 1984, 56, 1667.
100. Schlegel, V., Cotton, T. M., Department of Chemistry, Iowa State University. unpublished results.
101. Ni, R., Cotton, T. M. Anal. Chem. 1986, 58, 3159.
102. Otto, A. In Proc. Intern. Conf. On Vibrations in Adsorbed Layers, June 78, Surf. Sci. 1980, 92, 145.
103. Burstein, E., Chen, Y. J., Chen, C. Y., Lundquist, S., Tossatti, E. Solid State Commun. 1979, 29, 567.
104. Chen, C. Y., Burstein, E., Lundquist, S. Solid State Commun. 1979, 32, 63.
105. Murray, C. A., Allara, D. L., Rhinewine, M. Phys. Rev. Lett. 1981, 46, 57.

106. Wood, T. H., Zwemer, D. A., Shank, C. V., Rowe, R. E. Chem. Phys. Lett. 1981, 82, 5.
107. Cotton, T. M., Uphaus, R. A., Möbius, D. J. Phys. Chem. 1986, 90, 6071.
108. Kovacs, G. J., Loutfy, R. O., Vincett, P. S., Jennings, C., Aroca, R. Langmuir 1986, 2, 689.
109. Wetzel, H., Gerischer, H. Chem. Phys. Lett. 1980, 76, 460.
110. Creighton, J. A., Blatchford, C. G., Albrecht, M. G. J. Chem. Co., Faraday Trans. 2 1979, 75, 790.
111. Weitz, D. A., Garoff, S., Gramila, T. J. Opt. Lett. 1982, 7, 168.
112. Glass, A. M., Liao, P. F., Bergman, J. G., Olson, D. H. Opt. Lett. 1980, 5, 368.
113. Liao, P. F., Bergman, J. G., Chemla, D. S., Wokaun, A., Melngailis, J., Hawryluk, A. M., Economou, N. P. Chem. Phys. Lett. 1981, 82, 355.
114. Smardzewski, R. R., Colton, R. J., Murday, J. S. Chem. Phys. Lett. 1979, 68, 53.
115. Murray, C. A., Bodoff, S. Phys. Rev. Lett. 1984, 52, 2273.
116. Weitz, D. A., Garoff, S., Gersten, J. I., Nitzan, A. J. Chem. Phys. 1983, 78, 5324.
117. Zwemer, D. A., Shank, C. V., Rowe, J. E. Chem. Phys. Lett. 1980, 73, 201.

118. Eesley, G. L. Phys. Lett. 1981, 81A, 193.
119. Zeman, E. J., Carron, K. T., Schatz, G. C., Van Duyne, R. P. J. Chem. Phys. 1987, 87, 4189.
120. Kim, J. -H, K., Cotton, T. M., Uphays, R. A., Möbius, D. J. Phys. Chem. 1989, 93, 3713.
121. Sverdlov, L. M., Kovner, M. A., Krainov, E. P., Eds., Vibrational Spectra of Polyatomic Molecules, Wiley: New York, 1974.
122. Erdheim, G. R., Birke, R. L., Lombardi, J. Chem. Phys. Lett. 1980, 69, 495.
123. Moskovits, M., DiLella, D. P. J. Phys. Chem. 1980, 73, 6068.
124. Gao, P., Weaver, M. J. J. Phys. Chem. 1985, 89, 5040.
125. Patterson, M. L., Weaver, M. J. J. Phys. Chem. 1985, 89, 5046.
126. Moskovits, M., DiLella, D. P. Chem. Phys. Lett. 1982, 85, 243.
127. Albrecht, A. C. J. Chem. Phys. 1961, 34, 1476.
128. Albrecht, A. C., Hutley, M. C. J. Chem. Phys. 1971, 55, 4438.
130. Creighton, J. A. In Advances in Spectroscopy, Clark, R. J. H., Hester, R. E., Eds.; John Wiley and Sons: New York, 1988; Vol. 16, p 37.
130. Moskovits, M., Suh, J. S. J. Phys. Chem. 1984, 88, 5526.

131. Moskovits, M., DiLella, D. P., Maynard, K. J. Langmuir 1988, 4, 67.
132. King, F. W., Van Duyne, R. P., Schatz, G. C. J. Chem. Phys. 1978, 69, 4472.
133. Chambers, J. A., Buck, R. P. J. Ram. Spectrosc. 1985, 16, 171.
134. Takahashi, M., Fujita, M., Ito, M. Chem. Phys. Letts. 1984, 102, 122.